Identification and Characterization of Genes Essential for Human Brain Development

Dissertation Advisor: Dr. Christopher A. Walsh Author: Vijay S. Ganesh

Identification and Characterization of Genes Essential for Human Brain Development

Abstract

The human brain is a network of ninety billion neurons that allows for many of the behavioral adaptations considered unique to our species. One-fifth of these neurons are layered in an epithelial sheet known as the cerebral cortex, which is exquisitely folded into convolutions called gyri. Defects in neuronal number clinically present with microcephaly (Greek for "small head"), and in inherited cases these defects can be linked to mutations that identify genes essential for neural progenitor proliferation. Most microcephaly genes are characterized to play a role in the centrosome, however rarer presentations of microcephaly have identified different mechanisms.

Charged multivesicular body protein/Chromatin modifying protein 1A (CHMP1A) is a member of the ESCRT-III endosomal sorting complex, but is also suggested to localize to the nuclear matrix and regulate chromatin. We show that loss-of-function mutations to human *CHMP1A* cause a rare microcephaly syndrome with reduced cerebellar volume. *CHMP1A* mutant cells show impaired proliferation, with increased expression of *INK4A*, a negative regulator of stem cell proliferation, and loss of enrichment of *INK4A* promoter DNA in chromatin immunoprecipitations performed against BMI1, indicating a loss of the normal repression of *INK4A* by BMI1. Defects in zebrafish produced by morpholino-based knockdown of the *CHMP1A* orthologue resembled those seen after *bmi1* knockdown, and were partially

rescued by *INK4A* orthologue knockdown. *Chmp1a* is expressed in dividing cells in the developing cerebral cortex and cerebellar external germinal layer, and *in vitro* knockdown assays using short hairpin RNA implicate a role in Wnt- and Shh-pathway signal transduction. Altogether, this suggests that CHMP1A serves as a critical link between cytoplasmic and nuclear signals that regulate neural progenitor proliferation.

Compared to microcephaly, polymicrogyria is a more heterogeneous brain malformation that has been suggested to implicate molecular mechanisms involved in pattern formation in the cortex. Many cases of polymicrogyria show an asymmetric distribution, and we demonstrate that these cases are strongly biased towards a right-predominant pattern. Using whole-exome sequencing in patients with polymicrogyria, we identify rare mutations in two primary microcephaly genes, *ASPM* and *WDR62.* Interestingly, some of these patients lack profound microcephaly, suggesting heretofore underappreciated pleiotropic effects of these centrosomal genes.

Table of Contents

Acknowledgements

After going through my own process of scientific writing, when I read manuscripts and dissertations now I am often struck more by what is excluded than what is included. A dissertation is like a bonsai tree -- defined not by ornamentation, but by what was pruned after careful aesthetic consideration. The finished product (one hopes) has the ironic appearance of something natural and minimally transformed, masking the thousands of tiny errors and corrections that went into its making. The bonsai tree itself is only half the story; the pot and its deep roots complete the composition. Similarly, the dissertation is not understood without seeing it in the context of what sustained it (and the author) over the years. The beauty and the promise of the work described over the next one hundred pages were obviously influenced by my effort and choices, but that effect pales in comparison to the role played by the nurturing and supportive environment of the pot I chose some five (or, in some ways, twelve) years ago.

Working in the Walsh Lab has been an amazing collaborative experience during a period of profound personal growth. It is a place filled with people I strive to emulate, doing work I find important and fulfilling, in a style conducive to my personality. Unsurprisingly, this starts from the top. The constraints and conventions of the Acknowledgements section limit a fuller narrative, but suffice to say that Chris Walsh is the consummate mentor. He sets an example by being *the* example, and convincing you (without platitudes) that you can do it too. He is the paragon of a physician-scientist: he would be great at either profession, but plays the combination spectacularly well. His self-deprecation and modesty mask a unique intellect and a remarkable capacity for memory and dynamic recall. Meetings with Chris have a peripatetic feel, because he has the polymathic ability to connect disparate ideas. He'll link Kant's *Critique of*

Pure Reason to thalamocortical circuit design, or cite the epic collapse of the 2011 Red Sox to suggest why we can't discount statistically unlikely linkage evidence. It's very satisfying to watch, because it allays my concern that success in a specialized career comes at the cost of broad, balanced knowledge. Chris is also a role model for a not-insane work-life balance, and shatters the cynical notion that high achievement and real happiness are mutually exclusive.

I could go on. Like the sun, Chris provided not only warmth, but more importantly, the comfort in knowing that even after the darkest of days he will look upon you shiningly tomorrow. His faith in me felt oddly, but truly, unconditional.

Ganesh Mochida, Tim Yu, and Ann Poduri were all collaborators of mine on the major projects that constituted my tenure in the lab. They all have that magical combination of being compassionate clinicians charged with a talent and passion for research that is compelling to witness and impossible not to follow. All of them generously allowed me to find independent space within projects they ostensibly started. In addition, former postdocs Ed Gilmore and Tony Hill were a source of limitless friendship and altruism. Maria Lehtinen and Anthony LaMantia were also great collaborators and friendly beyond collegiality. I am grateful for the community of graduate students, in particular Gilad Evrony, whom I value as my closest and most like-minded friend in the lab, and the one person who I would want with me in the trenches (both for his company and his resourcefulness). Kutay "Deniz" Atabay, though he arrived only within the last year, has made his mark both through his hard and selfless work in assisting me, but also through engaging discussions on science and exploration.

Outside the lab, I have been helped tremendously from many sides of Harvard Medical School. From the guidance of my Dissertation Advisory Committee, consisting of Gabriel

Corfas, Elizabeth Engle, and Yang Shi, to the pragmatic and steady support of my M.D./Ph.D. advisor Chinfei Chen, to the constructive discussions with Rick Born. Karen Harmin, the program administrator, deserves special praise for her assistance at crucial times. David Cardozo can never be appreciated adequately for his empathy and unflinching student advocacy.

The HMS ecosystem also provided many rich collaborations that were essential to my projects, with Katie Kathrein and Leonard Zon facilitating a great collaboration with their zebrafish resources, and Adriana Eisner and Rosalind Segal providing acute expertise with Shh assays.

Most importantly, none of this would be possible without the backstop provided by my parents, the periodic ego-checking and good old fashioned horseplay provided by my brothers, and the insight provided by my sister-in-law, Nisha. My friendships with Athar Malik and Takahiro Soda, fellow M.D./Ph.D. colleagues since the beginning, have forged closer through the tempering process of graduate school. My core college friends Sean Creehan, Pat Donovan, and Chris and Georgia Shutzer, are a part of almost every great adventure and memory I could list over the past five years.

Lastly, this work and my graduate education would not be possible without the direct support of the United States, and its citizens' support for research and medical scientist training.

To the patients and their families,

whose continued participation in this study

provided the ultimate source of motivation,

and a necessary antidote for cynicism.

Chapter 1

Introduction

Introduction

We attribute many of the features that are most quintessentially human to adaptations that occurred in the brain. Grammatical language, technological innovation, and consciousness are all cognitive capacities that are unique to our species, or at the very least are sophisticated upgrades of more primitive capacities seen in primates: basic communication, tool use, and self-awareness. Whether these human adaptations are a direct product of natural selection, or evolutionary "spandrels" that emerged from more proximate selective forces (Gould and Lewontin, 1979), the substrate for these phenotypes resides in the information processing of a very large brain. The human brain consists of nearly ninety billion neurons and an approximately equal number of nonneuronal cells (Azevedo et al., 2010). One-fifth of these neurons are layered in an epithelial sheet known as the cerebral cortex, which is exquisitely folded inside the cranium in convolutions called gyri. The expansion of the size of the cerebral cortex is perhaps the cardinal feature that distinguishes modern humans from our primate ancestors. It is generally assumed that the size of the cerebral cortex is a proxy for the computational power of the brain, because of the apparent modularity of the cortical circuit (Hill and Walsh, 2005). Therefore, an essential scientific inquiry concerning the existential nature of the human brain is to understand the developmental processes and molecular mechanisms necessary for this expansion and folding.

In the 7-8 million years since humans diverged from the last common ancestor with chimpanzees, our brains expanded approximately threefold (Hill and Walsh, 2005). Strikingly, the size of the human brain nearly doubled compared to the early hominids of 2-2.5 million years ago (Carroll, 2003). However these measurements are based on brain mass relative to body mass,

and can be confounded by the large variation in body mass seen in primates and early hominids (Marino, 1998). When compared to a mouse, the relative brain size of a human (reported as the "encephalization quotient") is increased by approximately 15-fold (Fish et al., 2008). Suspiciously clean estimates of 100 billion neurons and one trillion glial cells in the human brain are strewn throughout the literature, though based on scant evidence (Kandel et al., 2000; Noctor et al., 2007). Estimates in neuronal number based on counts from histological sections offer a very wide range of possibilities, anywhere between 75 and 125 billion neurons in the cerebral cortex and cerebellum (Pelvig et al, 2008; Andersen et al., 1992). Moreover, when compared between orders, these estimates do not correct for the fact that human neurons are larger than mouse neurons, and so a larger brain does not automatically infer more neurons (Herculano-Houzel et al., 2007). Recent studies using more precise single-cell counting techniques with molecular markers have revised the estimate of neurons in the adult human brain downward, to roughly ninety billion (Azevedo, 2010). When compared to other primates using the same technique, the human brain is approximately ten percent larger than a linearly scaled-up version of a theoretical 75 kg primate's brain (Azevedo, 2010). While this ten percent increase is significant and may account for the remarkable emergent capacities of the human brain, it nevertheless is a more modest reassessment of recent human brain expansion.

Developmental steps for expanding the mammalian neuroepithelium

The increased size of the human cortex reflects not only an increase in neuronal number, but also added complexity to the basic cortical circuit diagram, most notably an expansion of upper cortical layers (Marin-Padilla, 1992). The basic six-layered neocortex evolved during the

transition from reptiles to mammals, prior to the dramatic increase in cortical surface area (Nieuwenhuys et al., 1999). Although the increased thickness of the upper layers of the human cerebral cortex is apparent, the expansion of the cortex predominantly reflects an increase in surface area (Caviness et al., 1995; Rakic, 1995). This evolutionary expansion in neuronal number is due to an increase in the number of rounds of progenitor cell proliferation. Cortical progenitors undergo eleven rounds of cell division in mice, approximately thirty in rhesus macaque, and more rounds in humans (Takahashi et al., 1999; Kornack and Rakic, 1998). Neuronal number and the direction of cortical expansion (lateral vs. radial) are determined not only by the number of progenitor cell divisions, but also the *mode* of division -- either symmetric or asymmetric. Symmetric divisions give rise to two identical cells equipotent in their self-renewal capacity, whereas asymmetric divisions yield one stem cell and one daughter cell with a more restricted cell fate potential (Morrison et al., 2006).

In the developing neuroepithelium of invertebrates, earlier evidence suggested that the fate of daughter cells of neural progenitors is exquisitely sensitive to the orientation of the mitotic spindle. At the onset of neurogenesis, apical neural progenitors divide symmetrically (Rakic, 1988). In these divisions, the mitotic spindle is oriented parallel to the neuroepithelium, resulting in an exponential expansion of the neural progenitor pool (Chenn and McConnell, 1995). Following the proliferative phase, the neural progenitors enter an asymmetric phase. In these divisions, the mitotic spindle rotates vertically until it is perpendicular to the plane of the neuroepithelium, yielding one neuron and one renewed neural progenitor (Chenn and McConnell, 1995; Haydar et al., 2003). The postmitotic neuron then migrates along a radial glial apical-basal process until it reaches its specified destination in the cortex, while the neural

progenitor remains at the apical surface to continue dividing (Noctor et al., 2004). Consistent with the finding that cleavage plane orientation affects daughter cell fate, several proteins are found to be asymmetrically inherited during neurogenic divisions -- including Notch (Chenn and McConnell, 1995), Numb (Cayouette et al., 2001), and Minibrain (Hammerle et al., 2002). Even the apical plasma membrane, and its transmembrane protein constituents (such as members of the Par family), are apparently asymmetrically distributed between the two daughter cells during vertical cleavage plane divisions (Kosodo et al., 2004). Hence, a putative mechanism appears to exist whereby asymmetric inheritance of neural progenitor cell components -- as a result of vertical orientation of the mitotic spindle -- confers different fates to the daughter cells.

However, there is some controversy whether mitotic spindle orientation determines whether progenitors in the VZ undergo symmetric or asymmetric cell divisions in mammals. Through time-lapse imaging of rat neocortical precursor cells, cleavage plane orientation was not necessarily associated with daughter cell fate, as previously thought (Noctor et al., 2008). Radial glial cells divided either symmetrically or asymmetrically depending on the stage of neurogenesis, despite generally dividing with 'vertical' cleavage planes oriented perpendicular to the ventricular surface (Noctor et al., 2008).

There are other paradigms besides spindle orientation that could underlie asymmetry of progenitor cell divisions. The 'mother centriole hypothesis' postulates that asymmetric inheritance of centrosomes in dividing radial glial progenitors determines which of two daughter cells will remain a progenitor and which will eventually differentiate into a neuron (Wang et al., 2009). In this model, the daughter cell that inherits the older mother centriole remains in the progenitor pool while the other daughter cell differentiates into a neuron.

Two classes of neural progenitor cells can be distinguished based on their location during mitosis: apical and basal progenitors. Apical progenitors (APs) are located in a pseudostratified layer bordering the lateral ventricle, known as the ventricular zone (VZ). APs share the characteristics seen in all epithelial cells: apical junctional complexes, and apicobasal bipolar morphology (the presence of apical and basal processes) (Fishell and Kreigstein, 2003; Huttner and Kosodo, 2005). In APs, the apical process contacts the ventricle directly, often presenting a primary cilium (Alvarez-Buylla et al., 1998; Gerdes et al., 2008). APs also migrate in a dynamic pattern called "interkinetic nuclear migration", in which the nucleus moves perpendicular to apical plane in synchrony with the cell cycle, migrating apically during the G2 phase of the cell cycle and undergoing mitosis only when the nucleus is at the apical surface (Messier, 1978; Takahashi et al., 1993). This continuous process during early neural development is what gives the VZ its pseudostratified appearance.

Basal progenitors (BPs) constitute the second class of neural progenitors in mammals, and are also known as "intermediate" or "subventricular zone" (SVZ) progenitors for their location in relation to the VZ (Kriegstein et al., 2006; Noctor et al., 2004). BPs arise from a slightly asymmetric apical divisions, migrate basally and retract their apical process before mitosis (Liu et al., 2008). BPs are found almost exclusively in the telencephalon and are only rarely observed in the hindbrain or spinal cord (Haubensak et al., 2004). In the telencephalon, BPs are generated from the onset of neurogenesis and increase in number as neurogenesis proceeds, eventually accumulating to form a secondary germinal layer, the SVZ. BPs have a round, non-polar morphology, and mostly divide symmetrically in one terminal division to form

two post-mitotic neurons (Haubensak et al., 2004; Miyata et al., 2004; Noctor et al., 2004; Attardo et al., 2008; Noctor et al., 2008).

Multiple subclasses of apical and basal progenitors have been identified and classified based on a combination of molecular markers, however a detailed description of these subtypes is outside the scope of this thesis. Briefly, one class of basal progenitors -- outer radial glia (oRG) -- have been identified predominantly in the primate brain, and characterized by an RG-like morphology but laking an apical process (Hansen et al., 2010). oRG do not express apically localized membrane proteins such as CD133, Par3, or aPKCl (Fietz et al., 2010), and divide asymmetrically in a horizontal cleavage plane to produce an oRG that retains the basal fiber, and a daughter cell that lacks a pial contact (Hansen et al., 2010). These daughter cells and oRGs form the outer subventricular zone (OSVZ), a region that arises late in primate neurogenesis but expands rapidly to become the dominant germinal layer in the neocortex (Lui et al., 2011). Whereas in rodents asymmetric divisions of the ventricular RG produce almost all of the neurons of the adult brain, in primates (including humans) the outer RG and OSVZ transit-amplifying cells are responsible for the dramatic expansion of brain size (Lui et al., 2011).

An intriguing correlation across different animals is that the presence of a sizeable OSVZ germinal layer correlates with having a gyrencephalic brain. Gyri are the intricate and reproducible folds of the neuroepithelium that maximizes the amount of cortical surface area that can be packed into a fixed volume. Gyri are not limited to primates; indeed, the feature appears in multiple different clades, including monotremes, marsupials, and placentals (Kriegstein, et al., 2006). While this suggests that the gyrencephalic cortex arose independently in multiple lineages, there might have been similar underlying mechanisms in each instance. An increase in

the number of RG, or an increase in the number of symmetric divisions, could expand the progenitor pool and pack more neuroepithelium into a limited cranial space. When mouse neuroepithelial cells were engineered to express a constitutively active form of β-catenin (a positive regulator of neural stem cell proliferation via the WNT signaling pathway), more neural progenitors were generated, as expected, and remarkably the mice developed an increased cortical surface area that displayed folds suggestive of gyri (Chenn and Walsh, 2002). The surface area of the lateral ventricles was also increased, consistent with the hypothesis that expansion of the VZ progenitors through lateral divisions increased both the neuronal number and ventricular surface area. By contrast, it has been suggested that expansion of the basal germinal layer, such as oRGs and OSVZ transit-amplifying cells, would allow for gyrification without expansion of lateral ventricle neuroependyma (Lui et al., 2011).

Proper sizing of the cortex is highly sensitive to precise control of the quantity and type of neural progenitor proliferation. The timing of the switch from symmetric to asymmetric divisions during neurogenesis is critical to ensure appropriate expansion of the neural progenitor pool. One way of quantifying this transition is by measuring cell cycle exit fraction, or the ratio of cells exiting the cell cycle, to cells remaining in the progenitor pool (Q/P ratio), at each progenitor cell division (Takahashi et al., 1996). Manipulating cell cycle exit fraction to delay this switch, by stably overexpressing β-catenin in neural progenitors, has been shown to lead to an expanded cerebral cortex (Chenn and Walsh, 2002). On the other hand, prematurely switching from symmetric to asymmetric divisions, such that the cell cycle exit fraction is higher at earlier

stages of neurogenesis, depletes the progenitor pool, leading ultimately to a smaller cortex (Chae and Walsh, 2007; Feng and Walsh, 2004).

Inherited or acquired mutations that disrupt the molecular processes critical for neural progenitor proliferation often manifest as profound brain malformations. Detailed clinical, pathological, and radiographic interrogation of these brain malformations allows for specific mechanistic hypotheses into role of the specific genes identified by the genetic mapping. Many of these disorders fall under the broad classification of "microcephaly".

Microcephaly

Microcephaly, Greek for "small head", is clinically defined as a head circumference less than two standard deviations below the mean for the person's age and gender (Mochida and Walsh, 2004). It is a genetically heterogeneous disorder, with each individual genetic cause being relatively rare, but collectively affecting approximately one percent of all Americans (Mochida and Walsh, 2001). The condition is subclassified into primary microcephaly, which presents at birth, and secondary microcephaly, which develops postnatally (Woods, 2004). This clinical distinction translates to a functional difference -- primary microcephaly is typically a developmental defect, while secondary microcephaly is typically neurodegenerative or due to some other progressive process (Dobyns, 2002). In autosomal recessive primary microcephaly (MCPH), the brain is small but architecturally normal, which implies a decrease in neural progenitor cell number (Woods, et al. 2005). At least seven genes have been identified as causes of primary autosomal recessive microcephaly (MCPH): *MICROCEPHALIN*, *WDR62*, *CDK5RAP2*, *CEP152*, *ASPM*, *CENPJ* and *STIL* (Bilguvar et al., 2010; Bond et al., 2002; Bond

et al., 2005; Guernsey et al., 2010; Jackson et al., 2002; Kumar et al., 2009). In all seven genes, microcephaly is the loss-of-function (or null) phenotype. All of these genes are expressed in the VZ of the embryonic mouse brain, and peak in expression during the period of neurogenesis (Bond and Woods, 2006). Furthermore, these genes implicate the critical role of mitotic spindle orientation and cell cycle timing in proper maintenance of the neural progenitor pool.

Cdk5rap2 and *Nde1* mutant mice are models of microcephaly. *Nde1* homozygous mutant mice, which are profoundly microcephalic, show defects in spindle orientation within progenitors. They also show an increased cell cycle exit fraction between E14.5 and E15.5, leading to a cell-fate change with generation of fewer superficial-layer neurons and more deep-layer neurons. A slight increase in apoptosis is observed (Feng and Walsh, 2004). Likewise, *Cdk5rap2* homozygous mutant mice show defects in spindle orientation within VZ progenitors, as well as premature cell cycle exit and resulting depletion of superficial-layer neurons. Unlike the *Nde1* mutant mice, the *Cdk5rap2* mutant mice show only a modest increase in deep-layer neurons and a significant increase in apoptosis (Lizarraga et al., 2010). While both studies show a correlation between spindle orientation defects and changes in cell cycle exit fraction, neither demonstrates a causal relationship between the two.

ASPM has also been implicated in regulating mitotic spindle orientation. Loss-of-function of *Asp*, the Drosophila homolog of *ASPM*, led to disorganization of gamma-tubulin ring complexes and disruption of microtubule organizing center (MTOC) activity (do Carmo Avides and Glover, 1999; Wakefield et al., 2001). Spindle orientation defects were observed with *ASPM* RNAi in cultured human U2OS osteosarcoma cells (Higgins et al., 2010). A mouse *Aspm* RNAi study using *in utero* electroporation also suggested spindle orientation defects (Fish et al., 2006).

However, analysis of *Aspm* homozygous mutant mice revealed no changes in spindle orientation or the ratio of symmetric to asymmetric cell divisions in the neuroepithelium (Pulvers et al., 2010).

Alternatively, *ASPM* may affect proliferation by acting on the Wnt signaling pathway rather than spindle orientation. Wnt signaling promotes neural progenitor proliferation (Chenn and Walsh, 2002), and a genome-wide siRNA screen identified *ASPM* as a positive regulator of Wnt signaling (Major et al., 2008). *In vivo* RNAi of *Aspm* in the developing mouse cortex causes proliferation defects, which are rescued by co-expression of stabilized β-catenin (Buchman et al., 2011). These findings suggest that the Wnt pathway may mediate defects in neurogenesis associated with *ASPM* loss-of-function, with possible implications for other MCPH genes.

Mitotic spindle orientation is not the only paradigm to explain microcephaly. In addition to the seven MCPH genes, two genes have been identified for other autosomal recessive disorders in which microcephaly is a predominant feature among other distinguishing radiological abnormalities. Both of these genes -- *COH1* and *ARFGEF2* -- implicate the role of vesicle-mediated intracellular protein transport in neural progenitor proliferation (Kolehmainen et al., 2003; Sheen et al., 2004), though the detailed mechanisms are not understood. It is interesting to note that *CHMP1A*, a new gene we have discovered for a subtype of microcephaly, appears to have roles in both neural progenitor proliferation and endosomal vesicle transport.

References

Alvarez-Buylla, A., García-Verdugo, J. M., Mateo, A. S., & Merchant-Larios, H. (1998). Primary neural precursors and intermitotic nuclear migration in the ventricular zone of adult canaries. The Journal of neuroscience : the official journal of the Society for Neuroscience, 18(3), 1020–1037.

Andersen, B. B., Korbo, L., & Pakkenberg, B. (1992). A quantitative study of the human cerebellum with unbiased stereological techniques. The Journal of Comparative Neurology, 326(4), 549–560. doi:10.1002/cne.903260405

Attardo, A., Calegari, F., Haubensak, W., Wilsch-Bräuninger, M., & Huttner, W. B. (2008). Live imaging at the onset of cortical neurogenesis reveals differential appearance of the neuronal phenotype in apical versus basal progenitor progeny. PLoS ONE, 3(6), e2388. doi:10.1371/journal.pone.0002388

Azevedo, F. A. C., Carvalho, L. R. B., Grinberg, L. T., Farfel, J. M., Ferretti, R. E. L., Leite, R. E. P., Filho, W. J., et al. (2009). Equal numbers of neuronal and nonneuronal cells make the human brain an isometrically scaled-up primate brain. The Journal of Comparative Neurology, 513(5), 532–541. doi:10.1002/cne.21974

Bilgüvar, K., Oztürk, A. K., Louvi, A., Kwan, K. Y., Choi, M., Tatli, B., Yalnizoğlu, D., et al. (2010). Whole-exome sequencing identifies recessive WDR62 mutations in severe brain malformations. Nature, 467(7312), 207–210. doi:10.1038/nature09327

Bond, J., & Woods, C. G. (2006). Cytoskeletal genes regulating brain size. Current opinion in cell biology, 18(1), 95–101. doi:10.1016/j.ceb.2005.11.004

Bond, J., Roberts, E., Mochida, G. H., Hampshire, D. J., Scott, S., Askham, J. M., Springell, K., et al. (2002). ASPM is a major determinant of cerebral cortical size. Nature genetics, 32(2), 316–320. doi:10.1038/ng995

Buchman, J. J., Durak, O., & Tsai, L.-H. (2011). ASPM regulates Wnt signaling pathway activity in the developing brain. Genes & development, 25(18), 1909–1914. doi:10.1101/gad.16830211

Carroll, S. B. (2003). Genetics and the making of Homo sapiens. Nature, 422(6934), 849–857. doi:10.1038/nature01495

Caviness, V. S., Takahashi, T., & Nowakowski, R. S. (1995). Numbers, time and neocortical neuronogenesis: a general developmental and evolutionary model. Trends in neurosciences, 18(9), 379–383.

Cayouette, M., Whitmore, A. V., Jeffery, G., & Raff, M. (2001). Asymmetric segregation of Numb in retinal development and the influence of the pigmented epithelium. The Journal of neuroscience : the official journal of the Society for Neuroscience, 21(15), 5643–5651.

Chae, T. H., & Walsh, C. A. (2007). Genes that control the size of the cerebral cortex. Novartis Foundation symposium, 288, 79–90– discussion 91–8.

Chenn, A., & McConnell, S. K. (1995). Cleavage orientation and the asymmetric inheritance of Notch1 immunoreactivity in mammalian neurogenesis. Cell, 82(4), 631–641.

Chenn, A., & Walsh, C. A. (2002). Regulation of cerebral cortical size by control of cell cycle exit in neural precursors. Science (New York, NY), 297(5580), 365–369. doi:10.1126/science.1074192

do Carmo Avides, M., & Glover, D. M. (1999). Abnormal spindle protein, Asp, and the integrity of mitotic centrosomal microtubule organizing centers. Science (New York, NY), 283(5408), 1733–1735.Wakefield, J. G., Bonaccorsi, S., & Gatti, M. (2001). The drosophila protein asp is involved in microtubule organization during spindle formation and cytokinesis. The Journal of cell biology, 153(4), 637–648.

Dobyns, W. B. (2002). Primary microcephaly: new approaches for an old disorder. American journal of medical genetics, 112(4), 315–317. doi:10.1002/ajmg.10580

Feng, Y., & Walsh, C. A. (2004). Mitotic spindle regulation by Nde1 controls cerebral cortical size. Neuron, 44(2), 279–293. doi:10.1016/j.neuron.2004.09.023

Fietz, S. A., Kelava, I., Vogt, J., Wilsch-Bräuninger, M., Stenzel, D., Fish, J. L., Corbeil, D., et al. (2010). OSVZ progenitors of human and ferret neocortex are epithelial-like and expand by integrin signaling. Nature neuroscience, 13(6), 690–699. doi:10.1038/nn.2553

Fish, J. L., Dehay, C., Kennedy, H., & Huttner, W. B. (2008). Making bigger brains-the evolution of neural-progenitor-cell division. Journal of cell science, 121(17), 2783–2793. doi:10.1242/jcs.023465

Fish, J. L., Kosodo, Y., Enard, W., Pääbo, S., & Huttner, W. B. (2006). Aspm specifically maintains symmetric proliferative divisions of neuroepithelial cells. Proceedings of the National Academy of Sciences of the United States of America, 103(27), 10438–10443. doi:10.1073/pnas.0604066103

Fishell, G., & Kriegstein, A. R. (2003). Neurons from radial glia: the consequences of asymmetric inheritance. Current opinion in neurobiology, 13(1), 34–41.

Gerdes, J. M., & Katsanis, N. (2008). Ciliary function and Wnt signal modulation. Current topics in developmental biology, 85, 175–195. doi:10.1016/S0070-2153(08)00807-7

Gould, S. J., & Lewontin, R. C. (1979). The spandrels of San Marco and the Panglossian paradigm: a critique of the adaptationist programme. Proc R Soc Lond, B, Biol Sci, 205(1161), 581–598.

Guernsey, D. L., Jiang, H., Hussin, J., Arnold, M., Bouyakdan, K., Perry, S., Babineau-Sturk, T., et al. (2010). Mutations in centrosomal protein CEP152 in primary microcephaly families linked to MCPH4. American journal of human genetics, 87(1), 40–51. doi:10.1016/j.ajhg.2010.06.003

Hämmerle, B., Vera-Samper, E., Speicher, S., Arencibia, R., Martínez, S., & Tejedor, F. J. (2002). Mnb/Dyrk1A is transiently expressed and asymmetrically segregated in neural progenitor cells at the transition to neurogenic divisions. Developmental biology, 246(2), 259–273. doi:10.1006/dbio.2002.0675

Hansen, D. V., Lui, J. H., Parker, P. R. L., & Kriegstein, A. R. (2010). Neurogenic radial glia in the outer subventricular zone of human neocortex. Nature, 464(7288), 554–561. doi:10.1038/nature08845

Haubensak, W., Attardo, A., Denk, W., & Huttner, W. B. (2004). Neurons arise in the basal neuroepithelium of the early mammalian telencephalon: a major site of neurogenesis. Proceedings of the National Academy of Sciences of the United States of America, 101(9), 3196–3201. doi:10.1073/pnas.0308600100

Haydar, T. F., Ang, E., & Rakic, P. (2003). Mitotic spindle rotation and mode of cell division in the developing telencephalon. Proceedings of the National Academy of Sciences of the United States of America, 100(5), 2890–2895. doi:10.1073/pnas.0437969100

Herculano-Houzel, S., Collins, C. E., Wong, P., & Kaas, J. H. (2007). Cellular scaling rules for primate brains. Proceedings of the National Academy of Sciences of the United States of America, 104(9), 3562–3567. doi:10.1073/pnas.0611396104

Higgins, J., Midgley, C., Bergh, A.-M., Bell, S. M., Askham, J. M., Roberts, E., Binns, R. K., et al. (2010). Human ASPM participates in spindle organisation, spindle orientation and cytokinesis. BMC cell biology, 11, 85. doi:10.1186/1471-2121-11-85

Hill, R. S., & Walsh, C. A. (2005). Molecular insights into human brain evolution. Nature, 437(7055), 64–67. doi:10.1038/nature04103

Huttner, W. B., & Kosodo, Y. (2005). Symmetric versus asymmetric cell division during neurogenesis in the developing vertebrate central nervous system. Current opinion in cell biology, 17(6), 648–657. doi:10.1016/j.ceb.2005.10.005

Jackson, A. P., Eastwood, H., Bell, S. M., Adu, J., Toomes, C., Carr, I. M., Roberts, E., et al. (2002). Identification of microcephalin, a protein implicated in determining the size of the human brain. American journal of human genetics, 71(1), 136–142. doi:10.1086/341283

Kandel, E. R., & Squire, L. R. (2000). Neuroscience: breaking down scientific barriers to the study of brain and mind. Science (New York, NY), 290(5494), 1113–1120.

Kolehmainen, J., Black, G. C. M., Saarinen, A., Chandler, K., Clayton-Smith, J., Träskelin, A.-L., Perveen, R., et al. (2003). Cohen syndrome is caused by mutations in a novel gene, COH1, encoding a transmembrane protein with a presumed role in vesicle-mediated sorting and intracellular protein transport. American journal of human genetics, 72(6), 1359–1369.

Kornack, D. R., & Rakic, P. (1998). Changes in cell-cycle kinetics during the development and evolution of primate neocortex. Proceedings of the National Academy of Sciences of the United States of America, 95(3), 1242–1246.

Kosodo, Y., Röper, K., Haubensak, W., Marzesco, A.-M., Corbeil, D., & Huttner, W. B. (2004). Asymmetric distribution of the apical plasma membrane during neurogenic divisions of mammalian neuroepithelial cells. The EMBO journal, 23(11), 2314–2324. doi:10.1038/sj.emboj.7600223

Kriegstein, A., Noctor, S., & Martínez-Cerdeño, V. (2006). Patterns of neural stem and progenitor cell division may underlie evolutionary cortical expansion. Nature reviews Neuroscience, 7(11), 883–890. doi:10.1038/nrn2008

Kumar, A., Girimaji, S. C., Duvvari, M. R., & Blanton, S. H. (2009). Mutations in STIL, encoding a pericentriolar and centrosomal protein, cause primary microcephaly. American journal of human genetics, 84(2), 286–290. doi:10.1016/j.ajhg.2009.01.017

Liu, H.-K., Belz, T., Bock, D., Takacs, A., Wu, H., Lichter, P., Chai, M., et al. (2008). The nuclear receptor tailless is required for neurogenesis in the adult subventricular zone. Genes & development, 22(18), 2473–2478. doi:10.1101/gad.479308

Lizarraga, S. B., Margossian, S. P., Harris, M. H., Campagna, D. R., Han, A.-P., Blevins, S., Mudbhary, R., et al. (2010). Cdk5rap2 regulates centrosome function and chromosome segregation in neuronal progenitors. Development (Cambridge, England), 137(11), 1907–1917. doi:10.1242/dev.040410

Lui, J. H., Hansen, D. V., & Kriegstein, A. R. (2011). Development and evolution of the human neocortex. Cell, 146(1), 18–36. doi:10.1016/j.cell.2011.06.030

Major, M. B., Roberts, B. S., Berndt, J. D., Marine, S., Anastas, J., Chung, N., Ferrer, M., et al. (2008). New regulators of Wnt/beta-catenin signaling revealed by integrative molecular screening. Science signaling, 1(45), ra12. doi:10.1126/scisignal.2000037

Marín-Padilla, M. (1992). Ontogenesis of the pyramidal cell of the mammalian neocortex and developmental cytoarchitectonics: a unifying theory. The Journal of Comparative Neurology, 321(2), 223–240. doi:10.1002/cne.903210205

Marino, L. (1998). A comparison of encephalization between odontocete cetaceans and anthropoid primates. Brain Behav Evol, 51(4), 230–238.

Messier, P. E. (1978). Microtubules, interkinetic nuclear migration and neurulation. Experientia, 34(3), 289–296.

Miyata, T., Kawaguchi, A., Saito, K., Kawano, M., Muto, T., & Ogawa, M. (2004). Asymmetric production of surface-dividing and non-surface-dividing cortical progenitor cells. Development (Cambridge, England), 131(13), 3133–3145. doi:10.1242/dev.01173

Mochida, G. H., & Walsh, C. A. (2001). Molecular genetics of human microcephaly. Current opinion in neurology, 14(2), 151–156.

Mochida, G. H., & Walsh, C. A. (2004). Genetic basis of developmental malformations of the cerebral cortex. Archives of neurology, 61(5), 637–640. doi:10.1001/archneur.61.5.637

Morrison, S. J., & Kimble, J. (2006). Asymmetric and symmetric stem-cell divisions in development and cancer. Nature, 441(7097), 1068–1074. doi:10.1038/nature04956

Nieuwenhuys, R. (1999). The morphological pattern of the vertebrate brain. European journal of morphology, 37(2-3), 81–84.

Noctor, S. C., Martínez-Cerdeño, V., & Kriegstein, A. R. (2007). Contribution of intermediate progenitor cells to cortical histogenesis. Archives of neurology, 64(5), 639–642. doi:10.1001/archneur.64.5.639

Noctor, S. C., Martínez-Cerdeño, V., & Kriegstein, A. R. (2008). Distinct behaviors of neural stem and progenitor cells underlie cortical neurogenesis. The Journal of Comparative Neurology, 508(1), 28–44. doi:10.1002/cne.21669

Noctor, S. C., Martínez-Cerdeño, V., Ivic, L., & Kriegstein, A. R. (2004). Cortical neurons arise in symmetric and asymmetric division zones and migrate through specific phases. Nature neuroscience, 7(2), 136–144. doi:10.1038/nn1172

Pelvig, D. P., Pakkenberg, H., Stark, A. K., & Pakkenberg, B. (2008). Neocortical glial cell numbers in human brains. Neurobiology of aging, 29(11), 1754–1762. doi:10.1016/j.neurobiolaging.2007.04.013

Pulvers, J. N., Bryk, J., Fish, J. L., Wilsch-Bräuninger, M., Arai, Y., Schreier, D., Naumann, R., et al. (2010). Mutations in mouse Aspm (abnormal spindle-like microcephaly associated) cause not only microcephaly but also major defects in the germline. Proceedings of the National Academy of Sciences of the United States of America, 107(38), 16595–16600. doi:10.1073/pnas.1010494107

Rakic, P. (1988). Specification of cerebral cortical areas. Science (New York, NY), 241(4862), 170–176.

Rakic, P. (1995). A small step for the cell, a giant leap for mankind: a hypothesis of neocortical expansion during evolution. Trends in neurosciences, 18(9), 383–388.

Sheen, V. L., Ganesh, V. S., Topcu, M., Sebire, G., Bodell, A., Hill, R. S., Grant, P. E., et al. (2004). Mutations in ARFGEF2 implicate vesicle trafficking in neural progenitor proliferation and migration in the human cerebral cortex. Nature genetics, 36(1), 69–76. doi:10.1038/ng1276

Takahashi, T., Goto, T., Miyama, S., Nowakowski, R. S., & Caviness, V. S. (1999). Sequence of neuron origin and neocortical laminar fate: relation to cell cycle of origin in the developing murine cerebral wall. The Journal of neuroscience : the official journal of the Society for Neuroscience, 19(23), 10357–10371.

Takahashi, T., Nowakowski, R. S., & Caviness, V. S. (1993). Cell cycle parameters and patterns of nuclear movement in the neocortical proliferative zone of the fetal mouse. The Journal of neuroscience : the official journal of the Society for Neuroscience, 13(2), 820–833.

Takahashi, T., Nowakowski, R. S., & Caviness, V. S. (1996). The leaving or Q fraction of the murine cerebral proliferative epithelium: a general model of neocortical neuronogenesis. The

Journal of neuroscience : the official journal of the Society for Neuroscience, 16(19), 6183–6196.

Wakefield, J. G., Bonaccorsi, S., & Gatti, M. (2001). The drosophila protein asp is involved in microtubule organization during spindle formation and cytokinesis. The Journal of cell biology, 153(4), 637–648.

Wang, X., Tsai, J.-W., Imai, J. H., Lian, W.-N., Vallee, R. B., & Shi, S.-H. (2009). Asymmetric centrosome inheritance maintains neural progenitors in the neocortex. Nature, 461(7266), 947–955. doi:10.1038/nature08435

Woods, C. G. (2004). Human microcephaly. Current opinion in neurobiology, 14(1), 112–117. doi:10.1016/j.conb.2004.01.003

Woods, C. G., Bond, J., & Enard, W. (2005). Autosomal recessive primary microcephaly (MCPH): a review of clinical, molecular, and evolutionary findings. American journal of human genetics, 76(5), 717–728. doi:10.1086/429930

Chapter 2:

CHMP1A encodes an essential regulator of BMI1-INK4A in cerebellar development

Adapted from a manuscript in review:

***CHMP1A* encodes an essential regulator of BMI1-INK4A in cerebellar development**

Vijay S. Ganesh[1,4*], Ganeshwaran H. Mochida[1,2,3*], Maria I. de Michelena[5], Hugo Dias[6], Kutay D. Atabay[1], Katie L. Kathrein[7], Emily Huang[7], R. Sean Hill[1], Jillian M. Felie[1], Daniel Rakiec[1], Danielle Gleason[1], Anthony D. Hill[8], Athar N. Malik[4], Brenda J. Barry[1], Jennifer N. Partlow[1], Wen-Hann Tan[1], Laurie J. Glader[9], A. James Barkovich[10], William B. Dobyns[11], Leonard I. Zon[7], Christopher A. Walsh[1,2]

1 Division of Genetics, Manton Center for Orphan Disease Research and Howard Hughes Medical Institute, Department of Medicine, Children's Hospital Boston, Boston, MA, USA
2 Departments of Pediatrics and Neurology, Harvard Medical School, Boston, MA, USA
3 Pediatric Neurology Unit, Department of Neurology, Massachusetts General Hospital, Boston, MA, USA
4 Harvard-MIT Division of Health Sciences and Technology, Cambridge, MA, USA
5 Department of Morphologic Sciences, Cayetano Heredia University, Lima, Perú
6 Institute for Child Development, ARIE, Lima, Perú
7 Stem Cell Program and Division of Hematology/Oncology, Children's Hospital Boston and Dana-Farber Cancer Institute, Howard Hughes Medical Institute, Harvard Medical School, Boston, MA, USA
8 Department of Neurology, Children's Hospital Boston, Boston, MA USA
9 Complex Care Outpatient Program, Division of General Pediatrics, Children's Hospital Boston, Boston, MA, USA
10 Department of Radiology and Biomedical Imaging, University of California, San Francisco, San Francisco, CA, USA
11 Center for Integrative Brain Research, University of Washington, Seattle, WA, USA
* These authors contributed equally to the work.

Author Contributions

G.H.M. designed the study, interpreted clinical information and brain MRI, identified the disease locus, helped sequence candidate genes, analyzed the sequencing data to identify *CHMP1A* mutations, helped analyze the functional data, and wrote the manuscript. V.S.G. performed RT-PCR, western blot, mouse histology and immunohistochemistry, quantitative PCR, chromatin immunoprecipitations, zebrafish morpholino experiments, and wrote the manuscript. M.I.M. and H.D. ascertained Family 1 and provided clinical information. K.D.A. performed immunohistochemistry. K.L.K. performed the morpholino injections. E.H. and L.Z. assisted with the morpholino experiments. R.S.H. helped organize genetic data and calculate LOD scores. J.M.F. and D.G. organized patient samples and helped perform sequencing experiments. D.R. organized patient samples and helped perform microsatellite analysis. A.D.H. assisted immunohistochemical studies and imaging. A.N.M. assisted with the chromatin immunoprecipitations. B.J.B. and J.N.P. organized clinical information and patient samples. W.H.T. and L.J.G. provided clinical information of Family 3. A.J.B. interpreted brain MRI of the patients. W.B.D. ascertained Family 2 and provided clinical information. C.A.W. directed the overall research and wrote the manuscript.

Introduction

Charged multivesicular body protein 1A/Chromatin modifying protein 1A (CHMP1A) is a member of the ESCRT-III (endosomal sorting complex required for transport-III) complex (Howard et al., 2001; Tsang et al., 2006), but is also suggested to localize to the nuclear matrix and regulate chromatin structure (Stauffer et al., 2001). Here we show that loss-of-function mutations to human *CHMP1A* cause reduced cerebellar size (pontocerebellar hypoplasia) and reduced cerebral cortical size (microcephaly). *CHMP1A* mutant cells show impaired proliferation, with increased expression of *INK4A*, a negative regulator of stem cell proliferation, and a loss of enrichment of *INK4A* promoter DNA in chromatin immunoprecipitations performed against BMI1, indicating a loss of the normal repression of *INK4A* by BMI1. Defects in zebrafish brain produced by morpholino-based knockdown of the zebrafish *CHMP1A* orthologue resembled those seen after *bmi1* knockdown, and were partially rescued by *INK4A* orthologue knockdown, further supporting links between CHMP1A and BMI1-mediated regulation of *INK4A*. Chmp1a is expressed in dividing cells in the developing cerebral cortex and cerebellar external germinal layer, suggesting that CHMP1A serves as a critical link between cytoplasmic signals and BMI1-mediated chromatin modifications that regulate proliferation of CNS progenitor cells.

As part of ongoing studies of human disorders of neural progenitor proliferation, we identified three families characterized by underdevelopment of the cerebellum, pons, and cerebral cortex. In a consanguineous pedigree of Peruvian origin, three children in two branches were affected (**Figure 2.1a, b, e**; Family 1). Two additional pedigrees from Puerto Rico showed

similar pontocerebellar hypoplasia and microcephaly (**Figure 2.1c, d, e**; Family 2 and 3). Brain MRI of affected individuals from all families show severe reduction of the cerebellar vermis and hemispheres. Strikingly, the cerebellar folds ("folia") are relatively preserved despite the extremely small cerebellar size (**Figure 2.1a-d, Figure 2.2, Figure 2.3**). All affected individuals had severe pontocerebellar hypoplasia, though affected individuals in Family 1 showed better motor and cognitive function than those in Family 2 and 3 (See **Supplementary Note 1**, at end of chapter).

Figure 2.1

Brain MRI and linkage mapping of pontocerebellar hypoplasia with microcephaly.

(a-d) T1-weighted sagittal brain MRI images of an age-matched, neurologically normal individual (a) and affected individuals CH3102 (b), CH2402 (c), and CH2701 (d) are shown. Compared to control, affected individuals show mild reduction in cortical volume, thinning of the corpus callosum, and severe hypoplasia of the pons, vermis, and cerebellar hemispheres. (e) Family 1 is a consanguineous pedigree from Peru in which three children from two branches are affected. Family 2 and 3 are both from Puerto Rico. Below each child in Family 1 and 2 is their Affymetrix 250K Sty SNP data (red and blue = homozygous SNP call; yellow = heterozygous SNP call), showing a region of homozygosity shared by all affected individuals in distal chromosome 16q. The graph aligned with the SNP genotyping data shows multipoint LOD scores calculated from microsatellite maker analysis of Family 1. Genes in the region of LOD > 3 are indicated on the right of the graph.

Figure 2.1 (Continued)

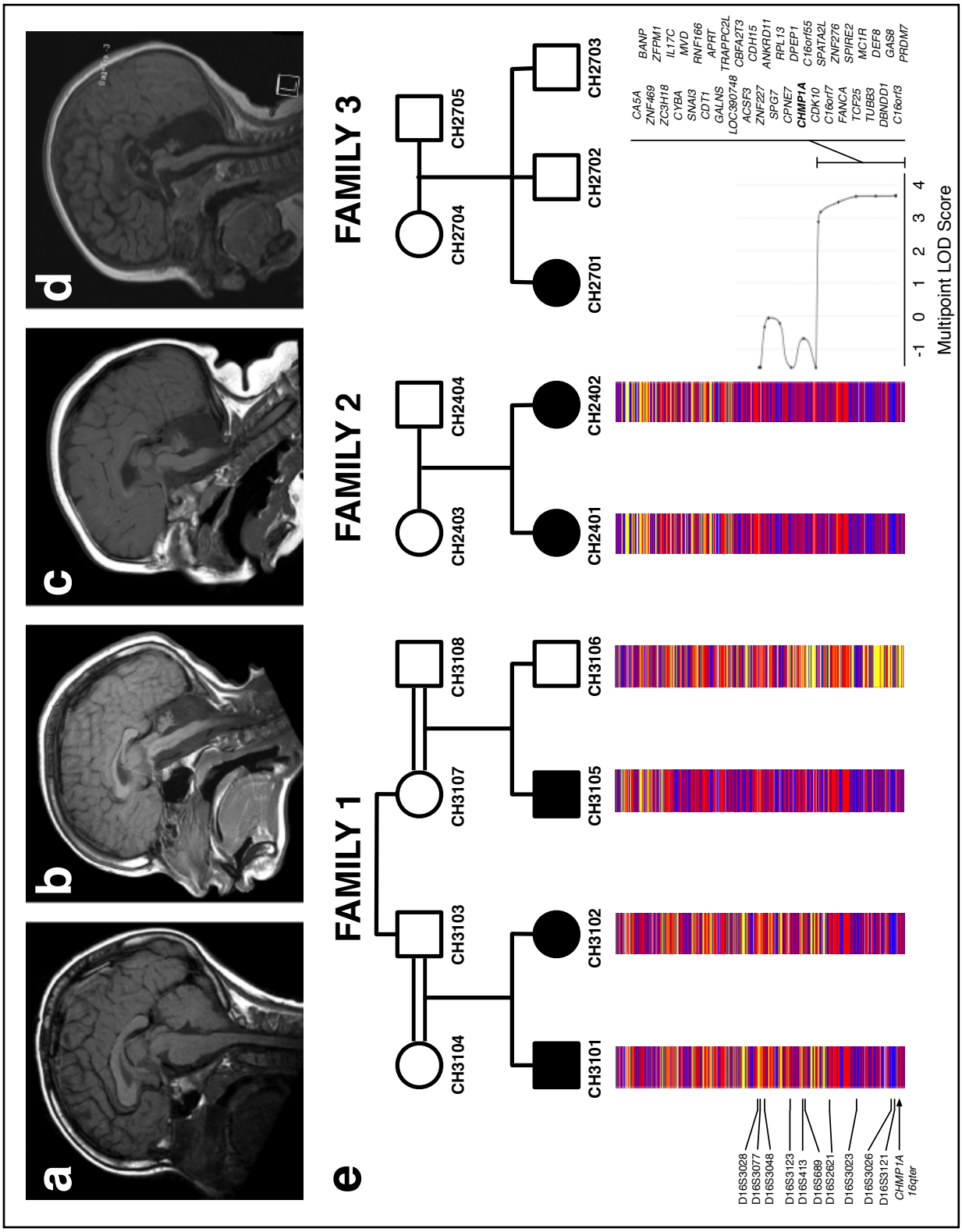

Figure 2.2

T1-weighted sagittal MRI from CH2402.

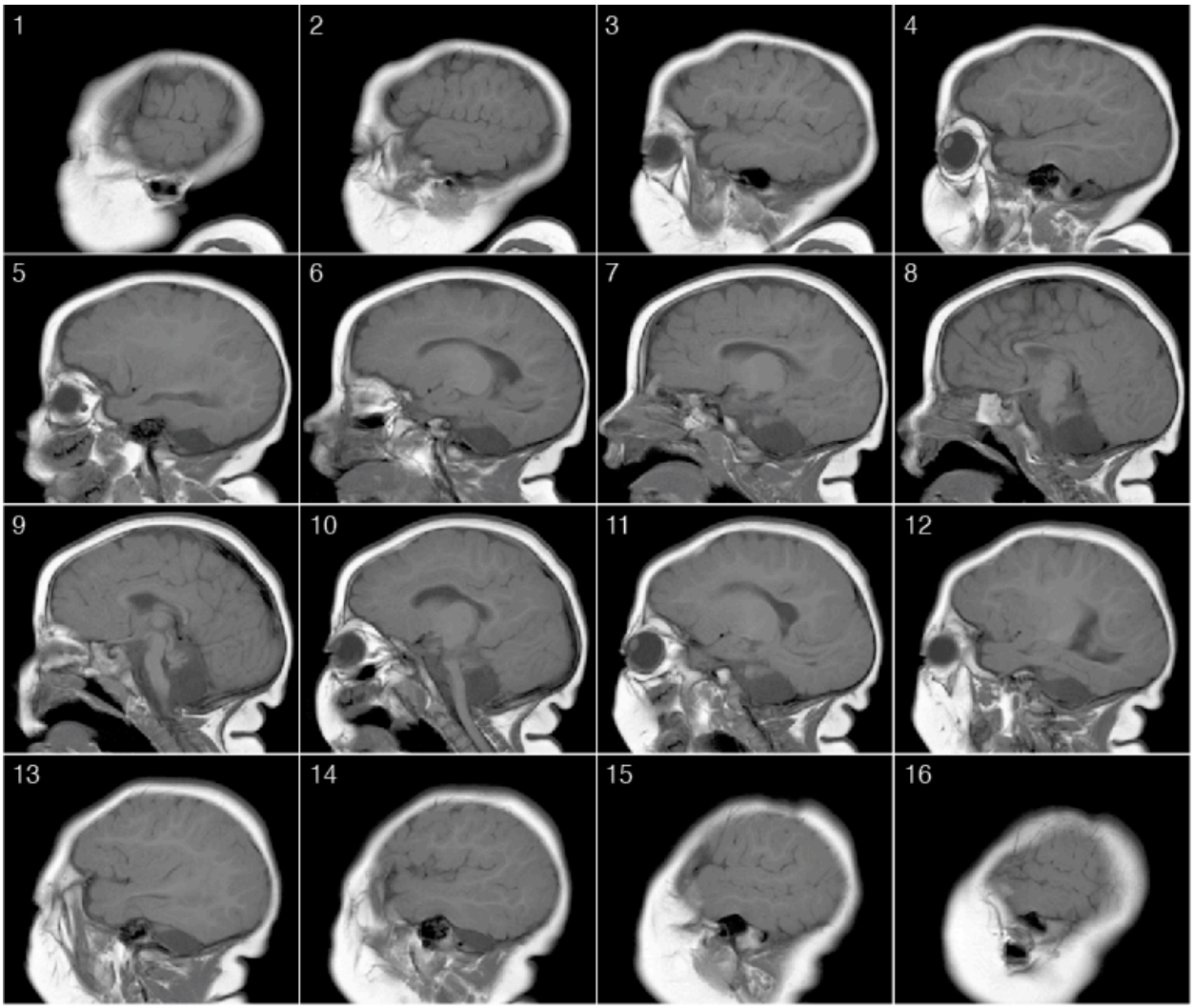

The extent of the cerebellar hypoplasia is most evident near the midline planes, around image 9-10.

Figure 2.3

T1-weighted sagittal MRI from CH3102.

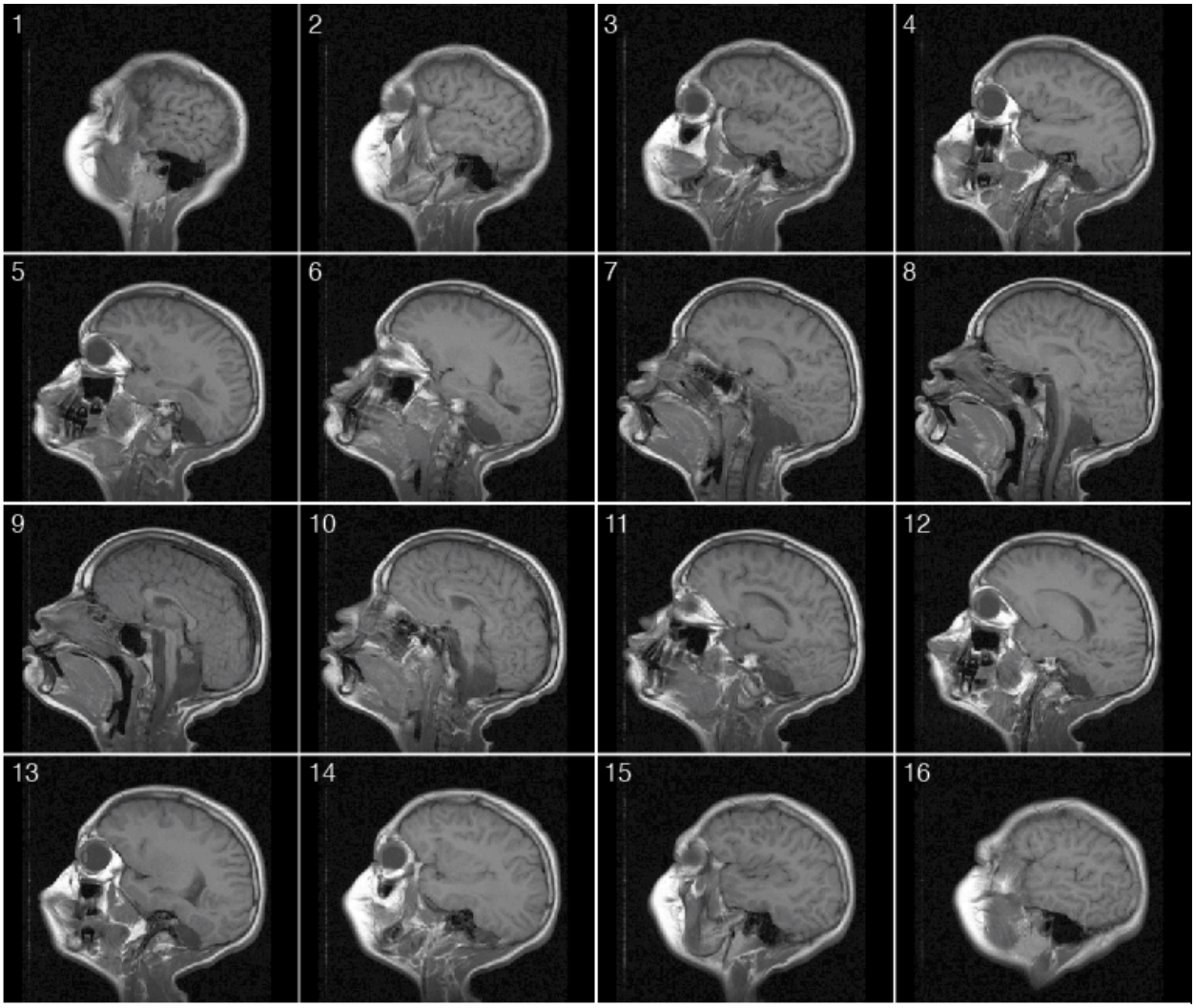

The extent of the cerebellar hypoplasia is most evident near the midline planes, around image 11-12.

Genome-wide linkage analysis of Family 1 and 2 using single nucleotide polymorphism (SNP) microarrays implicated only one region on chromosome 16q as linked and homozygous in all six affected individuals (**Figure 2.1e**; **Figure 2.4**), with a maximum multipoint LOD score of 3.68 (**Figure 2.1e**). Although Families 2 and 3 are not highly informative for linkage analysis, their shared homozygosity provides additional support for this locus. Furthermore, Families 2 and 3 shared the same haplotype (**Figure 2.4**), suggesting a founder effect. Sequencing of 42 genes within the candidate interval on 16q24.3 revealed homozygous variants predicted to be deleterious only in the *CHMP1A* gene. *CHMP1A* consists of seven exons encoding a 196 amino acid protein (See **Supplementary Note 2**, at end of chapter**)**. Affected individuals in Family 2 and 3 had a homozygous nonsense variant in exon 3, predicted to prematurely terminate translation (c.88C>T; Q30X; **Figure 2.5a**). Family 1 showed a homozygous variant in intron 2 of *CHMP1A* (c.28-13G>A; **Figure 2.5a**) predicted to create an aberrant splice acceptor site leading to an 11 base pair insertion into the spliced mRNA product (**Figure 2.6a**). The two mutations were absent from dbSNP, 281 neurologically normal European control DNA samples (562 chromosomes), the 1000 Genomes Project database, and approximately 5000 control exomes from the NHLBI Exome Sequencing Project. We sequenced *CHMP1A* in 64 patients with other cerebellar anomalies without finding additional mutations, but none of these patients shared the rare and distinctive pattern of hypoplasia seen in *CHMP1A* mutant patients.

Figure 2.4

Microsatellite marker haplotypes in the region of linkage on chromosome 16 in Families 1, 2, and 3.

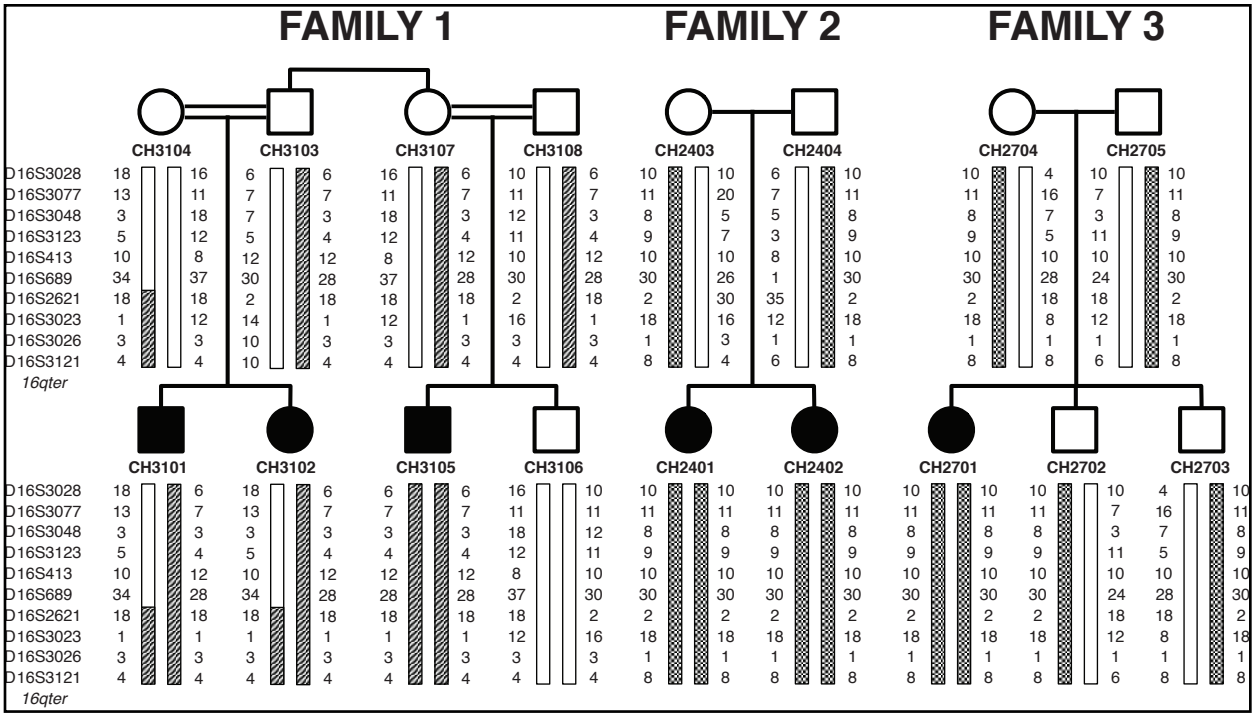

The affected individuals in Family 1,2 and 3 share a region of homozygosity on chromosome 16q24.3. Family 2 and 3 have the same homozygous haplotype. The minimal critical interval is defined by D16S689 and 16qter.

Figure 2.5

Loss-of-function mutations in *CHMP1A*, and dysregulation of *INK4A* in patient cell lines. (a) Chromatograms of genomic DNA sequencing show homozygous mutations in intron 2 (patient CH3101; c.28-13G>A) and in exon 3 (patient CH2401; c.88C>T). (b) A schematic diagram of full length CHMP1A, showing the relative contribution of each exon to the 196 amino acids of the protein. The expected effect of the mutation in CH2401 is a premature termination of translation after 29 amino acids. The intronic mutation in CH3101 creates a novel splice acceptor site, resulting in a termination of translation after 36 amino acids. (c) Western blot analysis of lysates from lymphoblastoid cell lines from CH2401 and CH3101 demonstrates a complete loss of expression of a 24 kD band detected by a CHMP1A antibody in control lysate (CTRL). Lysates from a cell line generated from the mother of CH3101 (CH3103) shows 50% of protein level relative to control. (d) Lymphoblastoid cell lines from patients CH2401 and CH3101 proliferate at a much lower rate compared to control cell lines. (e) qPCR of cDNA levels from human lymphoblastoid cell lines from patients CH2401 and CH3101 show a nearly two-fold increase in expression of *INK4A* relative to an unrelated, neurologically normal control cell line (normalized to *GAPDH* expression levels). The other transcribed isoform at the locus, *ARF*, shows no significant difference in expression level between patient cells and control. (f) ChIP-qPCR from lymphoblastoid cell lines using a BMI1 antibody shows an approximate eight-fold enrichment of *INK4A* promoter DNA relative to probes targeted 10kb upstream (10kb US) of the locus in a control cell line. This enrichment is reduced by nearly half in cell lines derived from a patient with a homozygous mutation in *CHMP1A* (CH2401). However, enrichment at the *ARF* promoter is not significantly different from the control cell line.

Figure 2.5 (Continued)

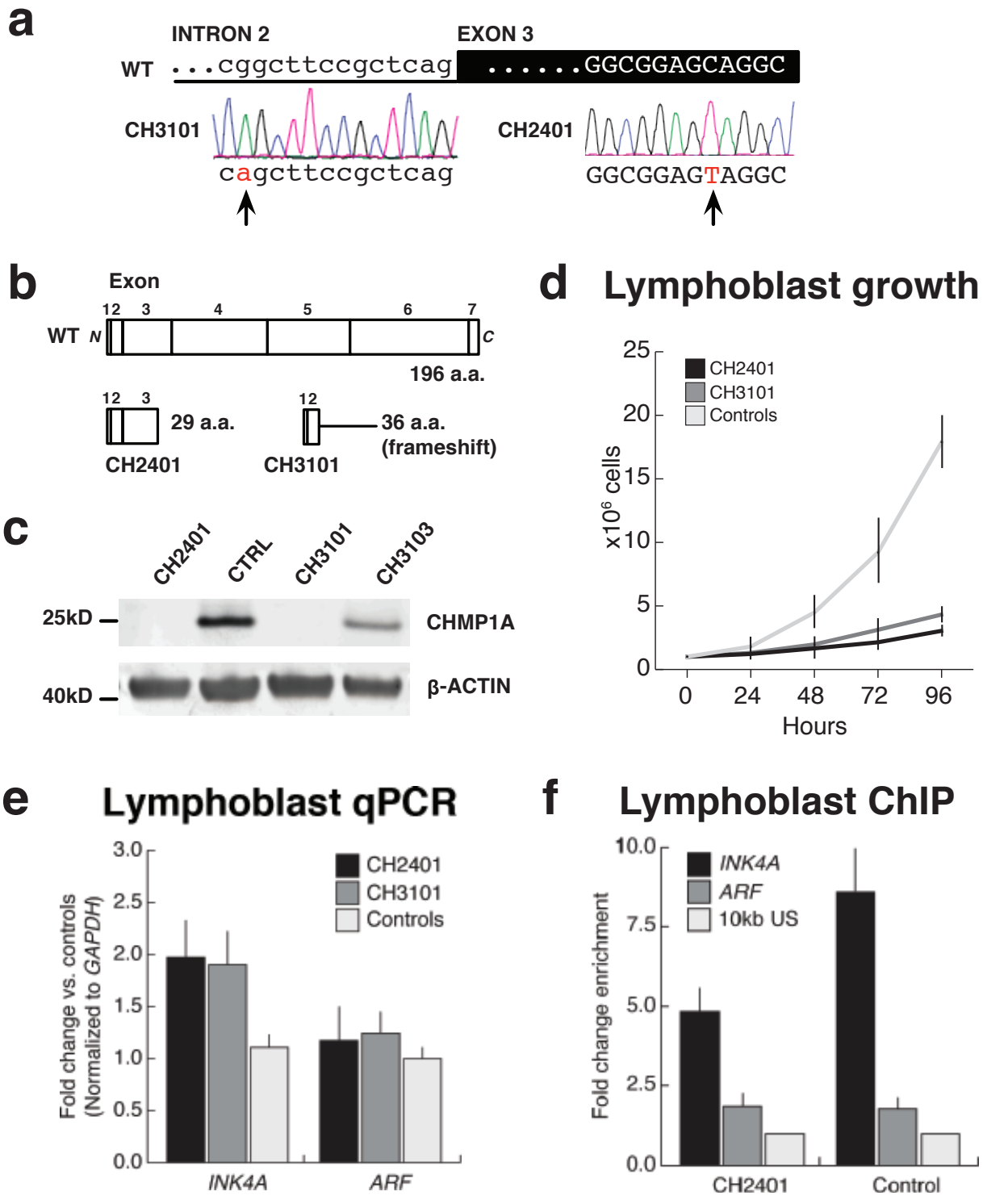

Figure 2.6

Analysis of aberrant splicing due to the intronic mutation in Family 1.

(a) NetGene2 (Brunak et al., 2001) web-based prediction was performed on the region surrounding the intron 2-exon 3 junction of *CHMP1A*, with and without the presence of the nucleotide change found in Family 1 (c.28-13G>A). Confidence values for predicted splice acceptors are scaled from zero to one, with a higher number indicating a greater probability of being a splice acceptor. In the wildtype sequence (WT), the annotated acceptor is predicted with a high confidence value (0.83). A cryptic splice acceptor 21 bp upstream of the annotated acceptor is also predicted (0.76). In the presence of the mutation (CH3101), the confidence value for the annotated acceptor decreases (0.69), and a novel acceptor 11 bp upstream is predicted (0.43). The confidence value for the cryptic acceptor 21 bp upstream is not affected the presence of the mutation. (b) *CHMP1A* cDNA from lymphoblastoid cell lines were sequenced. A control sample (CTRL) reveals a single transcript, which utilizes the annotated splice acceptor. An affected individual (CH3101) does not show any wildtype transcript, and instead reveals a transcript that utilizes the novel acceptor 11 bp upstream of the annotated acceptor (resulting in a 11 bp insertion), as well as a transcript that utilizes the cryptic acceptor 21 bp upstream of the annotated acceptor (resulting in a 21 bp insertion). The mother of CH3101 (CH3104) shows a similar tracing to control, suggesting that the abnormal transcripts are quite unstable.

Figure 2.6 (Continued)

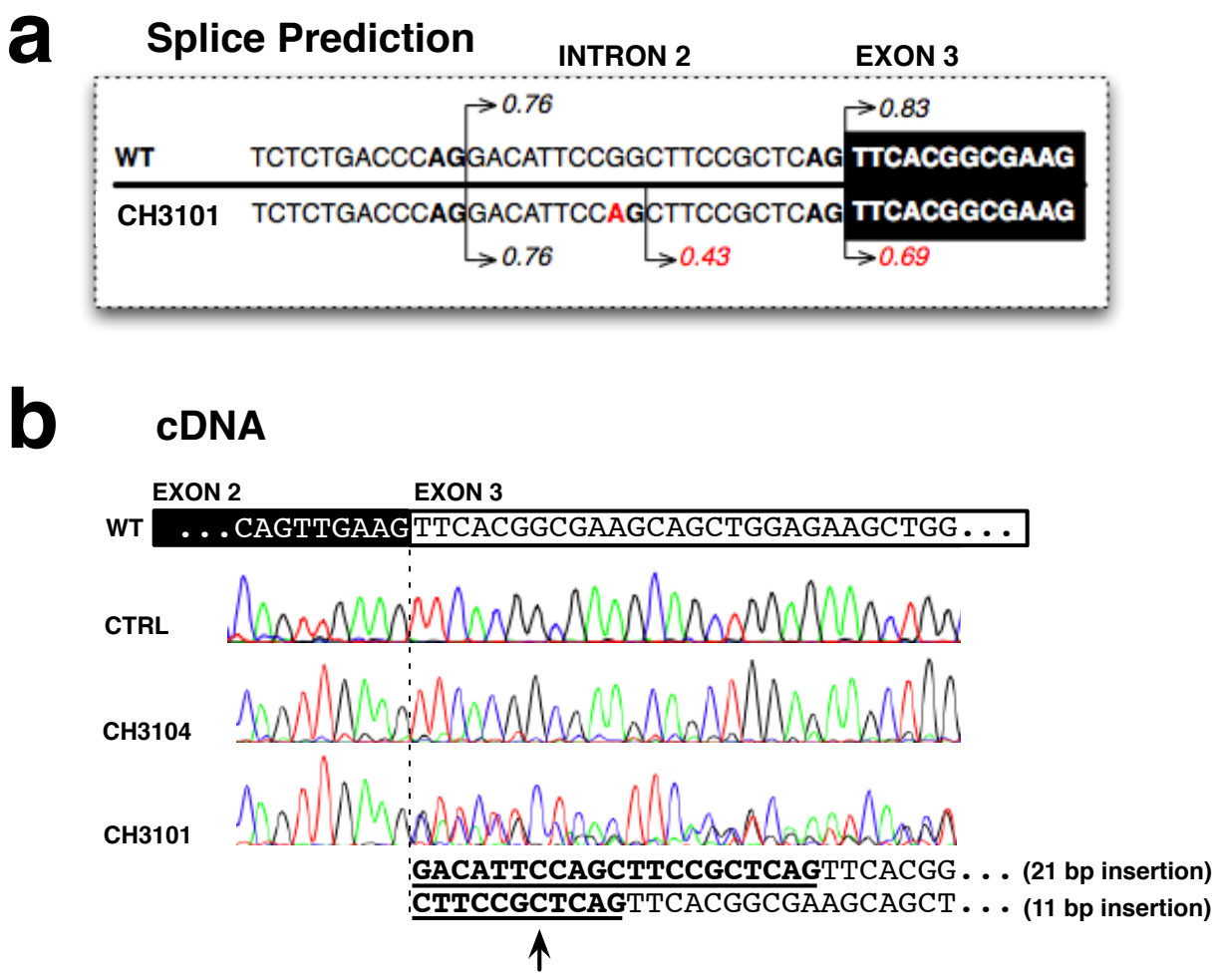

RT-PCR analysis of *CHMP1A* in lymphoblastoid cells from affected individuals from Family 1 (CH3101 and CH3105) identified the predicted aberrant transcript with the 11 base pair insertion and a second aberrant transcript with a 21 base pair insertion, but no normal *CHMP1A* transcript (**Figure 2.6b**). In the parents of affected children Family 1, and in unaffected control samples, only the normal transcript was detected, suggesting that the abnormal splice products are unstable. Western blot analysis revealed a single 24 kilodalton band in a normal control individual, but no corresponding band was detected in affected individuals from Families 1 or 2 (CH3101 and CH2401, respectively; **Figure 2.5c**). Normalized to the loading control, levels of CHMP1A were 50% in the parent (CH3104). Hence this genetic study establishes *CHMP1A* null mutations as the cause of pontocerebellar hypoplasia and microcephaly in these pedigrees.

CHMP1A has been assigned two distinct putative functions, as both a chromatin modifying protein, and a charged multivesicular body protein (Howard et al., 2001; Stauffer et al., 2001). CHMP1A was originally identified as a binding partner of the Polycomb group protein Pcl (Polycomblike) (Stauffer et al., 2001). In the nucleus, it has been suggested to recruit the Polycomb group transcriptional repressor BMI1 to heterochromatin, and overexpressed CHMP1A has been shown to arrest cells in S-phase (Stauffer et al., 2001). In the cytoplasm, CHMP1A is part of the ESCRT-III complex (endosomal sorting complex required for transport) Howard et al., 2001; Tsang et al., 2006). ESCRT-III complex localizes to endosomes and interacts with VPS4A and VPS4B (Stuchell-Brereton et al., 2007) to assist in the trafficking of ubiquitinated cargo proteins to the lysosome for degradation (Scita et al., 2006).

We investigated potential relationships of CHMP1A to Polycomb function by analysis of cell lines from two patients harboring different *CHMP1A* mutations (CH3101 from Family 1,

and CH2401 from Family 2), which show severely impaired doubling times compared to control cell lines, suggesting essential roles of CHMP1A in regulating cell proliferation (**Figure 2.5d**). In order to examine BMI1 function in these cells, we performed quantitative PCR analysis of expression of the BMI1 target locus *CDKN2A*, which in human encodes alternative transcripts *INK4A* and *ARF*. This revealed abnormally increased expression of *INK4A*, the isoform implicated in cerebellar development, but not of *ARF* (**Figure 2.5e**), suggesting de-repression of *INK4A*. Chromatin immunoprecipitation with a BMI1 antibody in control cell lines showed an approximately eight-fold enrichment of BMI1 binding at *INK4A* promoter DNA, relative to a control region 10kb upstream, whereas cells from an affected individual (CH2401) showed only about half this effect (**Figure 2.5f**). Enrichment of BMI1 at the *ARF* promoter was not substantial in this assay, and was similar in both control or patient cell lines, consistent with the specificity of regulation of the *INK4A* isoform by BMI1 (**Figure 2.5f**). Bmi1 suppresses the *Cdkn2a* locus via Polycomb-mediated H2A monoubiquitination, and is required for neural stem cell self-renewal (Molofsky et al., 2003). Our evidence suggests a role for CHMP1A in mediating BMI1-directed epigenetic silencing at the *INK4A* promoter, but not at the *ARF* promoter.

We further explored the relationship between CHMP1A and BMI1 using morpholino-based knockdown experiments in zebrafish. Knockdown of the zebrafish *CHMP1A* orthologue (*chmp1a*) resulted in reduced cerebellum and forebrain volume, similar to the effects of human *CHMP1A* mutations and zebrafish knockdown of *BMI1* orthologues (**Figure 2.7a-e**). The cerebellum consists of 5 major cells types, with the principal cell, known as the Purkinje cell, deriving from the ventricular epithelium, whereas granule cells derive from a separate progenitor pool known as the rhombic lip. Granule cell precursors then migrate over the outer surface of the

cerebellum and form the external germinal layer (EGL) before migrating radially past the Purkinje cells to settle in the internal granule layer (IGL) (Garel et al., 2011). Within the *chmp1a* morphant cerebellum, the internal granule and molecular layers were severely affected (**Figure 2.7a,b)**, which is consistent with the relatively preserved folia pattern of the human cerebellum (thought to be primarily established by Purkinje cells) and severely reduced volume (determined mainly by granule cell quantity).

Next, we tested genetic interactions between *chmp1a* and the zebrafish orthologue of *INK4A* (*ink4a*). Knockdown of *ink4a* alone did not result in noticeable abnormalities, and double knockdown of *chmp1a* and *ink4a* resulted in partial rescue of the brain morphology defects seen with *chmp1a* knockdown (**Figure 2.7f,g**). This was analogous to the rescue of the *Bmi1* knockout mouse cerebellar phenotype seen in the *Bmi1* and *Cdkn2a* double knockout mice (Jacobs et al., 1999). Of note, there are also parallels in brain morphology between individuals with *CHMP1A* mutations and *Bmi1*-deficient mice, which show cerebellar hypoplasia (Leung et al., 2004; van der Lugt et al., 1994) (**Figure 2.7h,i**). In *Bmi1*-null mice, the cerebellar architecture was generally preserved, but the thickness of the granular and molecular layers was markedly reduced (Leung et al., 2004), and *Bmi1*-deficient mice show a modest reduction in cerebral volume (Leung et al., 2004; Zencak et al., 2005), similar to *CHMP1A* mutant patients (**Supplementary Note 1,** at end of chapter).

Figure 2.7

Genetic links between *CHMP1A* and *BMI1* in zebrafish and mice.

(a, b) Compared to parasagittal section of control zebrafish 5 days post fertilization (a), zebrafish injected with *chmp1a* morpholino (MO) show a reduction in cerebellum and forebrain volume. Higher magnification images of the cerebellum (insets) highlight loss of molecular and internal granular layers in the mutant (arrowheads). (c-g) Compared to control zebrafish (c), morpholino-based knockdown of *chmp1a* (d) shows a reduction in head size, with the hindbrain more markedly reduced in thickness (asterisks), which is similar to the phenotype seen by knocking down the zebrafish orthologues of BMI1, *bmi1a* and *bmi1b* (e). When the *ink4a* morpholino is co-injected with the *chmp1a* morpholino, the *chmp1a* knockdown phenotype is partially rescued (f). Embryos were classified at 28 hours post fertilization as either normal, disrupted, or severely disrupted (see Online Methods) for each of uninjected controls, *ink4a* MO, *bmi1* MO *chmp1a* MO, *bmi1* MO coinjected with *ink4a* MO, and *chmp1a* MO coinjected with *ink4a* MO or human *CHMP1A* mRNA. (g). (h, i) Compared to the wildtype mouse cerebellum at P25 (h), sagittal cross-sectional area of the *Bmi1*-/- mouse cerebellum at the same age (i) is dramatically reduced, though foliation and structure of the lobules (indicated in Roman numerals) are generally preserved. Scale bars = 200μm (a, b), 200μm (c-f), 500μm (h, i). Asterisk = $p < 0.0001$, two-tailed Pearson's chi-squared test.

Figure 2.7 (Continued)

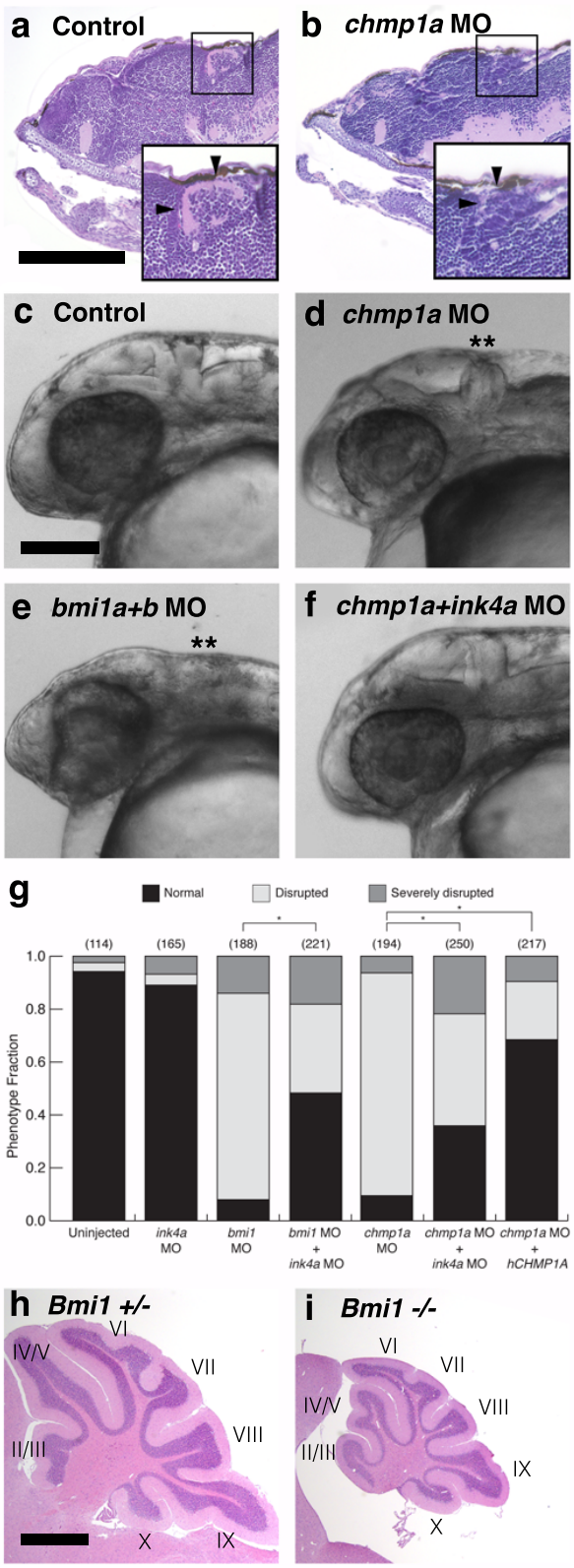

Though Chmp1a immunoreactivity is predominantly cytoplasmic, some nuclear localization is seen in some cell types. Confocal images of NIH 3T3 cells show prominent exclusion of Chmp1a from the nucleus, where Bmi1 is seen (**Figure 2.8a**). On the other hand, confocal images of HEK293T cells, while still showing predominantly cytoplasmic localization, show some nuclear immunoreactivity as well (**Figure 2.8b**). Primary cultures of cerebellar granule cells also show predominant cytoplasmic localization, along with a speckled nuclear pattern (**Figure 2.8c**). Overexpression of HA-tagged Chmp1a in cultured granule cells shows abundant nuclear Chmp1a with a punctate expression pattern, confirming the speckled nuclear localization of native Chmp1a (**Figure 2.8d**), and consistent with earlier reports that Chmp1a can appear in the nucleus (Stauffer et al., 2001). However, even with overexpression, Chmp1a and Bmi1 do not prominently co-localize within the nucleus, also in agreement with previous data (Stauffer et al., 2001).

Immunohistochemical studies of mouse developing cerebellum and cerebral cortex showed widespread expression of Chmp1a in dividing and postmitotic cells. Chmp1a immunoreactivity was robust in the cytoplasm of EGL cells and Purkinje cells and slightly lower in the cytoplasm of IGL cells at P2 (**Figure 2.8e,f**), and confocal images again suggest low levels of speckled immunoreactivity in the nuclei of these cells (**Figure 2.8e, f**). At later stages of cerebellar development (P4, P10 and P29), Chmp1a expression persisted in Purkinje cells and granular cells, but at lower levels compared to P2 (**Figure 2.9**). E14.5 cerebral cortex showed Chmp1a expression in the neuroepithelial cells, with highest expression near the ventricular surface (**Figure 2.8g**). A similar pattern was seen in E12.5 cerebral cortex (**Figure 2.9**). At E17.5, the expression at the ventricular surface decreased, but expression was noted in

postmitotic neurons (**Figure 2.9**). At P2, expression in postmitotic neurons of the cortical plate decreased before increasing again at P10 (**Figure 2.9**). These expression studies confirm that Bmi1 and Chmp1a are often expressed in the same cells. On the other hand, the absence of widespread subcellular co-localization of Bmi1 and Chmp1a suggests that the regulation of Bmi1 by Chmp1a is perhaps not mediated by direct physical interaction.

Our data suggest that CHMP1A is an essential CNS regulator of BMI1, which in turn is a key regulator of stem cell self-renewal. Chmp1a's dual cytoplasmic and nuclear localization, and its connection to the ESCRT-III complex, position Chmp1a as a potentially crucial link between cytoplasmic signals and the global regulation of stem cells via the Polycomb complex.

Figure 2.8

Chmp1a and Bmi1 expression in cultured cells and the developing mouse brain.

(a) Immunohistochemistry of NIH 3T3 cells shows cytoplasmic Chmp1a staining with exclusion from the nucleus, where Bmi1 is present. (b) Immunohistochemistry of HEK293T cells also shows cytoplasmic Chmp1a staining, with some nuclear immunoreactivity. (c) In dissociated cerebellar granule cells (Cb GC), endogenous Chmp1a localizes mostly to the cytoplasm, but also has a speckled nuclear localization. (d) When dissociated cerebellar granule cells are transfected with an HA-tagged Chmp1a overexpression construct (Cb GC OX), HA-Chmp1a is expressed robustly in the nucleus with prominent nuclear puncta (arrowheads). (e) In the developing cerebellum at postnatal day 2 (P2 Cb), Chmp1a is expressed primarily in the cytoplasm of cells in the external germinal layer (EGL), Purkinje cells (PC) and internal granule layer (IGL), with low level of speckled staining in the nucleus. (f) In P2 cerebellum, Bmi1 is expressed in the EGL and IGL cells that are positive for Chmp1a, and it primarily localizes to the nucleus. (g) In the developing cortex at E14.5, Chmp1a is expressed in both ventricular zone progenitors and cortical plate cells. Bmi1 is expressed in the same population of cells and at a level slightly lower than in the P2 cerebellum. LV = lateral ventricle. Scale bars = 20μm (a-g).

Figure 2.8 (Continued)

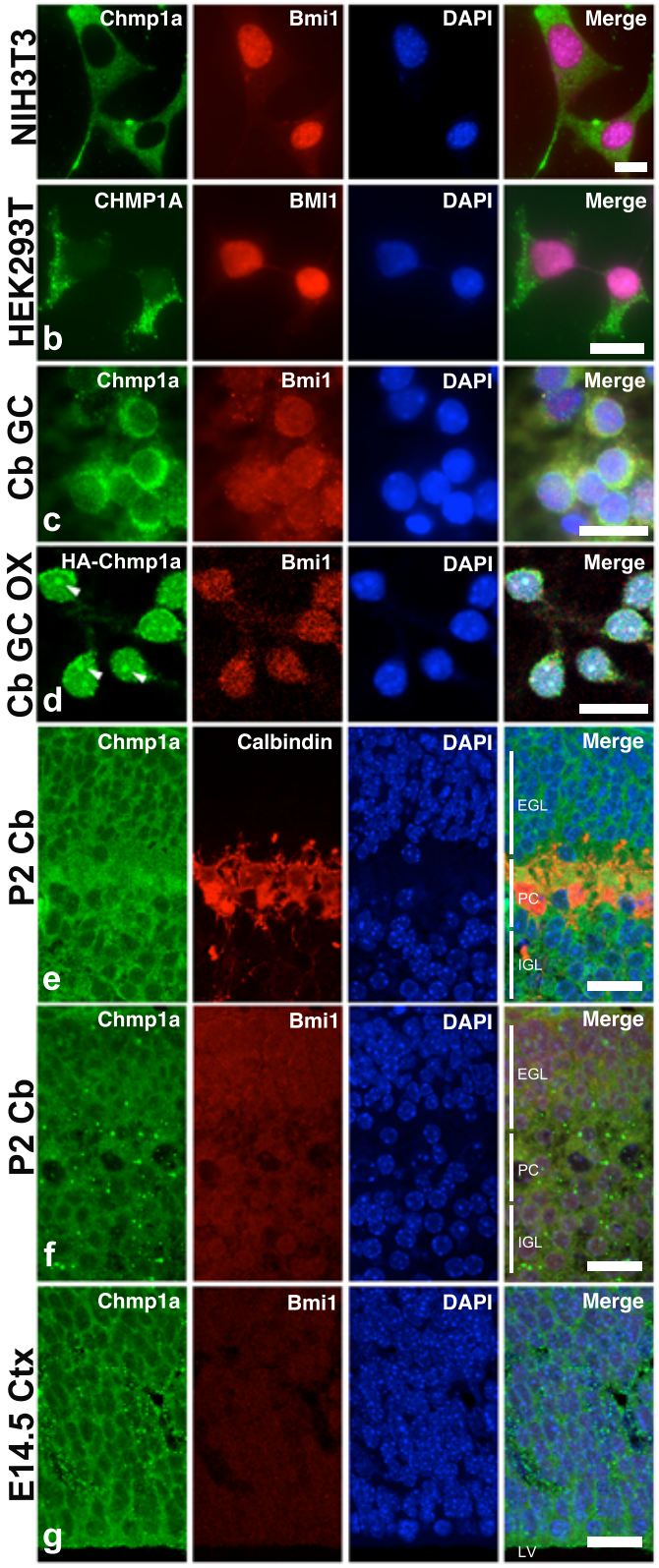

Figure 2.9

Expression of Chmp1a in the developing mouse cerebellum and cerebral cortex.

At P4 and P10, Chmp1a was expressed in the cytoplasm of external germinal layer cells, Purkinje cells, and internal granule layer cells, but at a slightly lower level than at P2 (**Figure 2.8**). At P29, Chmp1a expression remained in the molecular layer, Purkinje cells and granular layer cells. Like at P2, only faint nuclear Chmp1a staining was observed at these stages. In E12.5 cerebral cortex, Chmp1a showed ubiquitous cytoplasmic expression in the neuroepithelial cells, with highest expression in the ventricular surface. At E17, the expression at the ventricular surface decreased, but cytoplasmic expression was noted in postmitotic neurons. At P2 and P6, expression in postmitotic neurons of the cortical plate decreased before increasing again at P8 and P10. EGL= external germinal layer, PC = Purkinje cell layer, IGL = internal granule layer, ML = molecular layer, vz = ventricular zone, cp = cortical plate. Scale bars = 20μm.

Figure 2.9 (Continued)

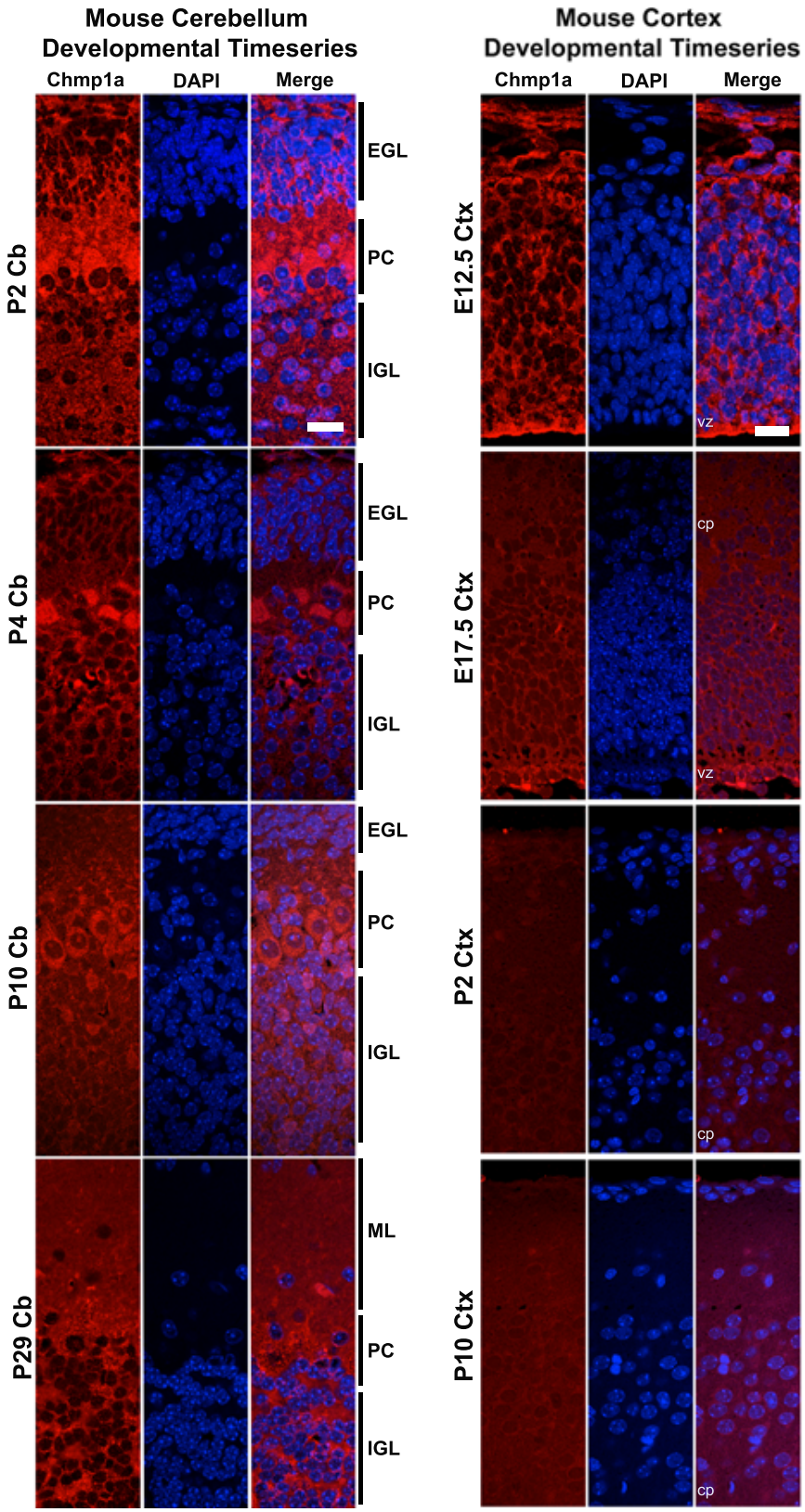

Supplemental Note 1

There are three affected individuals in Family 1 (CH3101, CH3102, and CH3105). CH3101 (female) was born at 33 weeks of gestation via Caesarean section. The pregnancy was complicated by hyperemesis gravidarum. At birth, her head circumference was 33cm (91st percentile), and weight was 2.2kg (57th percentile). She was found to have ventricular septal defect during the neonatal period, which later resolved. Her early motor and speech development were delayed. She started to walk independently at 8 years of age. She had bilateral equinocavovarus and claw foot deformities, which were worse on the left, and underwent orthopedic procedures for them. On examination at 16 years of age, her head circumference was 50cm (-4.0 SD), height was 138cm (-3.7 SD) and weight was 32kg (-3.2 SD). No dysmorphic features were noted. She spoke only in single words. She had poor social interaction. There were no oral motor difficulties. She had generalized hypotonia and walked with an ataxic gait. She had normal deep tendon reflexes. Her visual examination was remarkable for myopia, astigmatism and convergent strabismus. She had negative TORCH titers and her karyotype was normal. She underwent MRI of the brain at 12 years of age, which was remarkable for a very small cerebellar vermis and hemispheres. Brain stem was thin with a short pons and long medulla. There was no malformation of the cerebral cortex, but the cerebral white matter was moderately reduced in volume. The corpus callosum was fully formed, but thin. Myelination of the white matter was age-appropriate.

CH3102 (male), younger brother of CH3101, was born after an unremarkable pregnancy via Caesarean section at 38 weeks of gestation. At birth, his head circumference was 36cm (86th percentile), and weight was 2.8kg (8th percentile). He had delay in motor and speech

development, and also had feeding difficulties. He started to walk independently at 7 years of age. He had surgery for bilateral talipes valgus. On examination at 11 years of age, his head circumference was 50cm (-2.4 SD), height was 127cm (-2.4 SD), and weight was 26kg (-2.0 SD). No dysmorphic features were noted. He spoke only in single words, and had poor social interaction. He had low muscle tone, except in the lower extremities, which were hypertonic and showed dystonic posturing. He also showed involuntary, repetitive vertical head movements. He had increased deep tendon reflexes. Ophthalmologic examination was remarkable for myopia, astigmatism, convergent strabismus of the right eye, bilateral pseudoptosis, and limitation of extraocular movements. He had normal TORCH titers and normal karyotype. He had MRI of the brain initially at 2 years and 5 months of age. The findings were similar to that of his older sister (CH3101) including severe hypoplasia of the cerebellar vermis, cerebellar hemispheres, and pons. There was no malformation of the cerebral cortex, and the cerebral white matter was moderately diminished in volume, with a fully formed but thin corpus callosum. He had a repeat brain MRI at 12 years of age, and there was no change in these findings, suggesting that the condition is a developmental, rather than degenerative condition.

CH3105 (male) is a cousin of CH3101 and CH3102, and was born after 38 weeks of gestation via Caesarean section with a birth head circumference of 36cm (86th percentile) and weight of 2.97kg (17th percentile). There were no perinatal complications. He had delay in motor and speech development, but no feeding difficulties. He has not achieved independent walking yet. On examination at 7 years of age, his head circumference was 50cm (7th percentile), height was 115cm (10th percentile), and weight was 27kg (79th percentile). No dysmorphic features were noted. He spoke only in single words, and had poor social interaction,

similar to his affected cousins. He had esotropia. He had low muscle tone, and showed involuntary, repetitive vertical movement of his head, similar to CH3102. He had normal deep tendon reflexes. He had negative TORCH titers, Fragile X syndrome DNA testing, and ataxia gene sequencing panel. He had normal plasma amino acid, very long-chain fatty acid, and urine organic acid profiles. Serum transferrin electrophoresis was also normal. He underwent MRI of the brain at the age of 3 months. The findings were very similar to that of CH3101 and CH3102, and included a very small cerebellar vermis and hemispheres, a small pons, normal cerebral cortex, mild to moderate decrease in the cerebral white matter volume and a thin, but fully formed corpus callosum. Myelination of the cerebral white matter was thought to be slightly delayed for his age. None of the siblings in Family 1 has history of seizure.

There are two affected children in Family 2 (CH2401 and CH2402). CH2401 (female) was born after uncomplicated pregnancy at 36 weeks of gestation via Caesarean section due to breech presentation. Measurements at birth are not available. Joint stiffness was noted soon after birth, worse in the legs with hip dislocation. She had gastrointestinal issues including constipation and gastroesophageal reflux. Her development was severely delayed from early on, and she was found to have impaired ability to control swallowing. Examination at 2 years and 7 months of age revealed head circumference of 44cm (-2.8 SD), length of 82.5cm (-2.4 SD) and weight of 11.25kg (7^{th} percentile). She was found to have frequent babbling, but no communication with words or signs. She did not interact with her environment, and did not follow commands. She had mildly increased tone in the arms and moderately increased tone in the legs. She showed frequent involuntary movements including side-to-side head shaking and slow kicking movements of the legs. Ophthalmological examination at 2 years and 10 months of

age revealed no visual tracking. Her eye movements and pupils were normal with no nystagmus. She had esotropia, hyperopia and astigmatism. She was felt to have predominantly cortical visual impairment. On examination at 5 years of age, her head circumference was 44.8cm (-4.0 SD), length was 97cm (-2.3 SD), and weight was 14.5kg (4th percentile). She had a mild scoliosis. She did not show visual tracking, but responded to visual threat by blinking. Side-to-side head shaking was again noted. She was diffusely spastic, with brisk deep tendon reflexes. She had normal serum lactate and pyruvate, serum amino acids and urine organic acids. Carbohydrate-deficient transferrin analysis and testing for *MECP2* were also normal. She had MRI of the brain twice, at 4 months of age and at 4 years of age. They were remarkable for severe reduction in size of the cerebellum and pons, with a decreased cerebral white matter volume, a thin corpus callosum and grossly normal cerebral cortex. There was no progression of the findings between the two studies.

CH2402 (female) is a younger sister of CH2401. The course of the pregnancy was uncomplicated, but at 37 weeks of gestation, fetal decelerations were noted, and delivery was precipitous. Her Apgar scores were 8 and 9, and her birth weight was 2.9 kg (38th percentile). She was noted to be microcephalic during the newborn period, and had a right club foot and multiple joint contractures, most prominent in the hands. At 3 months of age, her head circumference was 37.4cm (-2.0 SD), length was 53cm (-2.6 SD), and weight was 6.4kg (89th percentile). She was noted to have mild asymmetry of the forehead and hollow temples. She had upturned nares, slightly tented upper lip, and mildly low set and posteriorly rotated ears. She showed no visual tracking or social smile. She had diminished spontaneous movements, but had frequent irregular small jerky movements, suggestive of chorea. On examination at 11 months of

age, her head circumference was 41.8cm (-2.4 SD), length was 68.3cm (6th percentile), and weight was 9.95kg (72nd percentile). She was noted to have brief visual tracking, but otherwise had gained few developmental milestones. Choreiform movements involving all body regions were again noted. She had diffusely increased muscle tone deep tendon reflexes. She had a normal karyotype and negative urine culture for cytomegalovirus. Echocardiogram was remarkable for patent foramen ovale. Renal ultrasound was normal. There was no history of seizure, and a video EEG monitoring showed no seizures or epileptiform activities. She had MRI of the brain twice, at 2 days of age and 10 months of age. They showed similar findings to her older sister (CH2401), including very small cerebellar vermis and hemispheres, small pons, no cortical malformations, severely reduced cerebral white matter with a fully formed but thin corpus callosum. Her MRI also revealed abnormal T2 hyperintensity diffusely in the cerebral white matter, in addition to reduced volume. There was no clear evidence of progression between the two studies.

CH2701 (female) was born after a full term, uncomplicated pregnancy. She reportedly did not cry at birth and had low Apgar scores. At birth, her head circumference was 34.3cm (39th percentile) and weight was 3.3kg (42nd percentile). She was noted to have arthrogryposis multiplex congenita. At 3 weeks of age, her head circumference was 36cm (39th percentile), length was 48cm (3rd percentile), and weight was 3.4kg (17th percentile). She had severe delay in her development. She never sat or stood independently. She developed some babbling, but no meaningful words. She was noted to have mild swallowing incoordination and esophageal dysmotility. At around 1 year of age, she started to have episodes of upward gaze deviation with head extension for a few seconds. She also developed episodes of clonic head movements to the

left. These episodes were felt to be seizures and she was placed on an anticonvulsant medication. She began to have vomiting with eating and started to lose weight after 1 year of age, requiring G-tube placement and Nissen fundoplication. She started to show developmental regression at around 18 months of age. On examination at 2 years 8 months of age, she was noted to be cachectic with severe wasting. Her head circumference was 41.5cm (-4.4 SD), length was 64cm (-7.4 SD), and weight was 5.3kg (-6.3 SD). She was noted to have long eyelashes, bushy eyebrows and synophrys. She had generalized hypertrichosis. By 5 years of age, her nutritional status significantly improved, and she started to show slow progress in her development again. On examination at 7 years of age, her head circumference was 48.0cm (-2.8 SD), length was 86.1cm (-6.8 SD), and weight was 13.0kg (-3.6 SD). She did not show visual fixation or tracking, but blinked to light. Her eyes intermittently showed conjugate upward deviation for a few seconds. She had low muscle tone on the trunk and increased tone on the hip and lower extremities. She was noted to have multiple joint contractures of the lower extremities. She was unable to roll over or sit independently. She was able to reach for objects. Her ophthalmological examination was remarkable for no measurable vision, but normal ocular structures and no cataracts. She had a normal karyotype and chromosomal microarray. Plasma amino acid and urine organic acid analyses did not show a recognizable pattern for a disorder of amino acid or organic acid metabolism. Complete blood count, serum immunoglobulin profile and T- and B-cell subsets were unremarkable. Work-up for congenital disorders of glycosylation included carbohydrate-deficient transferrin analysis, as well as phosphomannomutase and phosphomannoisomerase activity on skin fibroblast, which were all unremarkable. She had an MRI of the brain at 22 months of age. She had a markedly hypoplastic cerebellar vermis and

hemispheres and brainstem, especially pons. There was no malformation of the cerebral cortex, but the volume of the cerebral white matter was markedly diminished, with a very thin corpus callosum. She had a follow-up MRI of the brain at 7 years of age, and the findings were unchanged, compared to the prior study, except for slightly more prominent subarachnoid spaces in the anterior middle cranial fossa. Overall there was no clear evidence of progression of the previously noted findings.

Supplemental Note 2

Though another isoform has been annotated for the human *CHMP1A* locus on the UCSC Human Genome Browser, the evidence in support of this alternative isoform is weak, and it is not detectable in any other species. The putative alternative isoform (NM_001083314.1) is identical to *CHMP1A*, except it lacks exon 2. Exon 2 is 20 nucleotides in length, therefore the majority of the alternative isoform is in a different reading frame from *CHMP1A*. The alternative isoform is predicted to encode a protein of 240 amino acids. The mutation identified in Families 2 and 3 is predicted to result in a conservative missense change in this alternative isoform (p.A24V), whereas the mutation identified in Family 1 creates a frameshift and premature stop codon for both isoforms. While western blot analysis shows complete absence of CHMP1A in affected individuals from both families, similar western blot analysis using an antiserum against the predicted alternative isoform shows low or undetectable expression of the alternative isoform in both affected and unaffected individuals from Family 2 (CH2401) (data not shown). In mouse, only the transcript orthologous to *CHMP1A* has been annotated, and it has 97% amino acid identity to human CHMP1A. When exon 2 was removed from the mouse *Chmp1a* sequence, the resulting amino acid sequence would be dissimilar to the human alternative isoform, and only 21 amino acids in length. In the chimpanzee genome, the *CHMP1A* ortholog has not been annotated, but N-SCAN gene prediction software (Gross et al., 2006; Korf et al., 2001) predicts the presence of a *CHMP1A* homolog, with 95% amino acid identity to human CHMP1A. Again, removing exon 2 results in a highly dissimilar amino acid sequence from the human alternative isoform, with the resulting protein length being only 28 amino acids. Furthermore, the NHLBI Exome Sequencing Project Exome Variant Server lists 5

nonsense variants for the alternative isoform, but none for *CHMP1A*. Taken together, these findings strongly suggest that *CHMP1A* is the essential form.

Methods

URLs

UCSC Human Genome Browser: http://genome.ucsc.edu/

Primer3: http://frodo.wi.mit.edu/primer3/

NetGene2: http://www.cbs.dtu.dk/services/NetGene2/

dbSNP: http://www.ncbi.nlm.nih.gov/projects/SNP/

1000 Genomes Project: http://www.1000genomes.org/

NHLBI Exome Sequencing Project: http://evs.gs.washington.edu/EVS/

Genetic Screening

The genetic study was approved by Beth Israel Deaconess Medical Center and Children's Hospital Boston Institutional Review Boards. Appropriate informed consent was obtained from all involved human subjects.

The affected individuals and their parents from Family 1 and the affected individuals from Family 2 were subjected to genome-wide SNP screen with Affymetrix GeneChip Human Mapping 250K Sty Array, performed at the Microarray Core of the Dana Farber Cancer Institute. We carried out fine mapping using microsatellite markers identified using the UCSC Human Genome Browser (Kent et al., 2002), with synthesized fluorescent-labeled primers (Sigma-Genosys). Two point and multipoint LOD scores were calculated using Allegro (Gudbjartsson et al., 2000), assuming recessive inheritance with full penetrance and a disease allele frequency of 0.001. Sequencing primers were designed using Primer3 (Rozen et al., 2000), and genomic DNA was sequenced using standard Sanger technology. Neurologically normal Caucasian

control DNA samples were obtained from the Coriell Cell Repositories (Coriell Institute for Medical Research). All nucleotide numbers are in reference to *CHMP1A* isoform 2 cDNA (NM_002768, in which A of the ATG start site is +1) from the UCSC Genome Browser.

Analysis of *CHMP1A* splicing

Splice prediction software NetGene2 (Brunak et al., 1991) was used to determine the effect of the Family 1 allele on *CHMP1A* splicing. EBV-transformed lymphocytes were grown in RPMI-1640 with 15% (v/v) fetal bovine serum and 1% (v/v) penicillin/streptomycin in a humidified incubator at 37^{o}C in 5% CO_2. RNA was isolated using the RNeasy Mini Kit (Qiagen). Total RNA (5µg) was used for first-strand synthesis with oligo(dT) primers and the SuperScript III First-Strand Synthesis SuperMix (Invitrogen), and 1µl of the product was used for the subsequent PCR reaction, with primers from exon 1 to exon 5 of *CHMP1A* (NM_002768).

Proliferation assay of lymphoblastoid cell lines

EBV-transformed lymphoblastoid cell lines from eight control subjects and two patients (CH2401 and CH3101) were grown as described above. From each cell line, 20 million cells were grown, and then one million cells were aliquoted into four sets of five T25 flasks filled with 10ml of media. Each set was allowed to grow for 24, 48, 72, and 96 hours, respectively. Cell densities were estimated using a hemocytometer.

Quantitative PCR

EBV-transformed lymphoblastoid cell lines were grown and cDNA was generated as described above. *INK4A* and *ARF* levels were quantified using the StepOnePlus Real-Time PCR System (Applied Biosystems), with *GAPDH* as a control. Primer sequences used are as follows: *INK4A* (5'-CCCCTTGCCTGGAAAGATAC and 5'-AGCCCCTCCTCTTTCTTCC), *ARF* (5'-AACATGGTGCGCAGGTTC and 5'- GGGATGTGAACCACGAAAAC), and *GAPDH* (5'-CCAAGGTCATCCATGACAAC and 5'-GGCCATCCACAGTCTTCTG).

Chromatin Immunoprecipitation

EBV-transformed lymphoblastoid cells were counted and 100 million cells were fixed in 1% paraformaldehyde in PBS for ten minutes at room temperature, followed by a quenching step for 10 minutes at room temp with 30mM glycine. Cells were then washed twice with ice-cold PBS and flash frozen with liquid nitrogen. Cells were later thawed on ice, and serially washed for 10 minutes, pelleted at 3000 rpm for 10 minutes, and resuspended in three buffers (10mL Buffer 1: 50mM HEPES KOH pH 7.5, 140mM NaCl, 1.0mM EDTA pH 8.0, 10% glycerol, 0.5% NP-40, 0.25% Triton X-100; 10mL Buffer 2: 200mM NaCl, 1.0mM EDTA pH 8.0, 0.5mM EGTA pH 8.0, 10mM Tris pH 8.0; 2mL Buffer 3: 10mM Tris pH 8.0, 1.0mM EDTA pH 8.0, 0.5mM EGTA pH 8.0). All three buffers were supplemented with protease inhibitor cocktail (Roche). The Buffer 3-contained cell lysates were sonicated (Misonix 3000) for sixteen cycles of 15 seconds ON and 2 minutes OFF at power setting 7.5, or until the DNA fragmentation was such that the vast majority of fragments were between 200-500bp. The equivalent volume corresponding to 20 million cells were precleared for 2 hrs with 20μL of pre-washed protein A/G plus sepharose beads (Santa Cruz Biotechnology, sc-2003), and spun for 1 minute at 6000 rpm.

5% of the supernatant was saved as the input DNA for each sample. Then 4µg of the BMI1 antibody (Abcam, ab14389) was applied to the remaining supernatant overnight at 4°C, on a rocking platform. The next day, 20µL of beads were incubated with the sample at 4 °C for 2 hrs, spun for 1 minute at 6000 rpm, the supernatant saved, and the beads washed 2x5 min in each of three serial salt washes (Wash Buffer 1 [Low Salt]: 0.1% SDS, 1.0% Triton X-100, 2mM EDTA, 20mM Tris-HCl pH 8.1, 150mM NaCl; Wash Buffer 2 [High Salt]: 0.1% SDS, 1.0% Triton X-100, 2mM EDTA, 20mM Tris-HCl pH 8.1, 500mM NaCl; Wash Buffer 3 [LiCl]: 250mM LiCl, 1.0% NP-40, 1.0% deoxycholic acid, 1.0mM EDTA, 10mM Tris pH 8.1). The beads were washed once more in TE Buffer, and then eluted with 100uL of elution buffer (10mM Tris pH 8.0, 1.0mM EDTA pH 8.0, 1% SDS) for 10 minutes at 65°C. The beads were spun at 6000 rpm for 1 minute, and a second elution was performed and combined with the first. The 200µL eluate was transferred to a new tube, and reverse crosslinked at 65°C overnight (12-16 hours). The next day, 10ug of RNAse A (New England Biolabs) was added for 2 hours at 37°C, followed by 100µg of proteinase K (New England Biolabs) for 2 hours at 37°C. DNA was extracted from the samples via phenol-chloroform extraction and column purification (Qiagen Qiaquick), and eluted with 2x50µL of EB Buffer. qPCR primers were assessed for specificity by their melt curves on the StepOnePlus (Applied Biosystems), and a standard curve was determined using four ten-fold serial dilutions for each primer using the input DNA samples. Fold-enrichments for each ChIP sample were normalized to input Ct. Primer sequences used are as follows: *INK4A* promoter (5'-CCAATTCCCCTGCAAACTTC and 5'-CAACGCACCGAATAGTTACG), *ARF* promoter (5'-ACATCACCGATCCTTTCTGG and 5'-TCCTTGCCCTGCTTTTACTG), 10 kb upstream (5'-AGGTTTTAGCCAAGGGGATG and 5'-ATGTTGTTGGGGCTACTTCC).

Zebrafish morpholino experiments

ATG-targeting morpholinos were designed against *chmp1a* (5'-CAGTGTGTCGTCCATGTCGCTGTCT), *bmi1-a* (5'-GCATCGTCATGGGATAGAAAAGAAC), *bmi1-b* (5'-CATTGTCATGGGAGTACGCCGACCT), and the *INK4A* zebrafish ortholog (*ink4a*; 5'-TAAAGCGCGTCTAAACCTACCTGTA) (GeneTools). In all experiments where *bmi1* morpholinos were used, *bmi1-a* and *bmi1-b* were injected together. Injections were performed at the one-cell stage. Optimal doses for the *chmp1a, bmi1a+b* and *ink4a* morpholinos were 4.5ng, 1.2ng, and 4.0ng, respectively. At 28 hours post fertilization (hpf), the embryos were visualized using a stereo microscope (Zeiss). A second ATG-targeting *chmp1a* morpholino was designed (5'-TCGGGTTATTCGCTGCTCTTCTGCT), and 3.0ng was injected at the one-cell stage, to check for phenocopying of the other *chmp1a* morpholino.

For the rescue experiment, morphants were screened at 28hpf and scored for the presence of a defect in the angle of the head to the tail (measured at the otic vesicle) or a deviation in the straightness of the tail (Kimmel et al., 1995). Human *CHMP1A* cDNA was PCR amplified from control human lymphoblastoid cell total RNA, using primers 5'-CCGGAAGTGGGGCGGCGACCCCG and 5'-TGTTTATTTACAACAGCATTCTA. The PCR product was subcloned into the pCS2+ vector, and 5' capped mRNA was synthesized *in vitro* using the mMESSAGE kit (Ambion). mRNA was diluted in 0.1M KCl, and titrated for the rescue experiments.

For the histological preparation, morphants were grown at 28^{o}C for 5 days, fixed overnight at 4^{o}C in paraformaldehyde (PFA), then embedded in 3% low-melt agarose blocks (in phosphate buffered saline), which were fixed again in 4% PFA/PBS overnight. The fixed agarose blocks were embedded in paraffin and sectioned at 5μm thickness in the sagittal plane. Sections were stained by standard techniques with hematoxylin and eosin, and visualized using a brightfield microscope (Nikon).

Immunocytochemistry and immunohistochemistry

NIH 3T3 and HEK293T cells were grown in DMEM with 10% (v/v) fetal bovine serum and 1% (v/v) penicillin/streptomycin, fixed and stained with antibodies against Chmp1a (1:200; Abcam, ab36679) and Bmi1 (1:250; Abcam, ab14389) using standard techniques, and visualized on a confocal microscope (Nikon).

All animal work was approved by Harvard Medical School, Beth Israel Deaconess Medical School and Children's Hospital Boston Institutional Animal Care and Use Committees.

Cerebellar granule neuron cultures were prepared as described (Bilimoria et al., 2008). Briefly, cerebella were dissected from euthanized postnatal day 5 mouse pups, meninges removed, and placed in ice cold HHGN (HBSS, 2.5mM HEPES, 35mM glucose, 4mM sodium bicarbonate, filter sterilized). The cerebella were washed with HHGN four times, then digested lightly with trypsin/DNase solution (5mL HHGN, 500μg DNase, 50mg trypsin), for 20 minutes at room temperature. The trypsin/DNase solution was removed and the cells were washed 3x with HHGN, then triturated in 8mL Basal Medium Eagle (with 800μg DNase) using a P1000 pipette until all clumps were dissociated. Cells were pelleted at 800rpm for 5min, and

resuspended slowly in 5mL plating medium (25mM KCl, 10% Hyclone bovine growth serum, in Basal Medium Eagle with 1% L-glutamine, 1% penicillin/streptomycin, filter sterilized). Coverslips coated the previous night at 4˚C with poly-L ornithine were washed 3 times with sterile water. Cell density was measured using a hemocytometer, and one million cells were plated on each coverslip with 500µL plating media, in a 24-well plate. After one day in vitro (DIV) in a 37˚C incubator, 20µL of 250µM AraC (cytosine-1-β-D-arabinofuranoside) was added to each well to arrest mitosis of non-neurons. At 2 DIV, the conditioned media was collected from each well, and the wells were washed with DMEM. The cells were then transfected with the HA-Chmp1a mammalian expression construct (EX-Mm15805-M06, GeneCopoeia). Transfection solution (87.6uL HBSS, 4.4µL of 2.5M calcium chloride, with 1.5µg of plasmid DNA) was prepared at room temperature, and 35µL of the transfection solution was added to a total of 400µL of conditioned media to each well. After 36 additional hours (4 DIV), cells were fixed with 4% paraformaldehyde for 20 minutes at room temperature, washed with PBS, and stained with antibodies against HA (1:100; Abcam, ab9110) and Bmi1 (1:250; Abcam, ab14389). Untransfected cells were processed similarly and stained with antibodies against Chmp1a (1:200; Abcam, ab36679) and Bmi1.

Tissues were perfused with 4% paraformaldehyde (PFA), dissected and fixed overnight in 4% PFA, then embedded in paraffin for sectioning. After rehydration of the slides in serial washes with xylene, 50% xylene/ethanol, 100%/70%/50%/30% ethanol, and finally PBS, the slides were boiled in antigen retrieval solution (R&D Systems) for 20 minutes. Slides were treated with PBST (PBS with 0.1% Tween-20) supplemented with 5% goat or donkey serum for 1 hour, followed by addition of antibodies against Bmi1 (1:100; Millipore, clone F6) or Chmp1a

(1:250; Abcam, ab36679 and ab104103) for overnight incubation at 4˚C. Slides were washed 3x5 minutes in PBST, then developed with secondary antibodies conjugated to Alexa Fluor dyes (Invitrogen) for 2 hours at room temperature. Slides were again washed 3x5 minutes in PBST, then mounted with Fluoromount-G (SouthernBiotech), and visualized on a confocal microscope.

Acknowledgements

We thank the patients and their families for their participation in this research. This research was supported by grants from the NINDS (2R01NS035129-12) to C.A.W., and by the Fogarty International Center (R21NS061772), Nancy Lurie Marks Family Foundation, the Dubai Harvard Foundation for Medical Research, the Simons Foundation, and the Manton Center for Orphan Disease Research. G.H.M. was supported by the Young Investigator Award of NARSAD as a NARSAD Lieber Investigator. V.S.G. is supported by the Medical Scientist Training Program of Harvard Medical School, with financial support from the NIGMS. C.A.W. and L.Z. are Investigators of the Howard Hughes Medical Institute. We thank Dr. Maarten van Lohuizen for providing the *Bmi1* knockout mice, Dr. Amy Wagers for help with breeding the *Bmi1* knockout mice, and Dr. Peter Baas for sharing patient DNA samples. Microscopy and image analyses were performed with support by the Cellular Imaging Core of the Children's Hospital Boston Intellectual and Developmental Disabilities Research Center.

References

Bilimoria, P.M. & Bonni, A. Cultures of cerebellar granule neurons. *CSH Protoc* **2008** (2008).

Brunak, S., Engelbrecht, J. & Knudsen, S. Prediction of human mRNA donor and acceptor sites from the DNA sequence. *J Mol Biol* **220**, 49-65 (1991).

Garel, C., Fallet-Bianco, C. & Guibaud, L. The fetal cerebellum: development and common malformations. *J Child Neurol* **26**, 1483-92 (2011).

Gross, S.S. & Brent, M.R. Using multiple alignments to improve gene prediction. *J Comput Biol* **13**, 379-93 (2006).

Gudbjartsson, D.F., Jonasson, K., Frigge, M.L. & Kong, A. Allegro, a new computer program for multipoint linkage analysis. *Nat Genet* **25**, 12-3 (2000).

Howard, T.L., Stauffer, D.R., Degnin, C.R. & Hollenberg, S.M. CHMP1 functions as a member of a newly defined family of vesicle trafficking proteins. *J Cell Sci* **114**, 2395-404 (2001).

Jacobs, J.J., Kieboom, K., Marino, S., DePinho, R.A. & van Lohuizen, M. The oncogene and Polycomb-group gene bmi-1 regulates cell proliferation and senescence through the ink4a locus. *Nature* **397**, 164-8 (1999).

Kent, W.J. et al. The human genome browser at UCSC. *Genome Res* **12**, 996-1006 (2002).

Kimmel, C.B., Ballard, W.W., Kimmel, S.R., Ullmann, B. & Schilling, T.F. Stages of embryonic development of the zebrafish. *Dev Dyn* **203**, 253-310 (1995).

Korf, I., Flicek, P., Duan, D. & Brent, M.R. Integrating genomic homology into gene structure prediction. *Bioinformatics* **17 Suppl 1**, S140-8 (2001).

Leung, C. et al. Bmi1 is essential for cerebellar development and is overexpressed in human medulloblastomas. *Nature* **428**, 337-41 (2004).

Molofsky, A.V. et al. Bmi-1 dependence distinguishes neural stem cell self-renewal from progenitor proliferation. *Nature* **425**, 962-7 (2003).

Rozen, S. & Skaletsky, H.J. Primer3 on the WWW for general users and for biologist programmers. . in *Bioinformatics Methods and Protocols: Methods in Molecular Biology.* (eds. Krawetz, S. & Misener, S.) 365-386 (Humana Press, Totowa, New Jersey, 2000).

Scita, G. & Di Fiore, P.P. The endocytic matrix. *Nature* **463**, 464-73 (2010).

Stauffer, D.R., Howard, T.L., Nyun, T. & Hollenberg, S.M. CHMP1 is a novel nuclear matrix protein affecting chromatin structure and cell-cycle progression. *J Cell Sci* **114**, 2383-93 (2001).

1000 Genomes Project Consortium. A map of human genome variation from population-scale sequencing. *Nature* **467**, 1061-73 (2010).

Stuchell-Brereton, M.D. et al. ESCRT-III recognition by VPS4 ATPases. *Nature* **449**, 740-4 (2007).

Tsang, H.T. et al. A systematic analysis of human CHMP protein interactions: additional MIT domain-containing proteins bind to multiple components of the human ESCRT III complex. *Genomics* **88**, 333-46 (2006).

van der Lugt, N.M. et al. Posterior transformation, neurological abnormalities, and severe hematopoietic defects in mice with a targeted deletion of the bmi-1 proto-oncogene. *Genes Dev* **8**, 757-69 (1994).

Zencak, D. et al. Bmi1 loss produces an increase in astroglial cells and a decrease in neural stem cell population and proliferation. *J Neurosci* **25**, 5774-83 (2005).

Chapter 3:

CHMP1A is implicated in neural progenitor proliferation through Wnt and Shh signaling pathways

Author Contributions

Vijay S. Ganesh primarily contributed to the project. Adriana Eisner performed the Shh luciferase experiments using constructs cloned by Vijay S. Ganesh, and Adriana Eisner and Rosalind Segal contributed to the design of the experiments. David Tischfield performed the *in utero* electroporations using constructs cloned by Vijay S. Ganesh, and Vijay S. Ganesh analyzed the results. Dilenny Gonzalez assisted in animal husbandry. Christopher A. Walsh contributed to the experimental design and oversaw the project.

Introduction

Charged multivesicular body protein/Chromatin modifying protein 1A (CHMP1A) is a member of the ESCRT-III endosomal sorting complex, but is also suggested to localize to the nuclear matrix and regulate chromatin. In the previous Chapter, we demonstrated how CHMP1A could play a role in regulating the chromatin-modifying effects of BMI1 on *INK4A*. Here we seek to explore alternative pathways implicated by Chmp1a loss-of-function. The endosomal sorting role of CHMP1A on the disease pathogenesis of pontocerebellar hypoplasia is not mutually exclusive from its role in regulating chromatin structure. Since the initial discovery of the ESCRT pathway, component proteins have been found play a crucial role in the formation of vesicles that bud away from the cytoplasm, trafficking ubiquitinated cargo to the lysosome for degradation (Hurley and Emr, 2006), or to the nucleus (Lutz et al., 2012). ESCRT-III proteins form a lattice on the endosomal membrane via N-terminal interactions, while their C-terminal domains act to recruit regulatory proteins that are required for function (such as VPS4) (McDonald et al., 2009).

It has also recently been described that ESCRT proteins also have a role in membrane abscission in the final stages of cell division, in a biophysical process not unlike its role in budding vesicles off from the plasma membrane (Wollert et al., 2009). Cytokinesis requires ESCRT-III in archaea, where ESCRT-III and VPS4 are also sufficient for membrane abscission, but it is not known if it is an absolute requirement in mammalian neurodevelopment (Lindas et al., 2008).

We sought to test if loss-of-function of *Chmp1a* in mouse has direct effects on neural development. Since ESCRT-III is involved in trafficking of membrane-bound components to the

lysosome and nucleus, it appears ideally positioned to regulate critical signal transduction steps involved in neural progenitor proliferation. Notably, Wnt and Shh pathways require the transduction of a ligand-bound membrane receptor interaction, culminating in translocation of a protein to the nucleus to affect transcription (beta-catenin in the case of canonical Wnt signaling; Gli1-3 in the case of Shh signaling) (Kim et al., 2009). Disruption of ESCRT-III may manifest is dysregulation of these canonical signaling pathways required for normal brain development. Alternatively, if the effect of Chmp1a in brain development is mostly due to its biophysical role in membrane abscission, then disruption to Wnt or Shh pathways may not be apparent.

We utilized a gene-trap line to assay for gross morphological deficits, as well as defects in cerebellar progenitor proliferation. In addition, we assayed for defects in Wnt- and Shh-stimulated transcription *in vitro* using shRNA targeted against *Chmp1a.* Our results indicate early post-natal lethality of some *Chmp1a* null mice, a decrease in brain and body size, but were unable to expose significant effects on the proliferation of cortical or cerebellar progenitor cells. However, *in vitro* assays robustly show a defect in both Wnt- and Shh-pathways in the presence of *Chmp1a* knockdown. Altogether this suggests compelling future directions in elucidating the precise role and contribution of *Chmp1a* and ESCRT-III in a cytoplasmic regulation of Wnt and Shh through multivescular bodies, perhaps in non-complementary roles to its function in Bmi1-mediated regulation of progenitor proliferation.

Methods

Chmp1a gene-trap mice

Cryopreserved sperm from a *Chmp1a*-targeting gene-trap line, B6;129P2-*Chmp1a*$^{Gt(XC472)Byg}$/Mmucd, was ordered from Bay Genomics. The gene-trap vectors used within BayGenomics contain a splice-acceptor sequence upstream of a reporter gene, β-geo (a fusion of β-galactosidase and neomycin phosphotransferase II). These vectors insert randomly into introns. The resulting insertional mutation creates a fusion transcript containing sequences from exons upstream to the insertion joined to the β-geo marker.

IVF was performed at the Beth Israel Deaconness Medical Center animal facility, with the sperm introduced into a 129sv female. The crosses of the resulting offspring were genotyped using the following PCR primers:
5'-GAGACAGCGGGTCCGTAAC, 5'-AACACACACTCGAACCGAAAG, 5'-GGTCCTAGTCGGAGGTCTCG
The gene-trap allele forms a 163bp band, whereas the wildtype band is 204bp. Mice heterozygous for the gene-trap allele will carry both bands.

Histology

To generate histopathological sections, surviving mice were sacrificed at postnatal day 20, perfused with PBS then 4% paraformaldehyde, organs carefully dissected out, then postfixed overnight in 4% paraformaldehyde. Tissues were embedded in paraffin blocks using standard techniques, then sectioned for H&E staining.

Western blotting

Postnatal day 20 mice were sacrificed, and organs harvested and flash frozen or homogenized using a pipet tip or syringe, in RIPA lysis buffer with protease and phosphatase inhibitors (Roche). Protein concentrations were measured using the BCA assay (Pierce), and western blot run using standard techniques in a 4-12% Bis-Tris Novex gel. Lysate from the spleens of homozygous genetrap, heterozygotes, and homozygous wildtype littermates were run and stained for levels of Chmp1a normalized to beta-actin. Antibodies used were chicken anti-Chmp1a (Abcam ab14389, 1:2000) and monoclonal mouse anti-beta-actin (clone AC-15, Abcam, 1:15,000).

BrdU pulse-chase in mouse cerebellum

For BrdU labeling, P6 pups were injected intraperitoneally with 100 ug BrdU/g body weight. Pups were sacked one hour later for analysis of S-phase cells, their brains dissected, fixed in 4% paraformaldehyde overnight at 4-degrees C, and processed for paraffin sectioning. Deparaffinized and rehydrated sections were treated with 4 N HCl for 10 min to denature DNA, neutralized for 5 min with 0.1 M sodium borate buffer (pH 8.5), followed by the addition of primary antibody (mouse anti-BrdU, Sigma, clone #: BU-33, 1:250 dilution). Nuclei were counterstained with DAPI. BrdU+ cells per field were counted, and averaged for all the sections through an entire folia, then compared between gene-trap (or knockout), and heterozygous or wildtype littermate controls.

shRNA construct design and cloning

Chmp1a knockdown constructs in the HuSH plasmid backbone (Origene) were cloned and tested in 3T3 cells for knockdown of co-transfected N-terminal HA-tagged Chmp1a (Genecopoeia, EX-Mm15805-M06). Clone 228 was used in subsequent experiments.

For the Shh luciferase assay, *Chmp1a* shRNA lentivirus constructs in the pLKO.2-puro backbone (Sigma) were cloned and tested against endogenous expression in 293T cells. Clone NM_145606.1-226s1c1 was used in subsequent experiments.

In utero electroporation

In utero electroporation was performed as described previously (Saito et al., 2006). Briefly, uterine horns of anesthetized pregnant dams at E13.5 were exposed through an incision in the peritoneum. DNA (3–4 mg/ml) was injected manually through the uterine wall into the lateral ventricle using pulled micropipettes. Four pulses of 40–55 V (50 ms duration) were applied across the uterine wall using a BTX ECM830 pulse generator. The uterus was then replaced in the abdominal cavity and embryonic development allowed to proceed normally, until E17.5, when the mother was sacrificed and the embryos dissected, drop fixed in 4% PFA, and subsequently embedded in paraffin for sectioning.

Wnt luciferase assay

Wnt luciferase assays were performed as described previously (Mao et al., 2009). Briefly 5x10^5 293T cells were seeded into 24-well plates and transfected with 0.8 μg of Super8XTOPFLASH or Super8XFOPFLASH (negative control) and 0.1 μg of pRL-TK using

Lipofectamine 2000 (Invitrogen). 24 hours after transfection, transfected cells were stimulated with Wnt3a-conditioned medium (Wnt3a CM) for 14 hours and TCF reporter activity was measured using the Dual-Luciferase Assay System (Promega). For the negative control experiments, 1.6 μg of β-catenin shRNA vector was transfected, or the *Chmp1a* shRNA plasmid cotransfected with 0.4 μg of at N-terminal beta-catenin binding site-deficient high mobility group (TCFdeltaN) construct using Lipofectamine 2000, and transfected cells were treated with Wnt3a (200 ng/ml). All firefly luciferase activities were normalized with Renilla luciferase activity.

Shh luciferase assay

Shh luciferase assays were performed using viral infection of Shh Light II cells (ATCC). Shh Light II is an NIH/3T3-derived cell line in 1999 (Sasaki et al., 1997), a Zeocin-selectable stable cell line with GLI-responsive Firefly luciferase reporter, pSV-Neo, pRL-TK constituitive Renilla-luciferase expression vector, and pVgRXR vector. It is compatible with the Dual-Luciferase reporter system (Promega). 50,000 cells were plated per 24-well plate along with pLKO-packaged lentiviruses carrying either scrambled control, target shRNA, LacZ-targeting shRNA (negative control), or Smo-targeting shRNA (negative control) plasmids. The cells were treated with puromycin selection after 24 hours, then treated the next day with Smoothened agonist (SAG) or vehicle control. After three days the cells were lysed and analyzed for renilla and firefly expression using a plate reader (Molecular Devices).

Results

Chmp1a gene-trap mice surviving perinatal lethality show defects in brain and body size

The vast majority of *Chmp1a* gt/gt mice did not survive the perinatal period between postnatal day zero (P0) and P8 (**Figure 3.1a**). Genotyping results at P20 of surviving mice demonstrate a substantial reduction in gt/gt homozygotes. At P0, 18% of pups are recovered and genotyped as gt/gt. In the P20 mice, protein levels of Chmp1a from spleen lysates show a doublet at the expected size (**Figure 3.1b**), and a faint level of Chmp1a expression in the gt/gt spleen, but far below wildtype levels. The brain and body size of the gt/gt mice are reduced compared to wildtype littermate controls, however the brain:body ratio is not substantially reduced (**Figure 3.1c**). Parasagittal sections of gt/gt mouse brain at P20 shows a modest decrease in overall brain size, perhaps slightly more of a decrease in cortical volume, but the cerebellum is not proportionally smaller (**Figure 3.1d,e**). No gross malformation or abnormality is apparent on histology.

Figure 3.1

***Chmp1a* gt/gt mice show perinatal lethality and reduced brain and body size.**

(a) The fraction of recovered mouse pups by their genotype, at the corresponding litter age shows a decrease in gt/gt survival in the postnatal period. (b) Chmp1a lysate levels from +/+, +/gt, and gt/gt P20 mouse spleen shows a substantial but not complete reduction in gt/gt on Western blot. Parallel lanes were loaded using 20ug or 50ug of total lysate. Beta-actin (Actb) was used as a loading control. (c) Both brain and body mass of the *Chmp1a* gt/gt mouse at P20 is reduced compared to littermate controls, however the brain:body ratio is not substantially changed in gt/gt. (d-e) H&E-stained sections of *Chmp1a* +/gt and *Chmp1a* gt/gt from comparable parasagittal planes shows a mild decrease in cortex and cerebellar size in the gt/gt mouse, without grossly apparent changes in morphology or cerebellar foliation.

Figure 3.1 (Continued)

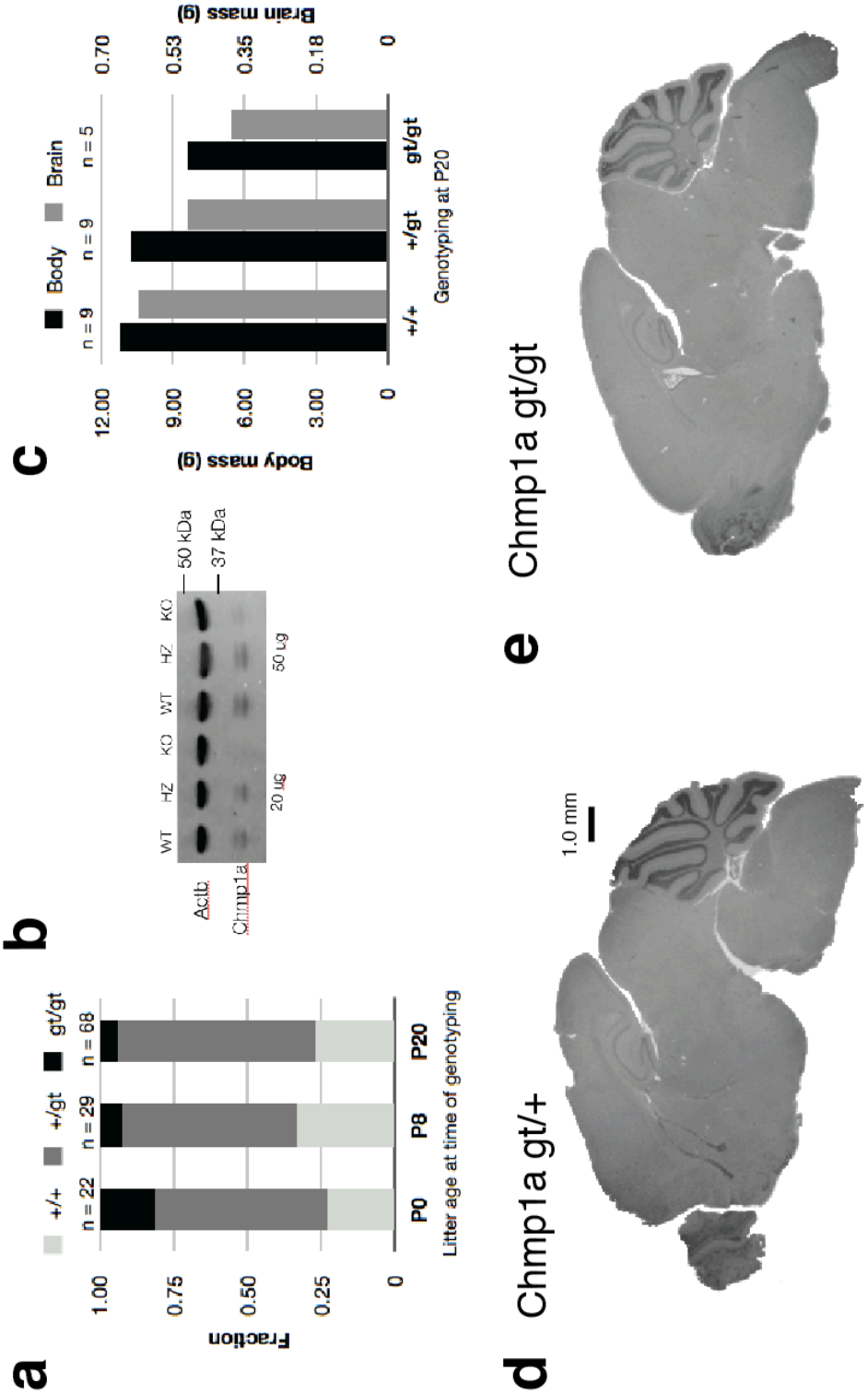

Chmp1a gene-trap mice show no profound defect in cortical or cerebellar proliferation

To more closely interrogate a possible subtle deficit on cerebellar granule cell proliferation in the *Chmp1a* gt/gt mice, we performed a BrdU pulse-chase experiment at P6. Compared to *Bmi1-/-* mice, which show a nearly 50% reduction in cells in S-phase in a given cerebellar field, *Chmp1a* gt/gt mice show a mild but not significant reduction (**Figure 3.2a**). Since the proportion of cells in S-phase is sensitive to the postnatal age, we repeated the experiment in another P6 litter, with similar results (**Figure 3.2a**).

To test for a role in cortical progenitor proliferation, we performed *in utero* electroporations in embryonic mice at E13.5, using shRNA constructs targeted against *Chmp1a*. GFP-positive transfected cells were counted in E17.5 brain sections (**Figure 3.2b**). The ratio of cells in the VZ/SVZ to the total number of cells in a radial column is a sensitive proxy for defects in the maintenance of cell proliferation and premature neuronal differentiation. In *Chmp1a* gt/gt embryos there is no significant change in the distribution of GFP-positive cells in the cortex compared to control (shRNA plasmid targeted against firefly luciferase) (**Figure 3.2b**).

Figure 3.2

***Chmp1a* loss-of-function shows no significant difference in cerebellar granule cell or cortical progenitor proliferation.**

(a) BrdU-positive cells per field were counted and average from sections of P6 cerebella from the *Bmi1-/-, Bmi1+/- , Chmp1a* +/gt, and *Chmp1a gt/gt* mice injected with intraperitoneal BrdU for 60 minutes. *Bmi1-/-* show a 50% reduction in cells in BrdU-positive cell fraction compared to heterozygous littermate controls, whereas a mild but not significant reduction is seen in *Chmp1a gt/gt.* (b) Representative images of E17.5 cortices from E13.5 electroporated embryos are shown on left. Quantification of GFP-positive cells is shown on the right. Dotted lines demarcate the boundary between the VZ/IZ and IZ/CP. LV = lateral ventricle, CP = cortical plate, VZ = ventricular zone, IZ = intermediate zone. pSil-Luci or Luci = pSilencer targeting firefly luciferase (positive control). pSil-shRNA-228 or 228 = pSilencer construct targeting *Chmp1a.* Error bars = S.E.M.

Figure 3.2 (Continued)

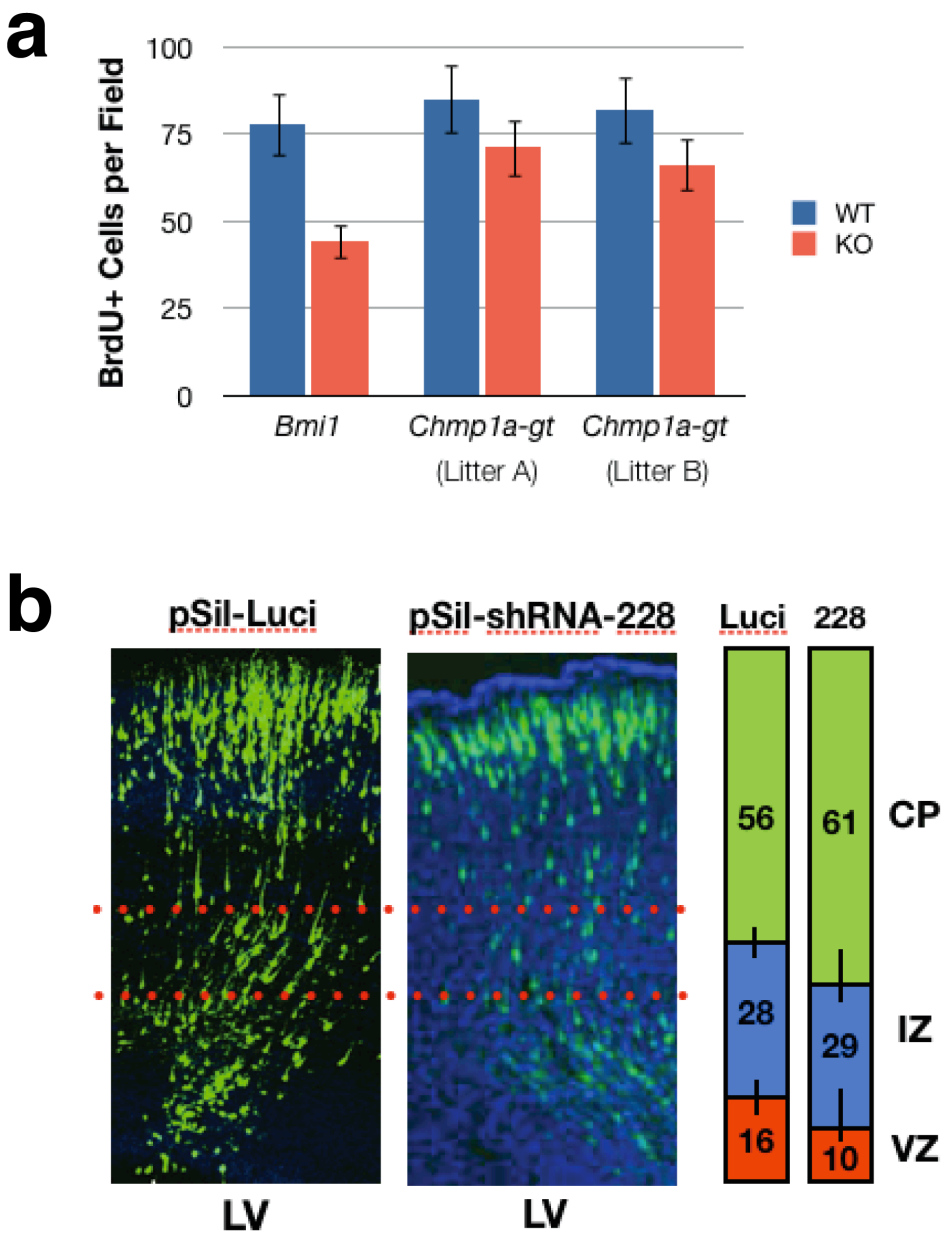

In vitro assays of *Chmp1a* knockdown show defects in Wnt- and Shh-pathway signal transduction

Given the possibility that small but detectable levels of protein in the *Chmp1a* gt/gt mice could be compensating for a true null phenotype, we explored *in vitro* approaches to probe the effects of *Chmp1a* knockdown. To assay for a role in Shh-stimulated signal transduction, we infected Shh Light II cells (ATCC) with lentivirus targeted against *Chmp1a*, and compared the effects on Gli1-luciferase transcription to negative controls (lentivirus containing scrambled shRNA, or targeted against LacZ) and a positive control (lentivirus targeted against Smo). Results of the stimulation with a Smoothened agonist (SAG, Millipore) were compared to unstimulated trials using vehicle. *Chmp1a* knockdown substantially decreased SAG-stimulated Gli1 transcription, with nearly 50% reduction in activity compared to an untargeted lentivirus (**Figure 3.3a**).

To discern the role of *Chmp1a* in regulating the Wnt pathway, we measured Wnt-activated transcription in the presence of reduced *Chmp1a* levels. We transfected 293T cells with our control or shRNA knockdown construct and a luciferase reporter construct containing eight copies of the TCF/LEF-binding site (8XSuperTOPFLASH), which can be bound and activated by a core component of the Wnt signaling pathway, beta-catenin (Molenaar et al. 1996). We confirmed that shChmp1a expression resulted in a significant decrease in Wnt- mediated luciferase reporter activation compared with controls (**Figure 3.3b**). This effect was titratable depending on the dose of shRNA (between 1.0 and 50ng of plasmid per well) (**Figure 3.3b**).

Figure 3.3

***Chmp1a* shRNA decreases both Wnt-activated and Shh-activated transcription.**

(a) Shh Light II stable cell lines containing Gli1-luciferase and dual-luciferase reporter constructs show a substantial decrease in Smoothened agonist (SAG) stimulated Gli1-luciferase transcription in the presence of *Chmp1a* shRNA lentivirus (shChmp1a) compared to lentivirus with a scrambled shRNA. The extent of induction of the pathway with no virus is shown at left. shLacZ is a negative control lentivirus containing shRNA targeting LacZ. shSmo is a positive control lentivirus containing shRNA against endogenous Smoothened. Similarly panel (b) shows the dual-luciferase reporter assay in 293T cells using Wnt3a conditioned medium (Wnt CM) to measure TCF/LEF-luciferase activity. Normalized to the induction seen with Wnt CM in the scrambled control, transfection with shRNA targeting *Chmp1a* shows a titratable decrease in Wnt-induced transcription (shChmp1a01 = 1.0ng HuSH plasmid (Origene) per well; shChmp1a50 = 50ng). shBcat = shRNA targeting beta-catenin, shChmp1a50+TCFdeltaN = cotransfection of shRNA targeting Chmp1a with an uninducible TCF/LEF-luciferase construct.

Figure 3.3 (Continued)

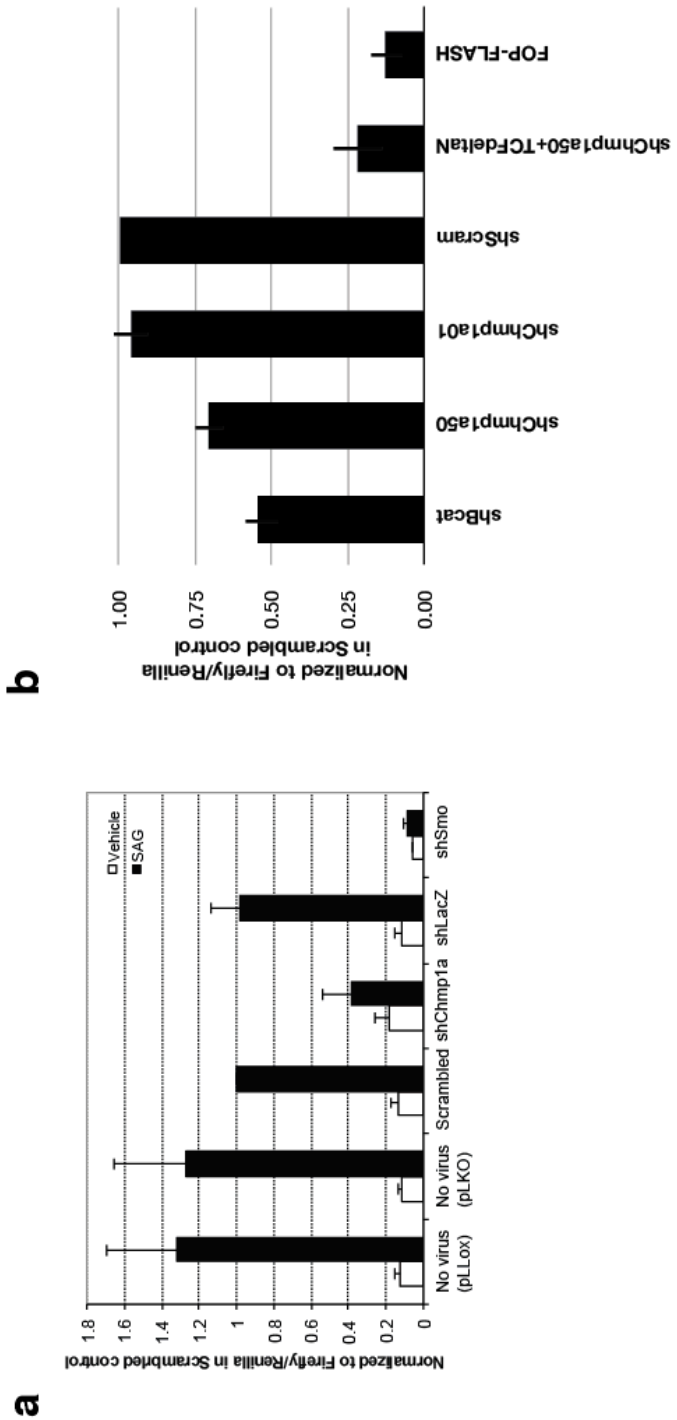

Discussion

While the surviving homozygous gene-trap *Chmp1a* mice described here have reduced brain and body size, the degree of cerebellar and cortical volume reduction is not as remarkable as seen in human patients with loss-of-function mutations to *CHMP1A* (Chapter 2), or as severe as in the *Bmi1-/-* mouse. Several explanations could reconcile this difference. First, the *Chmp1a* gene-trap mouse is derived from a mixed background of B6, 129P2, and 129sv, while the *Bmi1* mouse is in a pure background of C57Bl6. Inbred mouse strains vary widely in their behavior and brain size (Wahlsten et al., 2006; Sandberg et al., 2000; Inouye et al., 1980). Backcrossing the *Chmp1a*-gt line to a C57Bl6 background (ongoing), is one approach to resolving possible confounding strain-specific effects. Second, there is evidence of faint expression of normal-sized Chmp1a in the gt/gt spleen (**Figure 3.1b**), suggesting the possibility of some transcript escaping the En2 splice acceptor of the gene-trap. The overall levels are less than 1% of endogenous, however small amounts of Chmp1a could be sufficient to rescue any severe phenotype. Of note, the only human disease alleles identified to-date are complete loss-of-function; it is possible that hypomorphic alleles do not manifest with disease pathology. Third, the mice analyzed for histology and proliferative defects, by definition, survived the postnatal period where the lethality of the gt/gt haplotype appears most severe (**Figure 3.1a**). Other alleles on modifier genes could explain why the gt/gt mice that survive to P20 appear "rescued". Future work on characterizing the gt/gt mice at P0 could expose a more severe defect in an animal that would not survive the postnatal period. One human patient with homozygous *CHMP1A* mutations, CH2701, had severe feeding difficulty after birth with failure-to-thrive, and would not have survived if a percutaneous endoscopic gastronomy (PEG) tube was not placed. It is possible that

the *Chmp1a* gt/gt mice also have difficulty with peristalsis or feeding, and as a result are cannibalized by the mother.

The subsequent inability to demonstrate a defect in BrdU-incorporation in P6 pups (**Figure 3.2a**), or a defect in cortical progenitor proliferation or migration (**Figure 3.2b**), could be secondary to the reasons outlined above. In addition, the degree of microcephaly in the human *CHMP1A* patients suggests a mild deficit. *In utero* electroporation may not be sensitive enough to expose an analogously mild phenotype in the mouse. On the other hand, *Bmi1* shRNA electroporation at E13.5 showed a severe defect, disrupting nearly half of all cortical progenitors, out of proportion to the degree of microcephaly expected from the *Bmi1* knockout studies (Fasano et al., 2007; Zencak et al., 2005; Jacobs et al., 1999).

By contrast to the mild effects seen in the *Chmp1a* gt/gt mouse and *Chmp1a in utero* RNAi, knockdown of *Chmp1a in vitro* shows pronounced dampening of both Wnt- and Shh-stimulated transcriptional activity (**Figure 3.3**). Recent compelling evidence suggests that multivesicular bodies (MVBs) are critical for glycogen synthase kinase 3 (GSK3) sequestration, and that GSK3 is a "master regulator" of Wnt, Shh, and other signaling pathways to maintain neural progenitor proliferation (Taelman et al., 2010; Kim et al., 2009). The biochemical details of this model have been worked out in more detail with respect to Wnt signaling, whereby MVBs (through ESCRT-mediated processes) sequester Wnt-bound receptor complexes (of which GSK3 is member) inside endosomes, thereby preventing GSK3 from degrading beta-catenin. Accumulating beta-catenin effectively serves to maintain progenitor proliferation. Therefore defects in MVB sequestration of GSK3 would be predicted to lead to decreased levels of cytosolic beta-catenin, and decreased TCF/LEF transcription. Our data on decreased Wnt-

stimulated TCF/LEF-luciferase activity in the presence of *Chmp1a* shRNA, is consistent with this model (**Figure 3.3b**).

Defects in Shh-signaling with *Chmp1a* shRNA as shown in our data could provide an explanation for the cerebellar hypoplasia in patients lacking functional CHMP1A. Shh is a key mitogen for cerebellar granule cell proliferation (Wechsler-Reya et al., 1999; Hatten et al., 2011). Purkinje cells release Shh to control proliferation of the granule cell progenitors (Dahmane et al., 1999; Wang et al., 2001), and levels of Shh control the complexity of cerebellar foliation (Corrales et al., 2006). However, defects in Wnt3 also contribute to cerebellar patterning, and could contribute to the patient phenotype without invoking Shh. During the final maturation of Purkinje cells, elaborate dendritic arbors form trophic synapses on granule cells, and this process of crosstalk between the granule cells and Purkinje cell appears to involve Wnt3 (Salinas et al., 1994; van Amerongen et al., 2006).

In summary, we provide *in vitro* evidence that knockdown of *Chmp1a* disrupts both Wnt- and Shh-induced transcriptional pathways, and that these effects may contribute to the cortical and cerebellar phenotype in patients harboring *CHMP1A* mutations through its cytoplasmic role in MVB formation. These effects may be entirely independent from the role of Chmp1a in regulation of proliferation through Bmi1-*Ink4a*.

References

Corrales, J. D., Blaess, S., Mahoney, E. M., & Joyner, A. L. (2006). The level of sonic hedgehog signaling regulates the complexity of cerebellar foliation. Development (Cambridge, England), 133(9), 1811–1821. doi:10.1242/dev.02351

Dahmane, N., & Ruiz i Altaba, A. (1999). Sonic hedgehog regulates the growth and patterning of the cerebellum. Development (Cambridge, England), 126(14), 3089–3100.

Fasano, C. A., Dimos, J. T., Ivanova, N. B., Lowry, N., Lemischka, I. R., & Temple, S. (2007). shRNA knockdown of Bmi-1 reveals a critical role for p21-Rb pathway in NSC self-renewal during development. Cell Stem Cell, 1(1), 87–99. doi:10.1016/j.stem.2007.04.001

Hatten, M. E., & Roussel, M. F. (2011). Development and cancer of the cerebellum. Trends in neurosciences, 34(3), 134–142. doi:10.1016/j.tins.2011.01.002

Hurley, J. H., & Emr, S. D. (2006). The ESCRT complexes: structure and mechanism of a membrane-trafficking network. Annual review of biophysics and biomolecular structure, 35, 277–298. doi:10.1146/annurev.biophys.35.040405.102126

Inouye, M., & Oda, S. I. (1980). Strain-specific variations in the folial pattern of the mouse cerebellum. The Journal of Comparative Neurology, 190(2), 357–362. doi:10.1002/cne.901900209

Jacobs, J. J., Kieboom, K., Marino, S., DePinho, R. A., & van Lohuizen, M. (1999). The oncogene and Polycomb-group gene bmi-1 regulates cell proliferation and senescence through the ink4a locus. Nature, 397(6715), 164–168. doi:10.1038/16476

Kim, W.-Y., Wang, X., Wu, Y., Doble, B. W., Patel, S., Woodgett, J. R., & Snider, W. D. (2009). GSK-3 is a master regulator of neural progenitor homeostasis. Nature neuroscience, 12(11), 1390–1397. doi:10.1038/nn.2408

Lindås, A.-C., Karlsson, E. A., Lindgren, M. T., Ettema, T. J. G., & Bernander, R. (2008). A unique cell division machinery in the Archaea. Proceedings of the National Academy of Sciences of the United States of America, 105(48), 18942–18946. doi:10.1073/pnas.0809467105

Lutz, D., Wolters-Eisfeld, G., Joshi, G., Djogo, N., Jakovcevski, I., Schachner, M., & Kleene, R. (2012). Generation and Nuclear Translocation of Sumoylated Transmembrane Fragment of Cell Adhesion Molecule L1. Journal of Biological Chemistry, 287(21), 17161–17175. doi:10.1074/jbc.M112.346759

Macdonald, B. T., Tamai, K., & He, X. (2009). Wnt/beta-catenin signaling: components, mechanisms, and diseases. Developmental cell, 17(1), 9–26. doi:10.1016/j.devcel.2009.06.016

Mao, Y., Ge, X., Frank, C. L., Madison, J. M., Koehler, A. N., Doud, M. K., Tassa, C., et al. (2009). Disrupted in schizophrenia 1 regulates neuronal progenitor proliferation via modulation of GSK3beta/beta-catenin signaling. Cell, 136(6), 1017–1031. doi:10.1016/j.cell.2008.12.044

Saito, T. (2006). In vivo electroporation in the embryonic mouse central nervous system. Nature Protocols, 1(3), 1552–1558. doi:10.1038/nprot.2006.276

Salinas, P. C., Fletcher, C., Copeland, N. G., Jenkins, N. A., & Nusse, R. (1994). Maintenance of Wnt-3 expression in Purkinje cells of the mouse cerebellum depends on interactions with granule cells. Development (Cambridge, England), 120(5), 1277–1286.

Sandberg, R., Yasuda, R., Pankratz, D. G., Carter, T. A., Del Rio, J. A., Wodicka, L., Mayford, M., et al. (2000). Regional and strain-specific gene expression mapping in the adult mouse brain. Proceedings of the National Academy of Sciences of the United States of America, 97(20), 11038–11043.

Sasaki, H., Hui, C., Nakafuku, M., & Kondoh, H. (1997). A binding site for Gli proteins is essential for HNF-3beta floor plate enhancer activity in transgenics and can respond to Shh in vitro. Development (Cambridge, England), 124(7), 1313–1322.

Taelman, V. F., Dobrowolski, R., Plouhinec, J.-L., Fuentealba, L. C., Vorwald, P. P., Gumper, I., Sabatini, D. D., et al. (2010). Wnt signaling requires sequestration of glycogen synthase kinase 3 inside multivesicular endosomes. Cell, 143(7), 1136–1148. doi:10.1016/j.cell.2010.11.034

van Amerongen, R., & Berns, A. (2006). Knockout mouse models to study Wnt signal transduction. Trends in genetics : TIG, 22(12), 678–689. doi:10.1016/j.tig.2006.10.001

Wahlsten, D., Bachmanov, A., Finn, D. A., & Crabbe, J. C. (2006). Stability of inbred mouse strain differences in behavior and brain size between laboratories and across decades. Proceedings of the National Academy of Sciences of the United States of America, 103(44), 16364–16369. doi:10.1073/pnas.0605342103

Wang, V. Y., & Zoghbi, H. Y. (2001). Genetic regulation of cerebellar development. Nature reviews Neuroscience, 2(7), 484–491. doi:10.1038/35081558

Wechsler-Reya, R. J., & Scott, M. P. (1999). Control of neuronal precursor proliferation in the cerebellum by Sonic Hedgehog. Neuron, 22(1), 103–114.

Wollert, T., Wunder, C., Lippincott-Schwartz, J., & Hurley, J. H. (2009). Membrane scission by the ESCRT-III complex. Nature, 458(7235), 172–177. doi:10.1038/nature07836

Zencak, D., Lingbeek, M., Kostic, C., Tekaya, M., Tanger, E., Hornfeld, D., Jaquet, M., et al. (2005). Bmi1 loss produces an increase in astroglial cells and a decrease in neural stem cell population and proliferation. The Journal of neuroscience : the official journal of the Society for Neuroscience, 25(24), 5774–5783. doi:10.1523/JNEUROSCI.3452-04.2005

Chapter 4:

Genetic architecture and asymmetries of human polymicrogyria

Adapted from a manuscript in preparation:

Vijay S. Ganesh[1,3*], Annapurna Poduri[1,2*], Tim W. Yu[1], R. Sean Hill[1], Christina P. El Hosary[1], Jacqueline Rodriguez[1], Brenda J. Barry[1], Jennifer N. Partlow[1], Wen-Hann Tan[1], Jill M. Gotoff[4], A. James Barkovich[5], Christopher A. Walsh[1,2]

1 Division of Genetics, Manton Center for Orphan Disease Research and Howard Hughes Medical Institute, Department of Medicine, Children's Hospital Boston, Boston, MA, USA
2 Division of Epilepsy and Clinical Neurophysiology, Department of Neurology, Children's Hospital Boston, Boston, MA USA
3 Harvard-MIT Division of Health Sciences and Technology, Cambridge, MA, USA
4 Department of Pediatric Neurology and Clinical Neurophysiology, Geisinger Medical Center, Danville, PA USA
5 Department of Radiology and Biomedical Imaging, University of California, San Francisco, San Francisco, CA, USA

* These authors contributed equally to the work.

Author Contributions

V.S.G. and A.P. designed the study. V.S.G. analyzed the sequencing data, helped build the annotation pipeline, and wrote the manuscript. A.P. interpreted clinical information and brain MRI, helped analyze the sequencing data, and wrote the manuscript. T.W.Y. assisted with the annotation pipeline and analyzing the variants. C.P.E. and J.R. performed Sanger resequencing. R.S.H. helped organize genetic data and calculate LOD scores. B.J.B. and J.N.P. organized clinical information and patient samples. W.H.T. and L.J.G. provided clinical information. A.J.B. interpreted brain MRI of the patients. C.A.W. directed the overall research and wrote the manuscript.

Introduction

Polymicrogyria (PMG) is a highly epileptogenic congenital malformation of cortical development characterized by the appearance of excessive small folds of the cerebral cortex on neuroimaging, and pathological evidence of abnormal neuronal organization. Most patients with polymicrogyria present with epilepsy in childhood - often refractory to standard medical treatment - along with intellectual disability, motor dysfunction and speech disturbances (Inder et al., 1999). The severity of the clinical presentation and age at presentation depend mostly upon the extent of cortical involvement (Barkovich, 2010).

Polymicrogyria appears to be a highly heterogeneous disorder in terms of its pathogenesis, distribution, and pathological and radiographic features. It can affect variable portions of the cerebral cortex, and may be unilateral, bilateral, or asymmetrical. The most common location is around the sylvian fissure, particularly the posterior aspect of the fissure (Leventer, 2007). However, any part of the cerebral cortex, including the frontal, occipital, and temporal lobes, can be affected (Guerrini et al., 1997). Polymicrogyria may be an isolated malformation or it may be associated with other brain malformations, such as corpus callosum agenesis and hypogenesis, cerebellar hypoplasia (Barkovich et al., 2007), or periventricular or subcortical heterotopia (Wieck et al., 2005). Affected patients range from microcephalic, to normocephalic, to macrocephalic (Dobyns et al., 2008).

From its histopathological pattern, polymicrogyria is considered a disorder of cortical organization, since the disruption is consistent with perturbations to late-stage neuronal migration. However a definitive etiology remains unclear (Barkovich et al., 2005). Evidence for both genetic and non-genetic etiologies exists. Polymicrogyria can be induced by *in utero*

ischemic events and can be seen secondary to congenital infections such as cytomegalovirus (Levine et al., 1974). Polymicrogyria has a range of histologic appearances, all having in common a disorganization of the normal six-layered lamination of the cortex and fusion of the molecular layer across sulci (Barkovich et al., 1992).

Despite strong evidence for the heritability of polymicrogyria, their extreme heterogeneity and the confounding influence of non-genetic contributing forces (such as infection and ischemia) makes identifying genetic causes difficult. Nevertheless, using highly informative multiplex families, and organizing cases into clinical and radiographic subtypes in the hope of finding a cohort that shares a molecular defect, allows for a way forward in elucidating the genetics of this complex disease.

Genes and loci for polymicrogyria

Polymicrogyria has been associated with several chromosomal deletion and duplication syndromes including the common deletion 22q11.2 (DiGeorge) syndrome (Robin et al., 2006; Dobyns et al., 2008). A genetic basis for some forms of polymicrogyria has been proposed based on reports of familial recurrence consistent with autosomal dominant, autosomal recessive, or X-linked inheritance (Guerreiro et al., 2000). Three loci of interest for the bilateral perisylvian form of polymicrogyria have been identified on chromosome X (Villard et al., 2002; Santos et al., 2008), yet only one polymicrogyria patient mutation has been identified for any gene in these loci, the *SRPX2* gene at Xq22 (Roll et al., 2006).

Autosomal recessive polymicrogyria genes include *GPR56*, *RAB3GAP1* and *RAB3GAP2* (all three associated with bilateral fronto-parietal polymirogyria), *TUBA1A* (associated with perisylvian polymicrogyria), and *LAMC3* (associated with occipital polymicrogyria), among others (reviewed in Manzini and Walsh, 2011). Mutations in *TUBB2B* have recently been identified in four patients with asymmetric polymicrogyria, and functional studies suggest that this gene is required for neuronal migration (Jaglin et al., 2009). The identification of these genes offered the tantalizing possibility that the heterogeneous polymicrogyrias could be discrete entities in which a single genetic lesion correlates with a specific regional disruption in the cortex. Other more severe syndromes in which polymicrogyria is one feature have been described with mutations to *EOMES, PAX6, COL18A1,* and *KIAA1279* (**Table 4.1**), but still the vast majority of cases of polymicrogyria have yet to be explained by specific gene mutations. On the basis of these findings we hypothesized (1) that there are still many additional genetic causes for this genetically heterogeneous and epileptogenic malformation, and (2) that the identification and study of new genes for well-phenotyped, regionally specific forms of polymicrogyria will shed further light on the intricate and detailed processes that govern the organization of the human brain and lead to epilepsy when they are perturbed.

Asymmetric polymicrogyria

The most common form of polymicrogyria is that which occurs in the perisylvian regions, accounting for 60-70% of all cases (Leventer et al., 2001). Approximately 80% of perisylvian polymicrogyria is bilateral, though in the asymmetric cohort there are a few cases that are strikingly unilateral (Guerrini, 2010; Chang et al., 2006). The Sylvian fissure is a

particularly interesting structure that demarcates the separation between the temporal, frontal, and parietal lobes. The fissure forms between the inferior frontal lobe and superior temporal lobe. In a process called “operculization”, the developing insular cortex indents and is surrounded by the developing frontal, temporal, and parietal lobes (Quarello et al., 2008). Identifying genes that regulate the intricate biophysical steps involved in the folding of the Sylvian fissure may yield insight into the developmental biology human brain left-right asymmetry.

We focused our attention on the asymmetric cases within our collection of familial, or suspected familial, polymicrogyrias. We show that the asymmetric and unilateral cases are strongly biased towards right-predominant polymicrogyria. Using whole-exome sequencing in patients with polymicrogyria, we identify rare mutations in two primary microcephaly genes, *ASPM* and *WDR62*. Interestingly, some of these patients lack profound microcephaly, suggesting heretofore underappreciated pleiotropic effects of these centrosomal genes

Methods

Human studies

All human studies were reviewed and approved by the institutional review board of the Children's Hospital Boston, Beth Israel Deaconess Medical Center, and local institutions.

Patient recruitment

Consanguineous families were collected through the Children's Hospital Boston Brain Development and Genetics clinic, with referral centers in Turkey, Saudi Arabia, Kuwait, United Arab Emirates, Egypt, Oman, Jordan, and Pakistan. Inclusion criteria included a diagnosis of polymicrogyria or perisylvian syndrome by a neurologist or neuroradiologist, and multiple affected children and/or suspected consanguinity (first or second cousins). 54 families were recruited in total. Patients were phenotyped using staging criteria by A.J.B. We performed more extensive analysis of selected families that were most informative genetically.

Genome-wide linkage and homozygosity scans

Genome-wide SNP screens were performed at the Broad Institute and Dana Farber Institute. Families were genotyped using Affymetrix 500K (NspI/Sty) or Affymetrix 6.0 microarrays. Single- and multipoint LOD scores were calculated using Allegro, assuming a recessive mode of disease inheritance, full penetrance, and a disease allele frequency of 0.0001. Runs of homozygosity were determined using custom Perl scripts, allowing for no more than 2 consecutive heterozygous SNPs in a run and 3 heterozygous calls in every 10 consecutive SNPs.

Intervals homozygous for the same haplotype and shared by all affected individuals were used to narrow the locus in each family.

Copy number variant analyses

CNV analyses were performed using Birdsuite, PennCNV, Nexus and Affymetrix Genotyping Console. Criteria for CNV calling included the intersection of two or more algorithms, 10 or more probes (15 for Affymetrix 6.0 samples) and size >100 kb. Samples with a very large number of calls (120) were rejected, as they are typically the result of poor DNA hybridization. After CNV calling, results were compared to a reference catalog generated from 1258 HapMap samples and filtered to remove common variants.

Whole exome sequencing and data analysis

DNA samples were sequenced at the Broad Institute or Axeq. Whole blood DNA was subject to barcoded exome capture (SureSelect v2, Agilent Technologies, Inc., Santa Clara, CA) and single-end sequencing (Illumina, read length of 36 bp). Whole exome sequence was obtained on 35 affected children, with a mean target coverage of 85.6% at >=20X and a read depth of 158X.

Reads were processed using Picard and aligned using BWA to hg19. Variant calling was performed with the GATK software suite at the Broad Institute. Variants were filtered according to standard GATK variant quality score recalibration thresholds. On average 38,148 SNPs and 5,569 indels were called per sample. Variants were then annotated more fully with respect to predicted molecular effect, pathogenicity (SIFT, PolyPhen2) and presence in public databases

using Annovar and a series of custom scripts (Kumar et al., 2009; Adzhubei et al., 2010). Reported pathogenic variants were confirmed by Sanger sequencing.

Sanger resequencing

Sequencing by capillary electrophoresis was performed according to standard molecular biology practices at SeqWright, Inc. (Houston, Texas).

Results

Asymmetric perisylvian polymicrogyria is biased towards right-predominant cases

The clinical presentation of right-sided polymicrogyria does not appear to be more severe than the equally disrupted left-sided malformation, therefore ascertainment bias does not appear to confound an analysis of the asymmetries of perisylvian polymicrogyria. From our patient cohort that received high-quality MRIs, in which the extent of the malformation could be measured within and between each hemisphere, there appears to be a strong right-sided bias (**Figure 4.1a-g**). This bias is evident in those cases where the polymicrogyria was bilateral but asymmetric in its severity, with approximately a 3:1 ratio between right-predominant and left-predominant cases (**Figure 4.1h,** $p < 0.01$ using a two-tailed Pearson's chi-squared test). This ratio is even more biased towards the right side in the unilateral cases (**Figure 4.1h**; $p < 0.001$ using a two-tailed Pearson's chi-squared test).

Whole-exome sequencing identifies novel variants to known PMG genes

Since the presence of recurrent inherited and *de novo* CNVs could potentially confound a recessive analysis, we excluded families harboring rare, large, CNVs. Using whole-exome sequencing in the remaining cohort, we processed the samples using a pipeline described in the methods and schematized in **Figure 4.2**. We first screened known polymicrogyria genes under non-recessive inheritance, annotating 14 genes with evidence linking them to polymicrogyria (**Table 4.1**). Since we sought to define the contribution of rare, highly penetrant risk alleles to polymicrogyria in our cohort, we prioritized variants based on rarity (minor allele frequency, MAF <1% in known databases and our own dataset of 831 Middle Eastern individuals),

predicted protein effect (nonsense/frameshift, splice-altering, missense), and inheritance pattern (*de novo*, or segregating in the family in a manner consistent with X-linked or autosomal dominant inheritance). We first filtered for variants in known PMG genes, in regions of large haplotype blocks shared by all the affected individuals in the family (blocks determined from Affymetrix SNP arrays). From this analysis we identified novel variants in five different genes previously linked to polymicrogyria, that segregated with disease in the pedigrees (**Table 4.2**).

Figure 4.1

Examples of right-sided unilateral polymicrogyria.

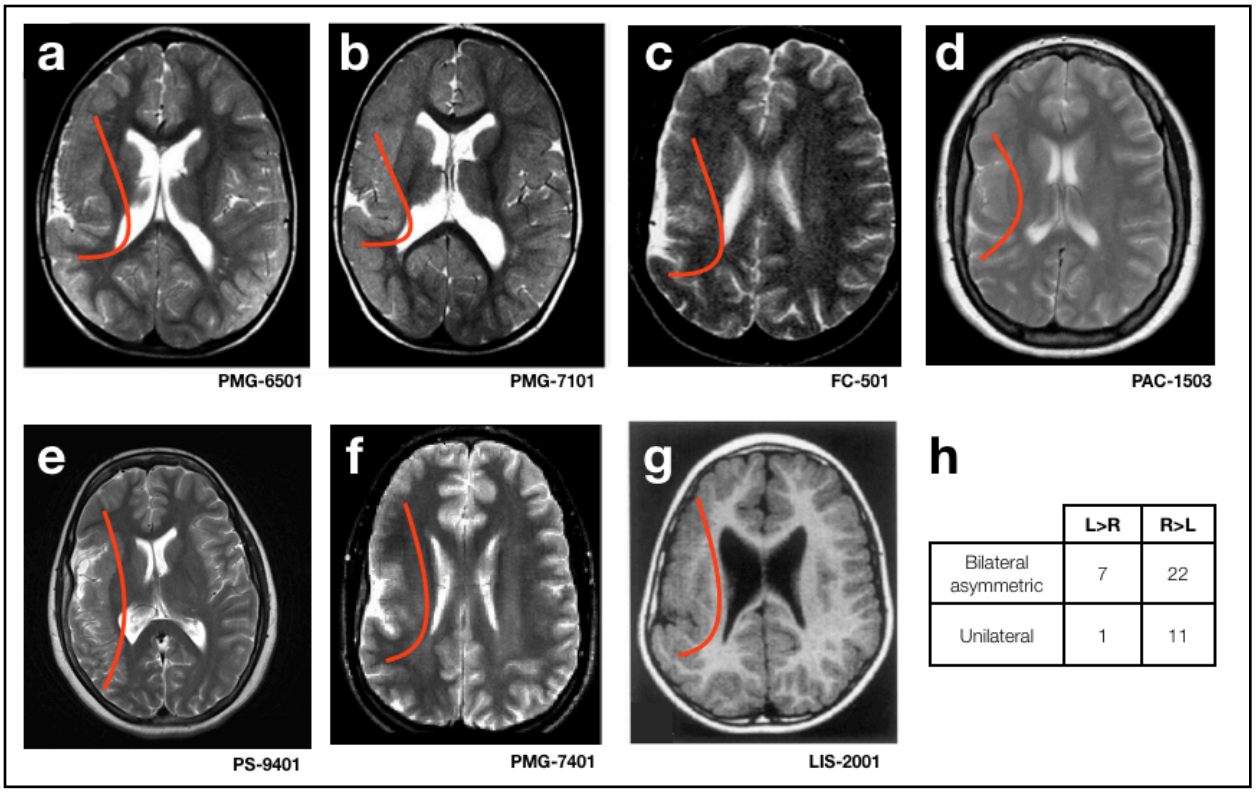

	L>R	R>L
Bilateral asymmetric	7	22
Unilateral	1	11

(a-g) Representative axial images from selected cases of right-sided unilateral polymicrogyria. Regions of polymicrogyria are outlined in red.

(h) Classification of the asymmetric polymicrogyria cases with high-quality MRI into bilateral and unilateral, and right-sided or left-sided predominant.

Figure 4.2

Schematic of whole-exome sequencing pipeline and variant annotation.

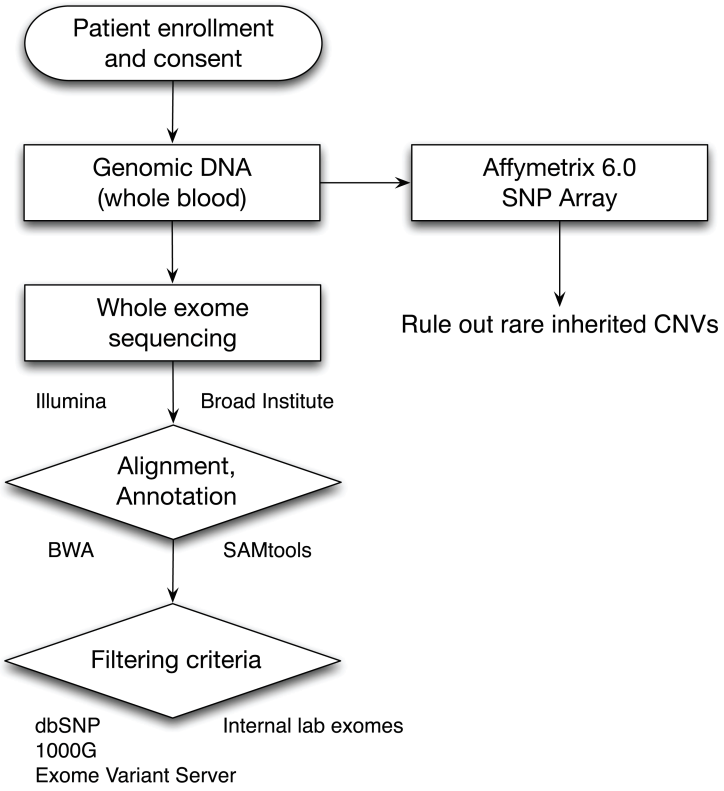

The internally developed pipeline for whole-exome variant analysis begins with patient consent and recruitment, and DNA collection from whole blood. An Affymetrix SNP array (6.0) is performed to generate linkage information in the familial cases, and to rule out any cases for high-throughput sequencing if a large, rare CNV is detected. Whole-exome sequencing was performed at Axeq and the Broad Institute on the Illumina pipeline. Raw data was batch processed for alignment and annotation. The variants were intersected with public databases, including dbSNP, 1000 Genomes, the NHLBI Exome Variant Server (EVS), Complete Genomics whole genomes, as well as our internal database of 831 exomes.

Table 4.1

Known genes and loci associated with polymicrogyria.

Locus	Gene	Inheritance	Reference
12q13.12	*TUBA1A*	Dominant	Jansen et al., 2011
6p25	*TUBB2B*	Dominant	Jaglin et al., 2009
16q24.3	*TUBB3*	Dominant	Poirier et al., 2010
21q22.3	*COL18A1*	Recessive	Paisán-Ruiz et al., 2009
3p21.3-p21.2	*EOMES*	Recessive	Baala et al., 2007
16q21	*GPR56*	Recessive	Piao et al., 2006
10q22.1	*KIAA1279*	Recessive	Brooks et al., 2005
9q34.12	*LAMC3*	Recessive	Barak et al., 2011
11p13	*PAX6*	Recessive	Mitchell et al., 2003
2q21.3	*RAB3GAP1*	Recessive	Morris-Rosendahl et al., 2010
1q41	*RAB3GAP2*	Recessive	Borck et al., 2011
22q11.2	*TUBA8*	Recessive	Abdollahi et al., 2009
19q13.12	*WDR62*	Recessive	Yu et al., 2010; Bilguvar et al., 2010; Nicholas et al., 2010
Xq21.33-q23	*SRPX2*	X-linked	Roll et al., 2006
1p36.3	Deletion		Dobyns et al., 2008
4q21.21-22.1	Deletion		Dobyns et al., 2008
6q26-qter	Deletion		Dobyns et al., 2008
22q11.2	Deletion		Dobyns et al., 2008
2p16.1-23	Duplication		Dobyns et al., 2008

A list of genes and loci associated with polymicrogyria, their observed inheritance pattern, and references from the literature.

Table 4.2

Identified rare variants to known PMG genes.

The exome data from our cohort was screened for rare variants to the list of known genes in **Table 1**. In cases where multiple patients were sequenced within the family, the variants shown were shared across all affected individuals, with an allele frequency < 1% in all the databases listed. Chr = chromosome; Position = basepair position of the variant (hg19); Ref = reference base (hg19); Obs = observed variant; Homozygous = Y if the variant is homozygous, N if heterozygous; AA Change = predicted amino acid change for that variant in the given transcript; 1000G = allele frequency in the 1000 Genomes database; NHLBI = allele frequency in the NHLBI Exome Variant Server; CG69 = allele frequency within 69 whole genome sequences from Complete Genomics; Lab AF = allele frequency within the 831 whole exomes in the internal Walsh Lab database; SNV = single nucleotide variant; SIFT = prediction algorithm from the J. Craig Venter Institute for the severity of nonsynonymous polymorphisms (< 0.05 considered damaging) (Kumar et al., 2009); PolyPhen2 = another prediction algorithm (higher score is better) (Adzhubei et al., 2010).

Table 4.2 (Continued)

Patient	Chr	Position	Reference	Observed	Homozygous	Gene	Transcript	Function	AA Change	1000G	NHLBI	CG69	Lab AF	SIFT	PolyPhen2
FC-500	6	3,225,082	T	C	N	*TUBB2B*	NM_178012	nonsynonymous SNV	p.N414S	0.000	0.000	0.000	0.000	0.000	0.000
PMG-16100	1	220,363,770	G	A	Y	*RAB3GAP2*	NM_012414	nonsynonymous SNV	p.P527L	0.001	0.000	0.000	0.017	0.000	0.999
PMG-14500	X	99,919,864	C	T	Y	*SRPX2*	NM_014467	nonsynonymous SNV	p.S150F	0.000	0.000	0.000	0.022	0.010	0.067
PAC-1500	19	36,558,782	ACA	-	N	*WDR62*	NM_001083961	nonframeshift deletion	p.251_252del				0.019		
PAC-1500	19	36,595,919	C	T	N	*WDR62*	NM_001083961	nonsynonymous SNV	p.R1516W				0.019	0.000	0.600
PMG-17800	19	36,574,073	G	A	N	*WDR62*	NM_001083961	nonsynonymous_SNV	p.G494R				0.000	0.012	0.821
PMG-17800	19	36,577,670	C	T	N	*WDR62*	NM_001083961	nonsynonymous_SNV	p.T575M				0.000	0.008	0.902
MC-23100	1	197,070,364	G	A	Y	*ASPM*	NM_018136	stopgain SNV	p.Q2673X				0.016		
PMG-5600	1	197,071,034	AT	-	Y	*ASPM*	NM_018136	frameshift deletion	p.2449_2449delfs				0.000		

TUBB2B

FC-500 is an American family with two affected boys with right unilateral PMG and left hemiparesis. The parents denied consanguinity. The PMG of boy patients involves the lateral right hemisphere with sparing of the frontal and occipital poles, reduced white matter in the right hemisphere, and a small right peduncle and pons. Interestingly, both also shared a slight asymmetry in the size of the caudate. Both patients harbored rare heterozygous variants to *TUBB2B* that were not found in 1000 Genomes, the NHLBI Exome Variant Server, or in our internal lab exome database. The variant results in a missense change in a highly conserved residue, p.N414S, and is predicted to be deleterious by SIFT and PolyPhen2 prediction algorithms (**Table 4.2**). A list of all the rare variants shared by the two affected patients is listed in **Table 4.3**.

TUBB2B has been identified as a gene for asymmetrical PMG (Jaglin et al., 2009), however the severity of the malformation in the published cases is much higher than in FC-500, which appears to have a unilateral right-sided distribution, rather than one in which both sides are severely affected but one side greater than the other (as seen in the previously published cases).

SRPX2

PMG-14501 is a consanguineous pedigree of Kuwait origin with one affected boy with right-sided perisylvian polymicrogyria. Exome sequencing identified 26 rare homozygous variants, including nonsense mutations to *HEXDC* and *HNRNPA1L2* (**Table 4.4**). No loss-of-function mutations to these genes were identified in any of our other PMG exomes. In addition, a

missense variant (p.S150F) was found in *SRPX2*, a known bilateral perisylvian PMG gene, with one patient mutation reported (p.Y72S) (Roll et al., 2006) (**Table 4.2**). In that report, the patient had an asymmetric malformation, with the PMG more severe on the left (Roll et al., 2006).

RAB3GAP2

PMG-16100 is a Moroccan consanguineous pedigree with diffuse bilateral polymicrogyria. Exome sequencing identified 19 homozygous rare variants, including a frameshift to *GPR179*, and no compound heterozygous candidate variants (**Table 4.5**). A homozygous missense change to a highly conserved residue in *RAB3GAP2* was predicted to be severely damaging by both SIFT and PolyPhen2 algorithms (p.P527L) (**Table 4.2**). A single case of an in-frame deletion of three amino acids to *RAB3GAP2* is reported to cause Warburg Micro syndrome (the predominant genetic lesion is to *RAB3GAP1*) (Borck et al., 2010). Bilateral fronto-parietal polymicrogyria is a noted feature of Warburg Micro syndrome (Aligianis et al., 2005).

Table 4.3: FC-500 rare variants shared between FC-501, 502.

Chrom	Position	Ref	Obs	Gene	Function	AA Change	1000G	NHLBI	Lab AF	SIFT	PolyPhen2
1	8073919	C	T	ERRFI1	nonsynonymous SNV	NM_018948:c.G740A:p.R247K		0.00	0.01	0.25	0.97
1	11580795	G	A	PTCHD2	nonsynonymous SNV	NM_020780:c.G2252A:p.R751H		0.00	0.01	0.07	0.03
1	36643701	AGA	-	MAP7D1	nonframeshift deletion	NM_018067:c.1607_1609del:p.536_537del			0.03		
1	46597520	T	C	PIK3R3;PIK3R3	splicing;synonymous SNV	NM_003629:c.A105G:p.P35P			0.01		
1	67794064	A	G	IL12RB2	nonsynonymous SNV	NM_001559:c.A661G:p.I221V			0.01	0.00	0.01
1	100349699	G	A	AGL	nonsynonymous SNV	NM_000645:c.G2281A:p.E761K			0.01	0.00	0.98
1	169586362	C	T	SELP	nonsynonymous SNV	NM_003005:c.G385A:p.E129K			0.01	0.01	0.07
1	173556912	C	T	SLC9A11	nonsynonymous SNV	NM_178527:c.G415A:p.V139I	0.00	0.00	0.01	0.17	0.48
1	205888027	C	T	SLC26A9	nonsynonymous SNV	NM_134325:c.G2197A:p.A733T			0.01	0.00	0.99
2	39088423	T	G	DHX57	nonsynonymous SNV	NM_198963:c.A1129C:p.T377P			0.01	0.00	0.92
2	46986696	A	T	SOCS5	nonsynonymous SNV	NM_144949:c.A1027T:p.I343L		0.00	0.01	0.86	0.00
2	130949588	C	T	TUBA3E	nonsynonymous SNV	NM_207312:c.G1169A:p.R390H		0.00	0.01	0.00	1.00
2	217543614	G	A	IGFBP5	nonsynonymous SNV	NM_000599:c.C526T:p.R176W			0.01	0.01	0.73
3	52822079	G	A	ITIH1	nonsynonymous SNV	NM_001166434:c.G1576A:p.G526S		0.00	0.01	0.40	0.00
4	47565681	A	T	ATP10D	nonsynonymous SNV	NM_020453:c.A2752T:p.M918L			0.01	0.03	0.99
4	120107272	G	A	MYOZ2	nonsynonymous SNV	NM_016599:c.G712A:p.G238R			0.01	0.00	1.00
5	71494593	C	A	MAP1B	nonsynonymous SNV	NM_005909:c.C5411A:p.T1804N			0.01	0.05	0.79
5	131705800	C	T	SLC22A5	nonsynonymous SNV	NM_003060:c.C136T:p.P46S		0.00	0.01	0.00	1.00
5	140222138	G	C	PCDHA8	nonsynonymous SNV	NM_031856:c.G1232C:p.S411T			0.01	0.04	0.51
5	141248571	T	C	PCDH1	nonsynonymous SNV	NM_032420:c.A466G:p.I156V			0.01	0.39	0.92
5	169535386	G	A	FOXI1	nonsynonymous SNV	NM_144769:c.G623A:p.G208E			0.01	0.01	1.00
5	172518171	A	G	C5orf41	nonsynonymous SNV	NM_001168393:c.A989G:p.Q330R	0.00	0.00	0.01	0.75	0.51
5	179228375	G	C	MGAT4B	nonsynonymous SNV	NM_014275:c.C517G:p.Q173E		0.00	0.01	1.00	0.00
5	179252155	C	T	SQSTM1	nonsynonymous SNV	NM_001142299:c.C431T:p.P144L		0.00	0.01	0.03	0.96
6	3225082	T	C	TUBB2B	nonsynonymous SNV	NM_178012:c.A1241G:p.N414S			0.01	0.00	0.58
6	11190609	A	G	NEDD9	nonsynonymous SNV	NM_006403:c.T1493C:p.I498T			0.01	1.00	0.07
6	108768498	C	A	LACE1;LACE1	splicing;nonsynonymous SNV	NM_145315:c.C889A:p.L297I			0.01	0.54	0.05
6	117710593	C	T	ROS1	nonsynonymous SNV	NM_002944:c.G1679A:p.R560H		0.00	0.01	0.46	0.00
8	27534087	T	A	SCARA3;SCARA3	splicing;synonymous SNV	NM_182826:c.T1371A:p.G457G			0.01		
9	124065263	C	T	GSN	nonsynonymous SNV	NM_001127664:c.C271T:p.R91W		0.00	0.01	0.01	0.31
9	131246994	C	A	ODF2	nonsynonymous SNV	NM_153439:c.C1194A:p.S398R		0.00	0.01	0.00	0.47
9	133759424	G	A	ABL1	nonsynonymous SNV	NM_005157:c.G1747A:p.G583S			0.01	1.00	0.00
9	135546172	G	T	GTF3C4	nonsynonymous SNV	NM_012204:c.G187T:p.A63S			0.01	0.39	0.02
9	136131635	G	A	ABO	nonsynonymous SNV	NM_020469:c.C482T:p.A161V		0.00	0.02		
9	136231723	A	C	SURF4	nonsynonymous SNV	NM_033161:c.T536G:p.F179C			0.01	0.01	0.61
10	120934038	T	C	PRDX3	nonsynonymous SNV	NM_014096:c.A182G:p.N61S			0.01	0.06	0.00
11	1080577	T	C	MUC2	nonsynonymous SNV	NM_002457:c.T1219C:p.Y407H			0.01	0.00	
11	1264872	C	G	MUC5B	nonsynonymous SNV	NM_002458:c.C6762G:p.S2254R	0.00	0.00	0.01		
11	124863097	G	T	CCDC15	nonsynonymous SNV	NM_025004:c.G2172T:p.E724D	0.00	0.00	0.01	0.20	
12	49425010	C	T	MLL2	nonsynonymous SNV	NM_003482:c.G13478A:p.S4493N			0.01		
12	49463531	C	G	RHEBL1	nonsynonymous SNV	NM_144593:c.G38C:p.G13A			0.01	0.02	0.50
12	68715393	C	T	MDM1	nonsynonymous SNV	NM_017440:c.G817A:p.D273N	0.00	0.00	0.01	0.01	0.03
12	113379485	G	T	OAS3	nonsynonymous SNV	NM_006187:c.G288T:p.E96D		0.00	0.01	0.08	
14	53066895	G	T	GPR137C	nonsynonymous SNV	NM_001099652:c.G553T:p.A185S		0.00	0.01	0.00	
14	63749908	G	A	RHOJ	nonsynonymous SNV	NM_020663:c.G472A:p.E158K		0.00	0.01	0.02	0.96
15	42632020	T	C	GANC	nonsynonymous SNV	NM_198141:c.T1997C:p.I666T			0.01	0.00	0.41
15	44856898	-	TCC	SPG11(NM_00116	splicing;				0.01		
16	52473280	G	A	TOX3	nonsynonymous SNV	NM_001146188:c.C1573T:p.P525S			0.01	0.11	
16	64984750	T	A	CDH11	nonsynonymous SNV	NM_001797:c.A1814T:p.N605I			0.01	0.00	1.00
17	8397095	CCT	-	MYH10	nonframeshift deletion	NM_005964:c.4070_4072del:p.1357_1358del			0.01		
17	18150068	CTC	-	FLII	nonframeshift deletion	NM_002018:c.2869_2871del:p.957_957del			0.01		
17	48614102	G	A	EPN3	nonsynonymous SNV	NM_017957:c.G185A:p.R62Q		0.00	0.01	0.01	0.99
17	64225442	G	A	APOH	nonsynonymous SNV	NM_000042:c.C56T:p.A19V			0.01	0.01	0.49
18	28588385	A	C	DSC3	nonsynonymous SNV	NM_001941:c.T1370G:p.L457W			0.01	0.01	0.02
19	1585142	G	A	MBD3	nonsynonymous SNV	NM_003926:c.C182T:p.T61I			0.01	0.02	0.00
19	33696362	C	T	LRP3	nonsynonymous SNV	NM_002333:c.C686T:p.P229L	0.00	0.00	0.01	0.01	0.97
19	38876170	G	C	GGN	nonsynonymous SNV	NM_152657:c.C1732G:p.R578G		0.00	0.01	0.74	0.13
19	39406347	C	T	SARS2	nonsynonymous SNV	NM_001145901:c.G1462A:p.G488S			0.01	0.00	0.91
19	43420568	A	-	PSG6	frameshift deletion	NM_001031850:c.136delT:p.S46fs			0.02		
19	43430060	C	T	PSG7	nonsynonymous SNV	NM_002783:c.G1108A:p.G370R		0.00	0.02		
19	44933513	C	A	ZNF229	nonsynonymous SNV	NM_014518:c.G1443T:p.K481N		0.00	0.02	0.02	0.70
19	50099897	C	G	PRR12	nonsynonymous SNV	NM_020719:c.C2305G:p.P769A		0.00	0.01	0.00	
19	54784318	C	T	LILRB2;LILRB2	splicing;nonsynonymous SNV	NM_001080978:c.G34A:p.G12R			0.01	0.01	0.30
19	56424650	C	G	NLRP13	nonsynonymous SNV	NM_176810:c.G533C:p.R178T			0.01	0.00	0.99
19	56482053	A	T	NLRP8	nonsynonymous SNV	NM_176811:c.A2525T:p.E842V			0.01	0.00	0.98
20	2464516	T	G	ZNF343	nonsynonymous SNV	NM_024325:c.A1091C:p.E364A			0.01	0.24	0.16
20	3025472	G	A	GNRH2	nonsynonymous SNV	NM_178331:c.G281A:p.R94Q		0.00	0.01	0.75	0.01
20	31627285	T	A	BPIFB6	nonsynonymous SNV	NM_174897:c.T1033A:p.W345R			0.01	0.87	0.01
20	44639214	C	T	MMP9	nonsynonymous SNV	NM_004994:c.C464T:p.T155I		0.00	0.01	0.06	0.79

Table 4.4: PMG-14501 homozygous rare variants and proband MRI.

Chrom	Position	Ref	Obs	Homozygous	Gene	Function	AA Change	1000G	NHLBI	Lab AF	SIFT	PolyPhen2
1	24078372	C	T	Y	TCEB3	nonsynonymous SNV	NM_003198:c.C1355T:p.T452I		0.00	0.01	0.19	0.09
2	1695771	C	T	Y	PXDN;PXDN	splicing;synonymous SNV	NM_012293:c.G273A:p.L91L		0.00	0.01		
2	152584305	G	A	Y	NEB	nonsynonymous SNV	NM_001164507:c.C194T:p.P65L		0.00	0.01	0.00	
3	38523926	G	T	Y	ACVR2B	nonsynonymous SNV	NM_001106:c.G1219T:p.V407L			0.01	0.01	0.09
4	186084022	G	A	Y	KIAA1430	nonsynonymous SNV	NM_020827:c.C1529T:p.A510V	0.00		0.02	0.40	
6	10784717	C	T	Y	MAK	nonsynonymous SNV	NM_001242957:c.G1405A:p.E469K	0.00	0.00	0.02	0.45	0.01
6	41652493	G	T	Y	TFEB	nonsynonymous SNV	NM_007162:c.C1275A:p.F425L			0.02	0.13	1.00
6	127768632	G	A	Y	KIAA0408	nonsynonymous SNV	NM_014702:c.C832T:p.P278S		0.00	0.02	0.75	0.97
7	98563504	A	G	Y	TRRAP	nonsynonymous SNV	NM_003496:c.A7087G:p.M2363V			0.01	0.95	0.01
7	99129858	G	C	Y	ZKSCAN5	nonsynonymous SNV	NM_145102:c.G2506C:p.G836R			0.01	0.00	0.19
8	99264792	C	T	Y	NIPAL2	nonsynonymous SNV	NM_024759:c.G275A:p.G92D		0.00	0.01	0.17	0.03
11	123777161	C	T	Y	OR8D4	nonsynonymous SNV	NM_001005197:c.C23T:p.T8I			0.02	0.22	0.00
13	46946451	T	C	Y	KIAA0226L	nonsynonymous SNV	NM_025113:c.A160G:p.I54V		0.00	0.01	0.19	
13	52603266	T	A	Y	UTP14C	nonsynonymous SNV	NM_021645:c.T326A:p.V109D		0.00	0.01	0.00	0.99
13	53216702	A	-	Y	HNRNPA1L2	frameshift deletion	NM_001011725:c.75delA:p.T25fs			0.02		
13	78477314	C	T	Y	EDNRB	nonsynonymous SNV	NM_001201397:c.G1048A:p.V350I	0.00		0.02	0.40	0.00
17	79428039	G	C	Y	BAHCC1	nonsynonymous SNV	NM_001080519:c.G6185C:p.G2062A			0.02	0.03	
17	80398977	C	-	Y	HEXDC	frameshift deletion	NM_173620:c.1087delC:p.P363fs			0.02		
17	80544008	C	A	Y	FOXK2	nonsynonymous SNV	NM_004514:c.C1508A:p.T503N			0.02	0.39	0.24
20	1532666	T	G	Y	SIRPD	nonsynonymous SNV	NM_178460:c.A92C:p.H31P			0.02	0.01	1.00
X	29417373	A	C	Y	IL1RAPL1	nonsynonymous SNV	NM_014271:c.A651C:p.E217D			0.02	0.04	0.84
X	48887979	C	T	Y	TFE3	nonsynonymous SNV	NM_006521:c.G1418A:p.G473D			0.02	0.05	0.14
X	51238861	C	G	Y	NUDT11	nonsynonymous SNV	NM_018159:c.G436C:p.G146R			0.02	0.14	0.00
X	69479141	G	A	Y	P2RY4	nonsynonymous SNV	NM_002565:c.C334T:p.R112C			0.02	0.00	1.00
X	99919864	C	T	Y	SRPX2	nonsynonymous SNV	NM_014467:c.C449T:p.S150F			0.02	0.01	0.07
X	129063580	AT	-	Y	UTP14A	frameshift deletion	NM_006649:c.2312_2313del:p.771_771del			0.02		

Table 4.5: PMG-16101 homozygous rare variants.

Chr	Position	Ref	Obs	Homozygous	Gene	Function	AA Change	1000G	NHLBI	Lab AF	SIFT	PolyPhen2
1	26517215	G	A	Y	CATSPER4	nonsynonymous SNV	NM_198137:c.G97A:p.G33R		0.000	0.017	0.000	0.000
1	220363770	G	A	Y	RAB3GAP2	nonsynonymous SNV	NM_012414:c.C1580T:p.P527L	0.001	0.000	0.017	0.000	0.999
3	118865127	GAA	-	Y	C3orf30	nonframeshift deletion	NM_152539:c.91_93del:p.31_31del			0.023		
5	72469090	G	A	Y	TMEM174	nonsynonymous SNV	NM_153217:c.G20A:p.R7H	0.002	0.000	0.008	0.430	0.002
5	147449998	C	T	Y	SPINK5	nonsynonymous SNV	NM_001127699:c.C194T:p.T65M			0.017	0.150	0.001
6	137113112	C	A	Y	MAP3K5	nonsynonymous SNV	NM_005923:c.G184T:p.A62S			0.017	0.060	0.000
6	146271591	G	A	Y	SHPRH	nonsynonymous SNV	NM_173082:c.C791T:p.P264L		0.000	0.017	0.070	0.000
11	55136032	C	T	Y	OR4A15	nonsynonymous SNV	NM_001005275:c.C673T:p.L225F			0.017	0.050	0.281
11	55339771	A	-	Y	OR4C16	frameshift deletion	NM_001004701:c.168delA:p.P56fs			0.010		
11	57506511	G	A	Y	TMX2;TMX2	splicing;nonsynonymous SNV	NM_015959:c.G614A:p.R205Q		0.000	0.017	0.020	0.770
11	58125600	A	G	Y	OR5B17	stoploss SNV	NM_001005489:c.T943C:p.X315Q	0.004	0.001	0.017	0.580	0.296
11	60971611	G	A	Y	PGA3	nonsynonymous SNV	NM_001079807:c.G89A:p.R30H			0.020	0.010	0.076
11	61113946	C	T	Y	DAK	nonsynonymous SNV	NM_015533:c.C1699T:p.R567W		0.001	0.008	0.000	0.787
11	62297175	T	C	Y	AHNAK	nonsynonymous SNV	NM_001620:c.A4714G:p.M1572V	0.001	0.001	0.015	0.120	0.354
11	63175665	G	A	Y	SLC22A9	nonsynonymous SNV	NM_080866:c.G1370A:p.G457E			0.017	1.000	0.000
12	7510040	G	C	Y	CD163L1	nonsynonymous SNV	NM_174941:c.C4322G:p.S1441W		0.000	0.017	0.000	0.768
17	36485517	CT	-	Y	GPR179	frameshift deletion	NM_001004334:c.3934_3935del:p.1312_1312del			0.017		
20	43547836	G	A	Y	PABPC1L	nonsynonymous SNV	NM_001124756:c.G656A:p.S219N			0.017	0.000	0.988
20	44576001	C	T	Y	PCIF1	nonsynonymous SNV	NM_022104:c.C1807T:p.R603C			0.017	0.030	0.995

WDR62

In addition to filtering for homozygous variants, we also searched for candidate compound heterozygous changes by looking for genes with two or more rare variants. We identified two families harboring rare compound heterozygous variants to *WDR62*.

PAC-1500 is a mixed ancestry pedigree from Pennsylvania, with three affected children with right-sided unilateral PMG, two unaffected siblings, and unaffected parents (**Figure 4.3a,b**). Haplotype analysis combined with exome sequencing converged on only one recessive candidate gene, with two variants to *WDR62*. The first variant is a three basepair deletion (p.251_252del, removal of a conserved histidine residue), and the second is a missense change of another conserved residue (p.R1521W) in the second to last amino acid residue of the peptide (**Table 4.2; Figure 4.3a**). All three affected patients have head circumferences within the normal range (**Figure 4.3b,c**).

PMG-17800 is also a mixed ancestry pedigree from the United Kingdom, with two children (one boy, one girl) affected with posterior predominant bilateral perisylvian polymicrogyria, and one unaffected sister. Both affected children had delayed speech and feeding difficulties. The parents are unaffected. As expected from an outbred pedigree, the two affected individuals share no homozygous variants. Screening for compound heterozygous variants, only one gene met the criteria for two or more variants in both affected individual, *WDR62* (**Table 4.2**). The two variants, p.G494R and p.T575M, are in highly conserved residues (**Table 4.2**). Haplotype analysis and Sanger sequencing (data not shown) confirmed that both alleles segregate together with disease. As with PAC-1500, both patients in PMG-17800 are reported to

be normocephalic, with PMG-17801 and PMG-17804 having birth head circumferences of 34 cm (20th percentile) and 33 cm (10th percentile), respectively.

Figure 4.3

Right-sided PMG segregates with a compound heterozygous mutation to *WDR62.*

(a) Pedigree of PAC-1500 and Sanger sequencing traces from *WDR62* variants identified on whole-exome sequencing confirm the segregation and phase of the compound heterozygous haplotype. The three basepair deletion allele on exon 7 and the point mutation on exon 32 are both highlighted in red. (b) T1-weighted axial MRI images from PAC-1501, 1502, and 1503 are shown below their corresponding pedigree symbol. Arrowheads indicate the extent of the unilateral right-sided polymicrogyria in each patient. (c) Head circumference data from each affected individual along with the age- and gender-adjusted percentile shows all three patients to be within the normal range.

Figure 4.3 (Continued)

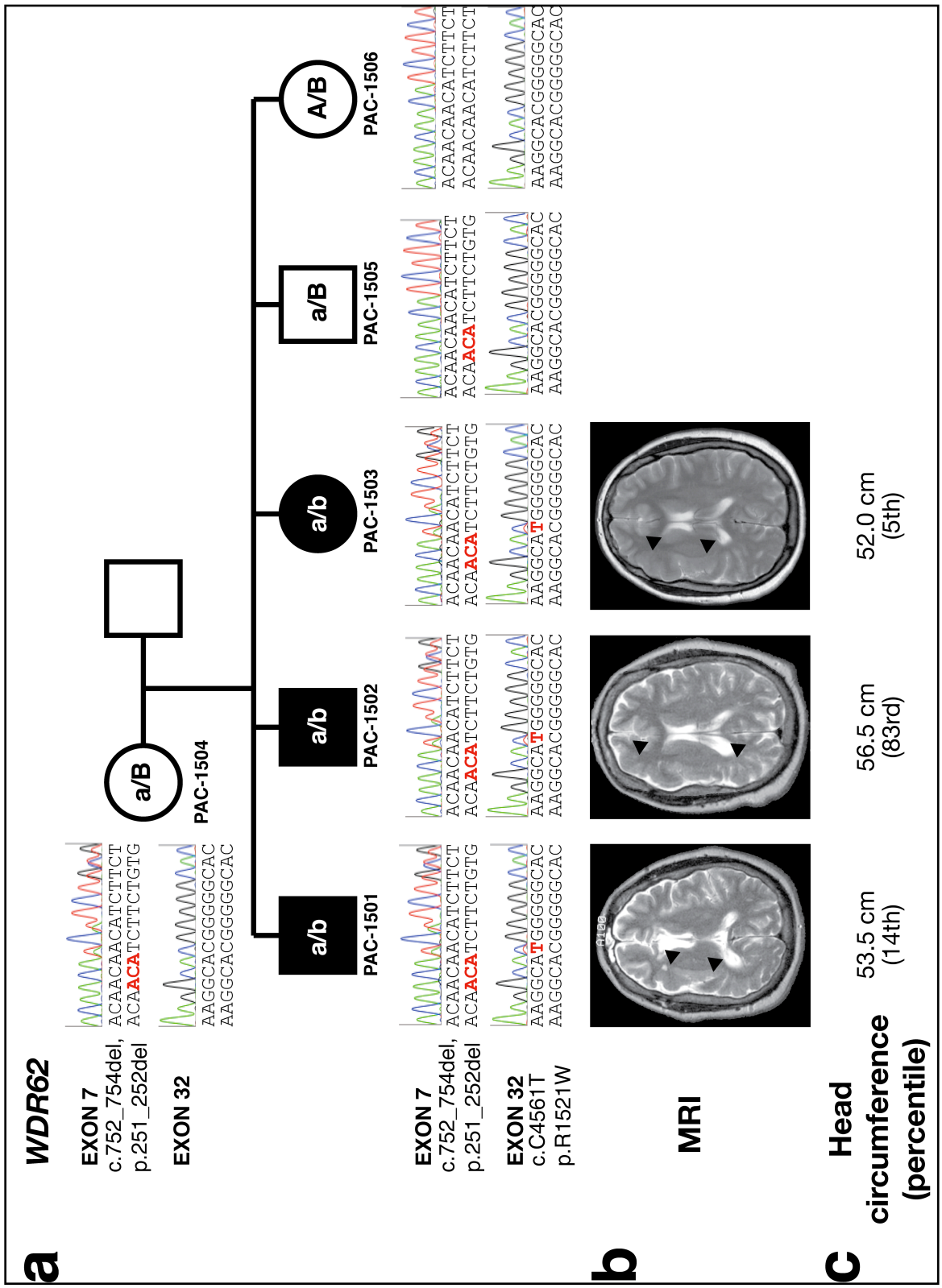

ASPM

Though not included in our screening list for known polymicrogyria genes, there is a case report of prematurely truncating frameshift *ASPM* mutation associated with unilateral PMG with microcephaly (Passemard et al., 2009). We have identified two additional novel truncating mutations in *ASPM* in two families with bilateral perisylvian polymicrogyria with microcephaly.

MC-23100 is a Kuwaiti pedigree with multiple loops of consanguinity (**Figure 4.4**). One branch of the family has three affected individuals with bilateral perisylvian polymicrogyria and severe microcephaly (head circumference -8 to -9 standard deviations from the mean for age and gender) (**Figure 4.4**). Two of these patients are identical twin girls (MC-23101, MC-23102), and the other is a boy (MC-23103). The parents are clinically unaffected. In another branch of the family, there is one affected girl with severe microcephaly without polymicrogyria or the clinical manifestations of perisylvian syndrome (MC-23106). Exome sequencing in MC-23102 and MC-23106 reveals only one shared homozygous rare variant that segregates with disease, a nonsense mutation to *ASPM* (p.Q2673X) (**Table 4.2**).

PMG-5600 is a pedigree with from Germany with two affected children (one boy and one girl) with diffuse bilateral polymicrogyria. The parents are unaffected and deny consanguinity. Microcephaly is not apparent from the MRI (data not shown), however birth head circumferences were not ascertained. Unexpected, a rare homozygous variant in *ASPM* was shared between both affected individuals, a frameshift deletion of two basepairs at position 197,071,034 on chromosome 1 (**Table 4.2**). No other shared homozygous variants passed the filtering criteria. There are two candidate compound heterozygous genes, each harboring two variants in both PMG-5601 and 5602. *GOLGA6L6* (p.R541W and p.E474X) and *DDX60*

(p.G79E and c.2671-1G>A, predicted to disrupt splicing at exon 21). Phasing and segregation of both alleles was not confirmed.

Figure 4.4

Pedigree structure of MC-23100, with proband MRI.

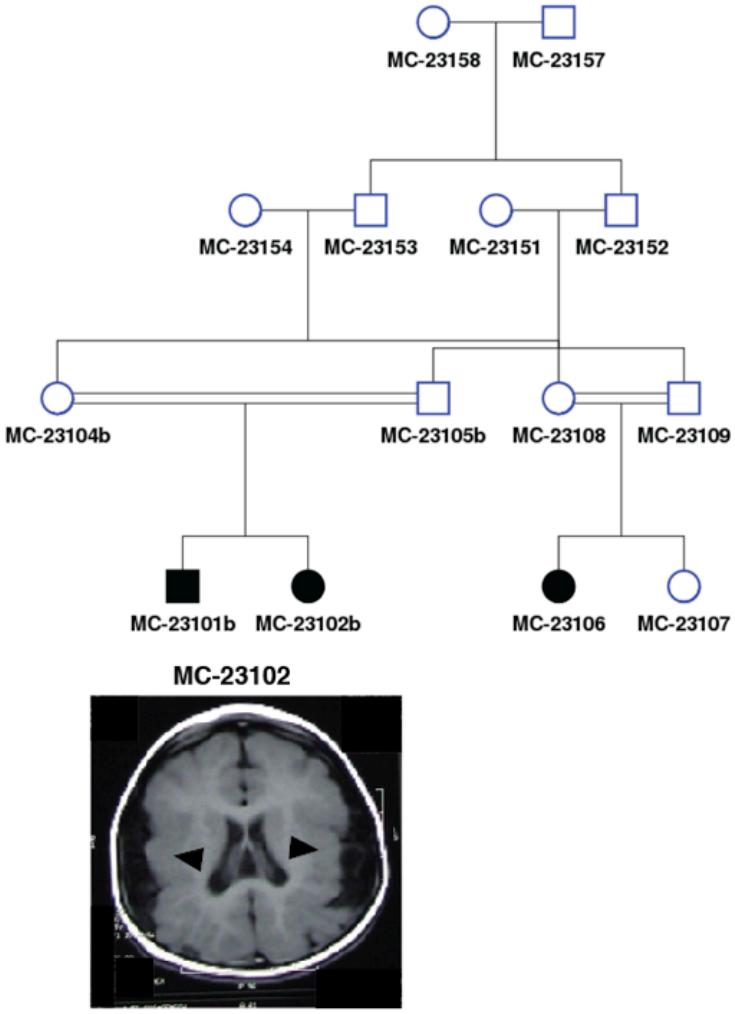

Black arrowheads indicate regions of polymicrogyria on coronal T1-weighted MRI for MC-23102. Double lines indicate consanguineous relationships.

Discussion

Previous work has suggested that unilateral perisylvian polymicrogyria is a distinct familial syndrome (Chang et al., 2005), and other groups have commented on the frequently asymmetric appearance of bilateral perisylvian polymicrogyria, but a statistical case has never been made (Leventer et al., 2010). Our data from a cohort of both familial mulitplex and simplex cases suggests that bilateral perisylvian polymicrogyria is somewhat biased towards a right-predominant pattern, and that unilateral polymicrogyria is substantially skewed towards a right-sided presentation (**Figure 4.1**). If we posit that the unilateral cases are hypomorphic presentations of a more severe syndrome, this suggests that the right perisylvian region is selectively vulnerable to developing PMG. Population-averaged, surface- and volume-based radiographic morphometry has demonstrated prominent left–right asymmetries in and near the Sylvian fissure (Van Essen, 2005). The sulcul depth and extent of the Sylvian fissure are the most variable features between and within individuals (Van Essen, 2005). Therefore, it seems likely that this region of developmental instability is particularly vulnerable to focal cortical malformations.

The identification of compound heterozygous variants in *WDR62* in patients with polymicrogyria was surprising because these patients lacked microcephaly. Compound heterozygous changes to *WDR62* have been reported in a familial case of bilateral perisylvian polymicrogyria with microcephaly and simplified gyral patterning (Murdock et al., 2011). The spectrum of *WDR62* phenotypes is remarkably variable (Yu et al., 2010; Bilguvar et al., 2010; Nicholas et al., 2010), and there appears to be no genotype-phenotype correlation, since almost

all mutations are truncations that are predicted to completely abrogate protein function. Some missense mutations in *WDR62* are responsible for milder form of microcephaly, with less severe reduction of brain size and less evidence for abnormal brain histology (Bilguvar et al., 2010; Nicholas et al., 2010; Yu et al., 2010). Nevertheless, the core phenotype of *WDR62* has always involved microcephaly (**Figure 4.5**), and this has steered the biological understanding of its key role towards one of facilitation of neural progenitor proliferation through maintenance of the mitotic spindle. In both PAC-1500 and PMG-17800, none of the affected patients show evidence of microcephaly at birth or later in life (**Figure 4.3**). This suggests that in the patients with these particular compound heterozygous haplotypes, that only specific domains of *WDR62* may be affected, and this hypomorphic presentation does not affect proliferation, but rather impacts more subtle roles of *WDR62* in later-stage cortical organization. For the first time we show that the core phenotype of *WDR62* does not necessary require microcephaly.

ASPM (abnormal spindle microcephaly) is the gene most commonly mutated in human microcephaly (Bond et al., 2002, 2003; Nicholas et al., 2009). Like Wdr62, Aspm protein localizes to the mitotic spindle and appears essential for normal mitotic spindle function (Fish et al., 2006; Kouprina et al., 2005). All but one of the almost one hundred reported mutations in *ASPM* represent truncations (Gul et al., 2006; Bond et al., 2002; Kousar et al., 2010; Nicholas et al., 2009), and like truncations in *WDR62*, are found throughout the coding region of the gene with no apparent correlation to disease severity. We show that certain rare truncating mutations to *ASPM* that are seemingly indistinguishable from any other truncation can present with bilateral perisylvian polymicrogyria, in addition to microcephaly (**Table 4.2**). This variability is

present even within the same family, where one branch of the family lacked any detectable PMG (**Figure 4.4**).

In summary, we used whole-exome sequencing in a cohort of polymicrogyrias, and identified novel variants in several known PMG genes but also in primary microcephaly genes *ASPM* and *WDR62*. This expands the clinical and radiographic phenotype of *ASPM* and *WDR62* mutations, and suggests that future gene discovery in polymicrogyria cases should screen for variants from a broad category of genes involved in cortical development, since missense or hypomorphic mutations can lead to different malformations that are not easily recognized as allelic.

Figure 4.5

PAC-1500 clinical presentation varies from the core *WDR62* phenotype.

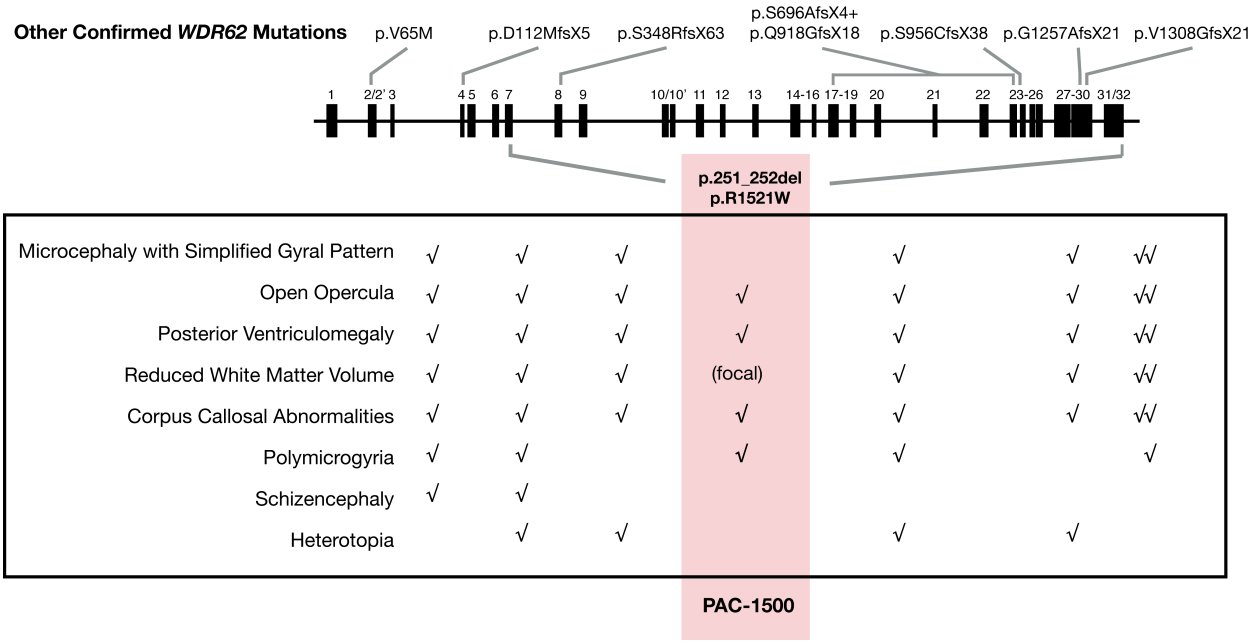

A schematic of the *WDR62* gene locus, with exons drawn as black boxes scaled to their relative length (intron distances not to scale). Above, *WDR62* mutations identified within our laboratory and in the literature are annotated relative to their position in the gene locus. The two *WDR62* alleles identified in PAC-1500 are annotated below the gene schematic. The core clinical phenotype of patients with *WDR62* mutations is listed and aligned with their corresponding variant. There is significant variability in the phenotype, but microcephaly with simplified gyral patterning is seen all previously identified cases, but not in PAC-1500.

References

Abdollahi, M. R., Morrison, E., Sirey, T., Molnár, Z., Hayward, B. E., Carr, I. M., Springell, K., et al. (2009). Mutation of the variant alpha-tubulin TUBA8 results in polymicrogyria with optic nerve hypoplasia. American journal of human genetics, 85(5), 737–744. doi:10.1016/j.ajhg.2009.10.007

Adzhubei, I. A., Schmidt, S., Peshkin, L., Ramensky, V. E., Gerasimova, A., Bork, P., Kondrashov, A. S., et al. (2010). A method and server for predicting damaging missense mutations. Nature Publishing Group, 7(4), 248–249. doi:10.1038/nmeth0410-248

Aligianis, I. A., Johnson, C. A., Gissen, P., Chen, D., Hampshire, D., Hoffmann, K., Maina, E. N., et al. (2005). Mutations of the catalytic subunit of RAB3GAP cause Warburg Micro syndrome. Nature genetics, 37(3), 221–223. doi:10.1038/ng1517

Baala, L., Briault, S., Etchevers, H. C., Laumonnier, F., Natiq, A., Amiel, J., Boddaert, N., et al. (2007). Homozygous silencing of T-box transcription factor EOMES leads to microcephaly with polymicrogyria and corpus callosum agenesis. Nature genetics, 39(4), 454–456. doi:10.1038/ng1993

Barkovich, A. J. (2010). Current concepts of polymicrogyria. Neuroradiology, 52(6), 479–487. doi:10.1007/s00234-009-0644-2

Barkovich, A. J., Gressens, P., & Evrard, P. (1992). Formation, maturation, and disorders of brain neocortex. AJNR. American journal of neuroradiology, 13(2), 423–446.

Barkovich, A. J., Kuzniecky, R. I., Jackson, G. D., Guerrini, R., & Dobyns, W. B. (2005). A developmental and genetic classification for malformations of cortical development. Neurology, 65(12), 1873–1887. doi:10.1212/01.wnl.0000183747.05269.2d

Barkovich, A. J., Millen, K. J., & Dobyns, W. B. (2007). A developmental classification of malformations of the brainstem. Annals of neurology, 62(6), 625–639. doi:10.1002/ana.21239

Bilgüvar, K., Oztürk, A. K., Louvi, A., Kwan, K. Y., Choi, M., Tatli, B., Yalnizoğlu, D., et al. (2010). Whole-exome sequencing identifies recessive WDR62 mutations in severe brain malformations. Nature, 467(7312), 207–210. doi:10.1038/nature09327

Bond, J., Roberts, E., Mochida, G. H., Hampshire, D. J., Scott, S., Askham, J. M., Springell, K., et al. (2002). ASPM is a major determinant of cerebral cortical size. Nature genetics, 32(2), 316–320. doi:10.1038/ng995

Bond, J., Scott, S., Hampshire, D. J., Springell, K., Corry, P., Abramowicz, M. J., Mochida, G. H., et al. (2003). Protein-truncating mutations in ASPM cause variable reduction in brain size. American journal of human genetics, 73(5), 1170–1177. doi:10.1086/379085

Borck, G., Wunram, H., Steiert, A., Volk, A. E., Körber, F., Roters, S., Herkenrath, P., et al. (2010). A homozygous RAB3GAP2 mutation causes Warburg Micro syndrome. Human Genetics, 129(1), 45–50. doi:10.1007/s00439-010-0896-2

Brooks, A. S., Bertoli-Avella, A. M., Burzynski, G. M., Breedveld, G. J., Osinga, J., Boven, L. G., Hurst, J. A., et al. (2005). Homozygous nonsense mutations in KIAA1279 are associated with malformations of the central and enteric nervous systems. American journal of human genetics, 77(1), 120–126. doi:10.1086/431244

Chang, B. S., Apse, K. A., Caraballo, R., Cross, J. H., Mclellan, A., Jacobson, R. D., Valente, K. D., et al. (2006). A familial syndrome of unilateral polymicrogyria affecting the right hemisphere. Neurology, 66(1), 133–135. doi:10.1212/01.wnl.0000191393.06679.e9

Dobyns, W. B., Mirzaa, G., Christian, S. L., Petras, K., Roseberry, J., Clark, G. D., Curry, C. J. R., et al. (2008). Consistent chromosome abnormalities identify novel polymicrogyria loci in 1p36.3, 2p16.1-p23.1, 4q21.21-q22.1, 6q26-q27, and 21q2. American journal of medical genetics Part A, 146A(13), 1637–1654. doi:10.1002/ajmg.a.32293

Fish, J. L., Kosodo, Y., Enard, W., Pääbo, S., & Huttner, W. B. (2006). Aspm specifically maintains symmetric proliferative divisions of neuroepithelial cells. Proceedings of the National Academy of Sciences of the United States of America, 103(27), 10438–10443. doi:10.1073/pnas.0604066103

Guerreiro, M. M., Andermann, E., Guerrini, R., Dobyns, W. B., Kuzniecky, R., Silver, K., Van Bogaert, P., et al. (2000). Familial perisylvian polymicrogyria: a new familial syndrome of cortical maldevelopment. Annals of neurology, 48(1), 39–48.

Guerrini, R. (2010). Polymicrogyria and epilepsy. Epilepsia, 51, 10–12. doi:10.1111/j. 1528-1167.2009.02434.x

Guerrini, R., Dubeau, F., Dulac, O., Barkovich, A. J., Kuzniecky, R., Fett, C., Jones-Gotman, M., et al. (1997). Bilateral parasagittal parietooccipital polymicrogyria and epilepsy. Annals of neurology, 41(1), 65–73. doi:10.1002/ana.410410112

Gul, A., Hassan, M. J., Mahmood, S., Chen, W., Rahmani, S., Naseer, M. I., Dellefave, L., et al. (2006). Genetic studies of autosomal recessive primary microcephaly in 33 Pakistani families: Novel sequence variants in ASPM gene. Neurogenetics, 7(2), 105–110. doi:10.1007/ s10048-006-0042-4

Inder, T. E., Hüppi, P. S., Warfield, S., Kikinis, R., Zientara, G. P., Barnes, P. D., Jolesz, F., et al. (1999). Periventricular white matter injury in the premature infant is followed by reduced cerebral cortical gray matter volume at term. Annals of neurology, 46(5), 755–760.

Jaglin, X. H., Poirier, K., Saillour, Y., Buhler, E., Tian, G., Bahi-Buisson, N., Fallet-Bianco, C., et al. (2009). Mutations in the beta-tubulin gene TUBB2B result in asymmetrical polymicrogyria. Nature genetics. doi:10.1038/ng.380

Jansen, A. C., Oostra, A., Desprechins, B., De Vlaeminck, Y., Verhelst, H., Régal, L., Verloo, P., et al. (2011). TUBA1A mutations: from isolated lissencephaly to familial polymicrogyria. Neurology, 76(11), 988–992. doi:10.1212/WNL.0b013e31821043f5

Kouprina, N., Pavlicek, A., Collins, N. K., Nakano, M., Noskov, V. N., Ohzeki, J.-I., Mochida, G. H., et al. (2005). The microcephaly ASPM gene is expressed in proliferating tissues and encodes for a mitotic spindle protein. Human molecular genetics, 14(15), 2155–2165. doi: 10.1093/hmg/ddi220

Kousar, R., Nawaz, H., Khurshid, M., Ali, G., Khan, S. U., Mir, H., Ayub, M., et al. (2010). Mutation analysis of the ASPM gene in 18 Pakistani families with autosomal recessive primary microcephaly. Journal of child neurology, 25(6), 715–720. doi:10.1177/0883073809346850

Kumar, P., Henikoff, S., & Ng, P. C. (2009). Predicting the effects of coding non-synonymous variants on protein function using the SIFT algorithm. Nature Protocols, 4(8), 1073–1081. doi: 10.1038/nprot.2009.86

Leventer, R. J., Cardoso, C., Ledbetter, D. H., & Dobyns, W. B. (2001). LIS1: from cortical malformation to essential protein of cellular dynamics. Trends in neurosciences, 24(9), 489–492.

Leventer, R. J., Guerrini, R., & Dobyns, W. B. (2008). Malformations of cortical development and epilepsy. Dialogues in clinical neuroscience, 10(1), 47–62.

Leventer, R. J., Jansen, A., Pilz, D. T., Stoodley, N., Marini, C., Dubeau, F., Malone, J., et al. (2010). Clinical and imaging heterogeneity of polymicrogyria: a study of 328 patients. Brain, 133(Pt 5), 1415–1427. doi:10.1093/brain/awq078

Levine, D. N., Fisher, M. A., & Caviness, V. S. (1974). Porencephaly with microgyria: a pathologic study. Acta neuropathologica, 29(2), 99–113.

Manzini, M. C., & Walsh, C. A. (2011). What disorders of cortical development tell us about the cortex: one plus one does not always make two. Current opinion in genetics & development, 21(3), 333–339. doi:10.1016/j.gde.2011.01.006

Murdock, D. R., Clark, G. D., Bainbridge, M. N., Newsham, I., Wu, Y.-Q., Muzny, D. M., Cheung, S. W., et al. (2011). Whole-exome sequencing identifies compound heterozygous mutations in WDR62 in siblings with recurrent polymicrogyria. American journal of medical genetics Part A, 155(9), 2071–2077. doi:10.1002/ajmg.a.34165

Nicholas, A. K., Khurshid, M., Désir, J., Carvalho, O. P., Cox, J. J., Thornton, G., Kausar, R., et al. (2010). WDR62 is associated with the spindle pole and is mutated in human microcephaly. Nature genetics, 42(11), 1010–1014. doi:10.1038/ng.682

Nicholas, A. K., Swanson, E. A., Cox, J. J., Karbani, G., Malik, S., Springell, K., Hampshire, D., et al. (2009). The molecular landscape of ASPM mutations in primary microcephaly. J Med Genet, 46(4), 249–253. doi:10.1136/jmg.2008.062380

Paisán-Ruiz, C., Scopes, G., Lee, P., & Houlden, H. (2009). Homozygosity mapping through whole genome analysis identifies a COL18A1 mutation in an Indian family presenting with an autosomal recessive neurological disorder. American journal of medical genetics. Part B, Neuropsychiatric genetics : the official publication of the International Society of Psychiatric Genetics, 150B(7), 993–997. doi:10.1002/ajmg.b.30929

Passemard, S., Titomanlio, L., Elmaleh, M., Afenjar, A., Alessandri, J. L., Andria, G., de Villemeur, T. B., et al. (2009). Expanding the clinical and neuroradiologic phenotype of primary microcephaly due to ASPM mutations. Neurology, 73(12), 962–969. doi:10.1212/WNL.0b013e3181b8799a

Piao, X., Chang, B. S., Bodell, A., Woods, K., BenZeev, B., Topcu, M., Guerrini, R., et al. (2005). Genotype-phenotype analysis of human frontoparietal polymicrogyria syndromes. Annals of neurology, 58(5), 680–687. doi:10.1002/ana.20616

Piao, X., Hill, R. S., Bodell, A., Chang, B. S., Basel-Vanagaite, L., Straussberg, R., Dobyns, W. B., et al. (2004). G protein-coupled receptor-dependent development of human frontal cortex. Science (New York, NY), 303(5666), 2033–2036. doi:10.1126/science.1092780

Poirier, K., Saillour, Y., Bahi-Buisson, N., Jaglin, X. H., Fallet-Bianco, C., Nabbout, R., Castelnau-Ptakhine, L., et al. (2010). Mutations in the neuronal ß-tubulin subunit TUBB3 result in malformation of cortical development and neuronal migration defects. Human molecular genetics, 19(22), 4462–4473. doi:10.1093/hmg/ddq377

Quarello, E., Stirnemann, J., Ville, Y., & Guibaud, L. (2008). Assessment of fetal Sylvian fissure operculization between 22 and 32 weeks: a subjective approach. Ultrasound in obstetrics & gynecology : the official journal of the International Society of Ultrasound in Obstetrics and Gynecology, 32(1), 44–49. doi:10.1002/uog.5353

Robin, N. H., Taylor, C. J., Mcdonald-Mcginn, D. M., Zackai, E. H., Bingham, P., Collins, K. J., Earl, D., et al. (2006). Polymicrogyria and deletion 22q11.2 syndrome: window to the etiology of a common cortical malformation. American journal of medical genetics Part A, 140(22), 2416–2425. doi:10.1002/ajmg.a.31443

Roll, P. (2006). SRPX2 mutations in disorders of language cortex and cognition. Human molecular genetics, 15(7), 1195–1207. doi:10.1093/hmg/ddl035

Santos, N. F., Secolin, R., Brandão-Almeida, I. L., Silva, M. S., Torres, F. R., Tsuneda, S. S., Guimarães, C. A., et al. (2008). A new candidate locus for bilateral perisylvian polymicrogyria mapped on chromosome Xq27. American journal of medical genetics Part A, 146A(9), 1151–1157. doi:10.1002/ajmg.a.32270

Van Essen, D. C. (2005). A Population-Average, Landmark- and Surface-based (PALS) atlas of human cerebral cortex. NeuroImage, 28(3), 635–662. doi:10.1016/j.neuroimage.2005.06.058

Villard, L., Nguyen, K., Cardoso, C., Martin, C. L., Weiss, A. M., Sifry-Platt, M., Grix, A. W., et al. (2002). A locus for bilateral perisylvian polymicrogyria maps to Xq28. American journal of human genetics, 70(4), 1003–1008. doi:10.1086/339433

Wieck, G., Leventer, R. J., Squier, W. M., Jansen, A., Andermann, E., Dubeau, F., Ramazzotti, A., et al. (2005). Periventricular nodular heterotopia with overlying polymicrogyria. Brain, 128(Pt 12), 2811–2821. doi:10.1093/brain/awh658

Yu, T. W., Mochida, G. H., Tischfield, D. J., Sgaier, S. K., Flores-Sarnat, L., Sergi, C. M., Topcu, M., et al. (2010). Mutations in WDR62, encoding a centrosome-associated protein, cause microcephaly with simplified gyri and abnormal cortical architecture. Nature genetics, 42(11), 1015–1020. doi:10.1038/ng.683

Discussion

The scope of this dissertation spans both ends of human disease genetics: extremely rare syndromes with low disease heterogeneity (such as microcephaly with pontocerebellar hypoplasia), and more prevalent, highly heterogeneous syndromes (such as polymicrogyria). The differences in the disease heterogeneity dictate different gene discovery strategies. In the rare syndromes, traditional techniques of linkage mapping in highly informative consanguineous pedigrees is possible because the low heterogeneity of the syndrome allows us to pool linkage scores across multiple families to arrive at a statistically significant locus. We discovered *CHMP1A* by combining the LOD scores of two pedigrees from different parts of the world, on the basis of their shared phenotypic distinctiveness. This is less fruitful in high-heterogeneity disease, since the inherent disease variability makes it difficult, if not impossible, to claim *a priori* that two pedigrees share the same molecular defect based on the phenotype. We attempted to focus our attention on the unilateral polymicrogyria cases in the hope that these malformations were allelic. That turned out not to be the case, but it was a pragmatic decision that could reasonably be made again. The era of high-throughput sequencing has increased the speed and decreased the cost of analyzing variants, and eventually will make the work of subcategorizing heterogeneous diseases into phenotypic groups increasingly moot. In the not-so-distant future, the initial categorizations will be made from the genotype, not the phenotype.

In Chapter 2 we identify a new gene for human microcephaly, *CHMP1A*. Because we had the ideal situation of highly informative families with a very rare disease, discovery of the variants was challenging but straightforward, leaving more opportunity to probe the biology of

the gene. We were struck by how similar the *Bmi1*-/- mouse brain phenotype resembled the rare constellation of morphological defects seen in our patients. This led us to hypothesize a mechanistic connection between *CHMP1A* and *BMI1*, and the bulk of Chapter 2 seeks to demonstrate through analysis of expression and zebrafish models that *INK4A* expression is downstream of *CHMP1A* and that disruption of BMI1-INK4A could explain the proliferative defects seen in the cortex and cerebellum.

CHMP1A is fascinating protein. It has two seemingly non-overlapping functions: a cytoplasmic role in ESCRT-III-mediated regulation of multivesicular bodies, and a role in the nuclear matrix regulating chromatin structure. As an aside, both of these functions were initially identified by the same research group in back-to-back papers in the same journal (Stauffer et al., 2001; Howard et al., 2001). In Chapter 3, rather than interrogating one specific molecule such as BMI1, we explored the possible non-nuclear roles of *CHMP1A*. We utilized the *Chmp1a* gene-trap mouse to characterize the loss-of-function phenotype *in vivo*, and tested for defects in Wnt and Shh pathways *in vitro.* The reduction in Wnt- and Shh-stimulated transcriptional activity in the presence of *Chmp1a* knockdown appears to support the proposed model of ESCRT-III mediating transduction of both Wnt and Shh pathways via GSK3 (Taelman et al., 2010; Kim et al., 2009).

In Chapter 4 we step into the breach of complex genetics with a search for genes for polymicrogyria using whole-exome sequencing. Here, pragmatic compromises needed to be made. We do not have highly informative families, so our filtering strategies need to be sophisticated to winnow down the list of variants to a manageable subset. Most of our polymicrogyria pedigrees are non-consanguineous, hence we need to build a pipeline to screen

for possible compound heterozygous candidate genes. We sought a screening approach, to first rule out patients that harbored rare, deleterious variants to previously published PMG genes. Our results identify novel rare variants, including compound heterozygous haplotypes, to *TUBB2B, RAB3GAP2,* and *SRPX2.* Interestingly, we also uncover variants to two primary microcephaly genes, *ASPM* and *WDR62*, that segregate with disease in multiplex families and are predicted to be deleterious. This expands the phenotypic spectrum of these two genes, and suggests roles beyond neural progenitor proliferation.

Proliferation and patterning defects converge on role in OSVZ progenitors

One curious feature of *WDR62* and *ASPM* from our data is that rare mutations appear to present with polymicrogyria without severe microcephaly, despite most published mutations presenting with profound microcephaly, often without polymicrogyria. One way to reconcile these effects is to propose that these genes may regulate neural progenitor proliferation in more subtle ways. Cortical size reduction in the *Aspm* knockout mice has been modest compared to the human phenotype (Pulvers et al., 2010; Manzini & Walsh, 2011), and an early look at a *Wdr62* gene-trap line also appears to show only a mild reduction in cortical volume (Tim W. Yu, personal communication). It is possible that though these genes are present at every mitotic spindle and regulate proliferation, their effect is most pronounced in a class of stem cells that are not abundant in the mouse, namely outer subventricular zone (OSVZ) progenitors (Lamonica et al., 2012).

Outer radial glia are characterized by a long radial process that reaches the pial surface, with the soma in the OSVZ, and a lack of an apical process (Hansen et al., 2010). A thick OSVZ

is only seen in gyrencephalic brains (Kriegstein, et al., 2006). One model for the role of *WDR62* and *ASPM* is that they regulate the organization and proliferation of progenitors in the OSVZ. Mild or hypomorphic effects would present with defects in gyrification without overt changes to overall brain size. And perhaps the most hypomorphic alleles would present with gyrification defects where the brain is biophysically most vulnerable and variable: in the Sylvian fissure (Van Essen, 2005). Severe effects on these genes would present with microcephaly because the OSVZ expands rapidly to become the dominant germinal layer in the neocortex (Lui et al., 2011). This mechanism of microcephaly would be of a different route than microcephaly secondary to disruption of ventricular radial glia proliferation (with *MCPH, CEP152,* etc.), but the effect may not be distinguishable radiographically.

CHMP1A **in tumor biology**

The *in vitro* data showing a reduction in Wnt- and Shh-stimulated transcription with *Chmp1a* shRNA, immediately suggests exploring the role of *CHMP1A* in human or mouse tumors. Medulloblastoma is the most common malignant brain tumor in children (Marino, 2005), and recent molecular subgrouping of a large array of medulloblastomas identified the critical signature of WNT and SHH disruption in over 30% of tumors (Cho et al., 2011). Inactivation of the Patched receptor, or activation of Smoothened, or overexpression of Shh itself was sufficient to induce tumors in mice (Vaillant et al., 2009). In fact, the nexus of WNT and SHH pathway disruptions in these tumors is suspicious for a more proximate role of GSK3. It is possible that ESCRT-III function plays a critical and necessary role in allowing these tumors to propagate.

Pleiotropy and heterogeneity in human disease

What connects *CHMP1A* to our findings with *WDR62* and *ASPM* is that in all three examples we have a gene that appears to have multiple roles in brain development. Pleiotropy has been suggested to play a key role in generating a complex brain (Kovas et al., 2006), and pleiotropic networks have been identified in nervous system function (Chesler et al., 2005). It should perhaps not be surprising that nature would map multiple functions onto each gene, to maximize the diversity capable from a limited set of genes. As we identify more alleles for syndromes that unexpectedly map back to primary microcephaly genes, we will begin to clarify functional domains or critical residues that mediate specific interactions. This will lead to specific hypotheses to genetically and biochemically dissociate the multiple roles of these genes in brain development.

In fact, elucidation of a pathway from genes identified from exome sequencing may be possible from our data. The identification of *RAB3GAP2* mutations, and the phenotypic similarity of those patients' MRI to the bilateral fronto-parietal polymicrogyria (BPPP) pattern seen with *GPR56* and *COL18A1* mutations, suggests a possible mechanistic connection between these three components. *Gpr56* is an orphan G-protein coupled receptor (Piao et al., 2004), for which *Col3a1* has recently been proposed as a ligand (Luo et al., 2011). Mutations to human *COL3A1* have not been identified in polymicrogyria, however loss-of-function mutations to a paralogous gene, *COL18A1,* are found in patients with Knobloch syndrome, in which BFPP is one radiographic feature (Keren et al., 2009). *RAB3GAP2* mutations are associated with Warburg Micro syndrome, which also has BFPP (Borck et al., 2010; Aligianis et al., 2005). *RAB3GAP2* is

involved in the vesicle trafficking of secretory proteins from the Golgi to the plasma membrane (Borck et al., 2010). So here we have three proteins with non-overlapping functions and subcellular localizations, all presenting with similar loss-of-function brain malformation phenotypes. A simple model is that RAB3GAP2 regulates the export of COL18A1 out of the cell, to then act as a ligand for GPR56 in regulating further downstream patterning.

Recent explosive human population growth over the past ten millenia has resulted in an excess of rare variants in the population (Keinan & Clark, 2012). As the world becomes more globalized and integrated, genetic admixture increases the probability that offspring will have compound heterozygous changes of private mutations, resulting in a range of hypomorphic presentations of severe diseases. Though the most severe loss-of-function mutations to *GPR56, COL18A1,* and *RAB3GAP2* appear as discrete syndromes, hypomorphic mutations might converge on a milder syndrome with BFPP as the shared cardinal feature. And we will recognize the allelic nature of the pathway only once we capture the full range of hypomorphic alleles. It will be an ongoing challenge to physician-scientists and research centers to integrate the subtleties of phenotypic information with the deluge of genetic data to maximize the capacity for discovery, while protecting patient privacy.

References

Aligianis, I. A., Johnson, C. A., Gissen, P., Chen, D., Hampshire, D., Hoffmann, K., Maina, E. N., et al. (2005). Mutations of the catalytic subunit of RAB3GAP cause Warburg Micro syndrome. Nature genetics, 37(3), 221–223. doi:10.1038/ng1517

Borck, G., Wunram, H., Steiert, A., Volk, A. E., Körber, F., Roters, S., Herkenrath, P., et al. (2010). A homozygous RAB3GAP2 mutation causes Warburg Micro syndrome. Human Genetics, 129(1), 45–50. doi:10.1007/s00439-010-0896-2

Chesler, E. J., Lu, L., Shou, S., Qu, Y., Gu, J., Wang, J., Hsu, H. C., et al. (2005). Complex trait analysis of gene expression uncovers polygenic and pleiotropic networks that modulate nervous system function. Nature genetics, 37(3), 233–242. doi:10.1038/ng1518

Cho, Y.-J., Tsherniak, A., Tamayo, P., Santagata, S., Ligon, A., Greulich, H., Berhoukim, R., et al. (2011). Integrative genomic analysis of medulloblastoma identifies a molecular subgroup that drives poor clinical outcome. Journal of Clinical Oncology, 29(11), 1424–1430. doi:10.1200/JCO.2010.28.5148

Hatten, M. E., & Roussel, M. F. (2011). Development and cancer of the cerebellum. Trends in neurosciences, 34(3), 134–142. doi:10.1016/j.tins.2011.01.002

Howard, T. L., Stauffer, D. R., Degnin, C. R., & Hollenberg, S. M. (2001). CHMP1 functions as a member of a newly defined family of vesicle trafficking proteins. Journal of cell science, 114(Pt 13), 2395–2404.

Keinan, A., & Clark, A. G. (2012). Recent Explosive Human Population Growth Has Resulted in an Excess of Rare Genetic Variants. Science (New York, NY), 336(6082), 740–743. doi:10.1126/science.1217283

Keren, B., Suzuki, O. T., Gérard-Blanluet, M., Brémond-Gignac, D., Elmaleh, M., Titomanlio, L., Delezoide, A.-L., et al. (2007). CNS malformations in Knobloch syndrome with splice mutation in COL18A1 gene. American journal of medical genetics Part A, 143A(13), 1514–1518. doi:10.1002/ajmg.a.31784

Kim, W.-Y., Wang, X., Wu, Y., Doble, B. W., Patel, S., Woodgett, J. R., & Snider, W. D. (2009). GSK-3 is a master regulator of neural progenitor homeostasis. Nature neuroscience, 12(11), 1390–1397. doi:10.1038/nn.2408

Kovas, Y., & Plomin, R. (2006). Generalist genes: implications for the cognitive sciences. Trends in Cognitive Sciences, 10(5), 198–203. doi:10.1016/j.tics.2006.03.001

Lamonica, B. E., Lui, J. H., Wang, X., & Kriegstein, A. R. (2012). OSVZ progenitors in the human cortex: an updated perspective on neurodevelopmental disease. Current opinion in neurobiology, 1–7. doi:10.1016/j.conb.2012.03.006

Luo, R., Jeong, S.-J., Jin, Z., Strokes, N., Li, S., & Piao, X. (2011). G protein-coupled receptor 56 and collagen III, a receptor-ligand pair, regulates cortical development and lamination. Proceedings of the National Academy of Sciences of the United States of America, 108(31), 12925–12930. doi:10.1073/pnas.1104821108

Manzini, M. C., & Walsh, C. A. (2011). What disorders of cortical development tell us about the cortex: one plus one does not always make two. Current opinion in genetics & development, 21(3), 333–339. doi:10.1016/j.gde.2011.01.006

Marino, S. (2005). Medulloblastoma: developmental mechanisms out of control. Trends in Molecular Medicine, 11(1), 17–22. doi:10.1016/j.molmed.2004.11.008

Paisán-Ruiz, C., Scopes, G., Lee, P., & Houlden, H. (2009). Homozygosity mapping through whole genome analysis identifies a COL18A1 mutation in an Indian family presenting with an autosomal recessive neurological disorder. American journal of medical genetics. Part B, Neuropsychiatric genetics : the official publication of the International Society of Psychiatric Genetics, 150B(7), 993–997. doi:10.1002/ajmg.b.30929

Piao, X., Hill, R. S., Bodell, A., Chang, B. S., Basel-Vanagaite, L., Straussberg, R., Dobyns, W. B., et al. (2004). G protein-coupled receptor-dependent development of human frontal cortex. Science (New York, NY), 303(5666), 2033–2036. doi:10.1126/science.1092780

Pulvers, J. N., Bryk, J., Fish, J. L., Wilsch-Bräuninger, M., Arai, Y., Schreier, D., Naumann, R., et al. (2010). Mutations in mouse Aspm (abnormal spindle-like microcephaly associated) cause not only microcephaly but also major defects in the germline. Proceedings of the National Academy of Sciences of the United States of America, 107(38), 16595–16600. doi:10.1073/pnas.1010494107

Stauffer, D. R., Howard, T. L., Nyun, T., & Hollenberg, S. M. (2001). CHMP1 is a novel nuclear matrix protein affecting chromatin structure and cell-cycle progression. Journal of cell science, 114(Pt 13), 2383–2393.

Taelman, V. F., Dobrowolski, R., Plouhinec, J.-L., Fuentealba, L. C., Vorwald, P. P., Gumper, I., Sabatini, D. D., et al. (2010). Wnt signaling requires sequestration of glycogen synthase kinase 3 inside multivesicular endosomes. Cell, 143(7), 1136–1148. doi:10.1016/j.cell.2010.11.034

Vaillant, C., & Monard, D. (2009). SHH pathway and cerebellar development. The Cerebellum, 8(3), 291–301. doi:10.1007/s12311-009-0094-8

Van Essen, D. C. (2005). A Population-Average, Landmark- and Surface-based (PALS) atlas of human cerebral cortex. NeuroImage, 28(3), 635–662. doi:10.1016/j.neuroimage.2005.06.058